

AD-A131 857

ENTHALPY - IMPROVED DIELECTRIC INSULATION FOR  
SUPERCONDUCTING WIRES(U) LAKE SHORE CRYOTRONICS INC  
WESTERVILLE OH W N LAWLESS ET AL MAY 82

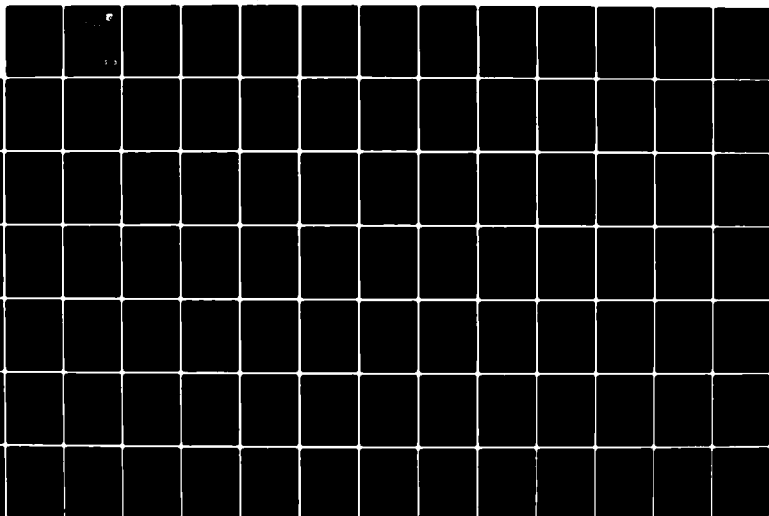
1/2

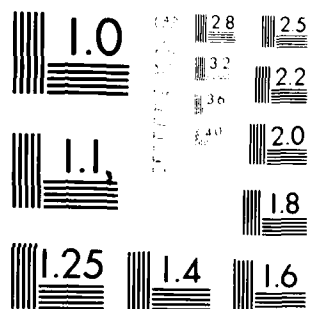
UNCLASSIFIED

AFWAL-TR-82-2056 F33615-80-C-2022

F/G 11/2

NL





MICROCOPY RESOLUTION TEST CHART  
NATIONAL BUREAU OF STANDARDS-1963-A

ADA131857

AFWAL-TR-82-2056



# ENTHALPY - IMPROVED DIELECTRIC INSULATION FOR SUPERCONDUCTING WIRES

W. N. LAWLESS, C. F. CLARK, AND R. W. ARENZ  
LAKE SHORE CRYOTONICS, INC.  
WESTERVILLE, OHIO 43081

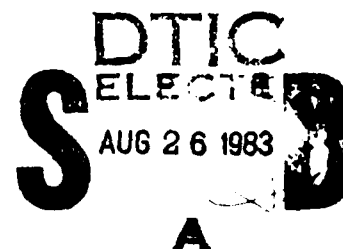
MAY 1982

FINAL REPORT FOR PERIOD JUNE 1980 - MARCH 1982

APPROVED FOR PUBLIC RELEASE; DISTRIBUTION UNLIMITED

DTIC FILE COPY

AERO PROPULSION LABORATORY  
AIR FORCE WRIGHT AERONAUTICAL LABORATORIES  
AIR FORCE SYSTEMS COMMAND  
WRIGHT-PATTERSON AIR FORCE BASE, OHIO 45433



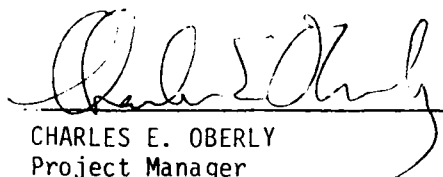
83 08 23 058

NOTICE

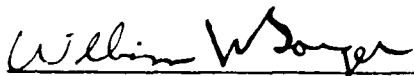
When Government drawings, specifications, or other data are used for any purpose other than in connection with a definitely related Government procurement operation, the United States Government thereby incurs no responsibility nor any obligation whatsoever; and the fact that the government may have formulated, furnished, or in any way supplied the said drawings, specifications, or other data, is not to be regarded by implication or otherwise as in any manner licensing the holder or any other person or corporation, or conveying any rights or permission to manufacture use, or sell any patented invention that may in any way be related thereto.

This report has been reviewed by the Office of Public Affairs (ASD/PA) and is releasable to the National Technical Information Service (NTIS). At NTIS, it will be available to the general public, including foreign nations.

This technical report has been reviewed and is approved for publication.



CHARLES E. OBERLY  
Project Manager  
Power Systems Branch  
Aerospace Power Division



WILLIAM U. BORGER  
Acting Technical Area Manager  
Power Systems Branch  
Aerospace Power Division

FOR THE COMMANDER



D. DAVID RANDOLPH, MAJOR, USAF  
Deputy Director  
Aerospace Power Division  
Aero Propulsion Laboratory

"If your address has changed, if you wish to be removed from our mailing list, or if the addressee is no longer employed by your organization please notify AFWAL/POOS, W-PAFB, OH 45433 to help us maintain a current mailing list".

Copies of this report should not be returned unless return is required by security considerations, contractual obligations, or notice on a specific document. -

UNCLASSIFIED

SECURITY CLASSIFICATION OF THIS PAGE (When Data Entered)

REPORT DOCUMENTATION PAGE		READ INSTRUCTIONS BEFORE COMPLETING FORM
1. REPORT NUMBER AFWAL-TR-82-2056	2. GOVT ACCESSION NO. AD-A131 857	3. RECIPIENT'S CATALOG NUMBER
4. TITLE (and Subtitle) Enthalpy - Improved Dielectric Insulation for Superconducting Wires		5. TYPE OF REPORT & PERIOD COVERED Final JUN 80 - MAR 82
7. AUTHOR(s) W. N. Lawless, C. F. Clark, and R. W. Arenz		6. PERFORMING ORG. REPORT NUMBER
9. PERFORMING ORGANIZATION NAME AND ADDRESS Lake Shore Cryotronics, Inc. 64 E. Walnut Street Westerville, Ohio 43081		8. CONTRACT OR GRANT NUMBER(s) F33615-80-C-2022
11. CONTROLLING OFFICE NAME AND ADDRESS Aero Propulsion Laboratory (POOS) Air Force Wright Aeronautical Lab., AFSC Wright-Patterson AFB OH 45433		10. PROGRAM ELEMENT, PROJECT, TASK AREA & WORK UNIT NUMBERS 62203F; 2301-S3-05
14. MONITORING AGENCY NAME & ADDRESS (if different from Controlling Office)		12. REPORT DATE May 1982
		13. NUMBER OF PAGES 136
		15. SECURITY CLASS. (of this report) UNCLASSIFIED
		15a. DECLASSIFICATION DOWNGRADING SCHEDULE
16. DISTRIBUTION STATEMENT (of this Report) Approved for public release; distribution unlimited.		
17. DISTRIBUTION STATEMENT (of the abstract entered in Block 20. If different from Report)		
18. SUPPLEMENTARY NOTES		
19. KEY WORDS (Continue on reverse side if necessary and identify by block number) Superconductor, Insulation, Dielectric, Heat Capacity, Thermal Conductivity, Ceramics		
20. ABSTRACT (Continue on reverse side if necessary and identify by block number) The objective of this investigation was to characterize the low - temperature thermal properties of several new, inorganic, dielectric materials which offer favorable enthalpy-stabilization advantages as dielectric insulators for superconductors.  Specific heat and thermal conductivity measurements are reported on four classes of materials: (1) SC-1 materials, which are refractory ceramics;		

UNCLASSIFIED

SECURITY CLASSIFICATION OF THIS PAGE(When Data Entered)

20. Abstract (continued)

(2) SC-2 materials, which can be hot-extruded onto NbTi at  $\approx 350^\circ\text{C}$ ; (3) SC-3 materials, which might be hot-extruded onto NbSn at  $\approx 600^\circ\text{C}$ ; and (4) Composites of powders of the SC-1 ceramics cast into glass and varnish matrices. Thermal properties' measurements at low temperatures are reported both in zero field and in intense magnetic fields up to 15 T, and a total of eighteen materials were studied.

A broad range of thermal properties are possible with these dielectric materials: Enthalpies (4.2  $\rightarrow$  6 K) range from 7.2 to 121 mJ/cm<sup>3</sup> (for comparison, the corresponding enthalpy for Pb is 30.3 mJ/cm<sup>3</sup>), and thermal diffusivities (at 5 K) range from 0.005 to 375 cm<sup>2</sup>/s (the corresponding value for Pb is 42 cm<sup>2</sup>/s). For the most favorable materials, the specific heat and thermal conductivity are unaffected by intense magnetic fields.

The ceramic + glass composites (Class 4 above) were chosen to be compatible with the 600-750°C reaction temperature range of NbSn, and it was found that a favorable solid-state reaction occurs between the ceramic and glass which leads to enhanced specific-heat properties in several cases. In a particularly noteworthy case (60% SC-1C ceramic + 40% 7570 glass), the composite has a much larger specific heat ( $\approx 0.07$  J/cm<sup>3</sup>K) than the bulk ceramic alone below 7 K. There is evidence that the low thermal conductivities of all the composites are due to Kapitza resistance, and suggestions are made for improving these conductivities.

The SC-2 and SC-3 type materials have near-metallic thermal conductivities near 4.2 K (i.e.,  $K \leq 7$  W/cm K), and in the case of SC-2 materials it is shown that boundary scattering does not degrade the thermal conductivity for coating thickness  $\geq 0.1$ -0.2 nm. Neither the SC-2 nor -3 materials contain paramagnetic ions, yet an expected dependence of the thermal conductivity on intense magnetic fields was found in these materials. The case of SC-3A is particularly dramatic: The thermal conductivity at 10.5 K has a large maximum at approximately 9 T.

Attempts to coat a NbTi wire (0.012" diam) with the SC-2B material by a hot-extrusion process ( $350^\circ\text{C}$ ) met with some success: A 16-ft section of wire was coated, and demanding bend tests ( $\sim \frac{1}{2}$ " radius) showed that the coating remained intact. This coating, however, was impractically thick, 0.019", due to the available extrusion die used, and a gap developed between the wire and the coating (seen in corona-discharge studies). Much thinner coatings on short sections ( $\sim$  inches) of the wire showed no evidence of a gap.

Recommendations are made for future studies of these dielectric coating materials, in areas of both applied and basic research.

UNCLASSIFIED

## FOREWORD

This final report was submitted by Lake Shore Cryotronics, Inc., Westerville, Ohio 43081, under Contract No. 33615-80-C-2022. The effort was sponsored by the Air Force Systems Command, Aeronautical Systems Division, Wright-Patterson AFB, Ohio 45433, with Dr C. E. Oberly, AFWAL/POOS-2, as Project Engineer. The time period covered by the report is June 1980 to March 1982, and Dr W. N. Lawless was technically responsible for the work performed.

The authors are grateful to Dr Charles Oberly at W-PAFB for encouragement in these studies and for helpful discussions. Special thanks are due to Scott Swartz at Penn State University for assistance in preparing some of the test samples, and also to Dr T. P. Gupta at the Westinghouse R&D Center for preparing all the ceramic + glass composites. The measurements in intense magnetic fields would not have been possible without the assistance and advice of L. G. Rubin (MIT) and Prof R. J. Sladek (Purdue University). Finally, Bruce Zeitlin at Intermagnetics General Corp. supplied the BNL NbTi wire, and R. Szupillo at Corning Glass Works supplied the rod of CIPG.

UNCLASSIFIED

Distribution For	
GR&I	<input type="checkbox"/>
TO	<input type="checkbox"/>
Announced	<input type="checkbox"/>
Classification	
Distribution/	
Availability Codes	
Avail and/or	Special
Dist	

## Table of Contents

<u>Section</u>	<u>Page</u>
I. Summary .....	1
II. Introduction .....	3
III. Dielectric Materials Studied .....	9
Pure Materials .....	9
Composite Materials .....	11
IV. Experimental Methods .....	12
Zero-Field Measurements .....	12
Measurements in Intense Magnetic Fields .....	14
Specific Heat Measurements .....	15
Thermal Conductivity Measurements .....	17
V. SC-1 Materials .....	17
Zero-Field Measurements .....	17
Magnetic-Field Measurements .....	22
SC-1A .....	22
SC-1B .....	24
SC-1C .....	27
SC-1D .....	31
VI. SC-2 Materials .....	36
Zero-Field Measurements .....	36
Magnetic-Field Measurements .....	45
VII. SC-3 Materials .....	52
Zero-Field Measurements .....	54
Magnetic-Field Measurements .....	57
VIII. SC-1C + Varnish Composite .....	62
Heat Transfer Sample .....	67
IX. SC-1B + Glass Composites .....	69
Specific Heat Measurements .....	71
Thermal Conductivity Measurements .....	77
X. SC-1C + Glass Composites .....	79
Specific Heat Measurements .....	80
Thermal Conductivity Measurements .....	88
XI. Wire Coating Studies (SC-2B on NbTi) .....	90
XII. Conclusions .....	96
XIII. Recommendations .....	106
Applied Materials' Research Areas .....	107
Basic Materials' Research Areas .....	109
System Safety Hazard Analysis Report .....	112
References .....	114
Appendix A1. Method for Measuring Specific Heats in Intense .....	116
Magnetic Fields at Low Temperatures using	
Capacitance Thermometry	



## List of Figures

	<u>Page</u>
Figure 1. Volumetric specific heats below 10 K for two dielectrics, SC-1C and SC-2B, compared to data on unfilled resins (Ref. 6).	6
Figure 2. Preliminary thermal conductivity data below 10 K for SC-2B compared to Pb and for the SC-1 class of materials compared to epoxies.	7
Figure 3. Volumetric specific heat data below 15 K for the SC-1 class of materials compared to Pb. The SC-1C material shown has a spinel:columbite ratio of 3:1 (see text).	19
Figure 4. Dependence of the specific heat of SC-1C on the spinel:columbite ratio (from Ref. 7). The 9/1-ratio material was used exclusively in the studies here.	20
Figure 5. Thermal conductivity data below 15 K for the SC-1 class of materials. Arrows indicate the temperatures of the specific heat maxima (Fig. 3), and data for glass (vitreous silica) are shown for comparison.	21
Figure 6. Magnetic-field dependence of the specific heat of SC-1A below 6.5 K at 2.5, 5.0, and 7.5 T. Zero-field data are shown for comparison.	23
Figure 7. Volumetric enthalpy of SC-1A relative to 3.87 K at 0, 2.5, 5.0, and 7.5 T.	25
Figure 8. Magnetic-field dependence of the specific heat of SC-1B below 9.5 K at 2.5, 5.0, and 7.5 T. Zero-field data are shown for comparison.	26
Figure 9. Volumetric enthalpy of SC-1B relative to 4.13 K at 0, 2.5, 5.0, and 7.5 T.	28
Figure 10. Magnetic-field dependence of the specific heat of SC-1C below 18 K at 7.5 and 15 T. Zero-field data are shown for comparison. Intense magnetic fields induce considerable structure in the specific heat in the neighborhood of the dominant 8 K peak.	29

# List of Figures (continued)

	<u>Page</u>
Figure 11. Specific heat of SC-1C at 7.5, 10.0, 12.5, and 15.0 T. Note the structure at 7.5 and 15.0 T.	30
Figure 12. Volumetric enthalpy of SC-1C relative to 4.91 K at 0, 7.5, and 15.0 T. At temperatures below about 7.5 K, the enthalpy is increased by intense magnetic fields.	32
Figure 13. Magnetic-field dependence of the specific heat of SC-1D below 18 K at 5.0, 7.5, and 15.0 T. Zero-field data are shown for comparison.	33
Figure 14. Volumetric enthalpy of SC-1D relative to 4.71 K at 0, 5.0, 7.5, and 15 T. At the two highest magnetic-field levels, the enthalpy is increased over the zero-field enthalpy for temperatures below 7 K.	35
Figure 15. Volumetric specific heat data for the SC-2 and SC-3 materials plotted as $CT^{-5}$ to emphasize the non-Debye, "ferroelectric" modes in the SC-2 materials (see text).	38
Figure 16. Thermal conductivities of the SC-2 materials showing near-metallic thermal-conductivity values with maxima near 5 K.	40
Figure 17. Thermal conductivity data measured on thin (0.49 mm) fibers of SC-2A. Shown for comparison are data on bulk SC-2A and on commercial copper.	42
Figure 18. Thermal conductivity data measured on thin (0.64 mm) bars of SC-2B. Shown for comparison are data on bulk SC-2B and on commercial copper.	43
Figure 19. Magnetic-field dependence of the specific heat of SC-2A below 13 K at 2.5 and 5.0 T. Zero-field specific heat data are shown for comparison.	46
Figure 20. Volumetric enthalpy of SC-2A relative to 4.40 K at 0 and 5 T. The enthalpy of SC-2A is unaffected by intense magnetic fields.	47

# List of Figures (continued)

	<u>Page</u>
Figure 21. Magnetic-field dependence of the specific heat of SC-2B below 15 K at 2.5 and 5.0 T. Zero-field specific heat data are shown for comparison.	48
Figure 22. Volumetric enthalpy of SC-2B relative to 4.29 K at 0 and 5 T. The enthalpy of SC-2B is slightly depressed by an intense magnetic field.	49
Figure 23. Magnetic-field-dependence of the thermal conductivities of SC-2A and -2B at constant temperature. A field-sweep method was used, and the two samples were measured under identical conditions. Four to eight points were measured at each field level.	53
Figure 24. Thermal conductivities of the SC-3 materials (bulk samples, zero field). Data for commercial copper are shown for comparison, and these SC-3 materials have the largest thermal conductivities of any of the materials studied.	55
Figure 25. Thermal conductivity data measured on thin (0.64 mm) bars of SC-3A. These data reveal stronger boundary-scattering effects than the data for SC-2A (Fig. 17) or SC-2B (Fig. 18).	56
Figure 26. Magnetic-field dependence of the specific heat of SC-3B below 17 K at 2.5, 5.0, and 7.5 T. Zero-field data are shown for comparison.	58
Figure 27. Volumetric enthalpy of SC-3B relative to 3.94 K at 0, 2.5, 5.0, and 7.5 T. The enthalpy of SC-3B is depressed slightly by intense magnetic fields at temperatures above 6 K.	59
Figure 28. Magnetic-field dependence of the thermal conductivity of SC-3A at 10.45 K. Several points were measured at each field level, and a large maximum appears in the thermal conductivity at about 9 T.	61

# List of Figures (continued)

	<u>Page</u>
Figure 29. Specific heat of the SC-1C + G.E. 7031 composite (zero field). The density of the composite is estimated to be 3.3 g/cm <sup>3</sup> , and the volumetric scale shown is based on this density.	64
Figure 30. Thermal conductivity of the SC-1C + 7031 composite (zero field). The conductivity data follow a T <sup>2</sup> law at the lowest temperatures, and thermal diffusivity data are also shown [estimated using Eq. (3) and the data in Fig. 29].	65
Figure 31. Specific heat data for the SC-1B + 7570 composites at 30, 45, and 60 wt % of the ceramic powder. Also shown for comparison are specific heat data for the bulk ceramic.	72
Figure 32. Specific heat data for the SC-1B + 7052 composites at 30, 45, and 60 wt % of the ceramic powder. Also shown for comparison are specific heat data for the bulk ceramic.	73
Figure 33. Specific heat data for the SC-1B powders <u>alone</u> in the composites with 7570 glass. Specific heat data for bulk SC-1B are also shown, and note that the SC-1B powders in the composites have reduced specific heats, indicating a solid-state reaction between the ceramic and the glass.	75
Figure 34. Specific heat data for the SC-1B powders <u>alone</u> in the composites with 7052 glass. In contrast to the case of the 7570 glass (Fig. 33), there is apparently no solid-state reaction between the SC-1B powder and the 7052 glass.	76
Figure 35. Thermal conductivities of the composites of SC-1B and 7570 glass (upper plot) and 7052 glass (lower plot).	78
Figure 36. Specific heat data for the SC-1C + 7052 composites at 30, 45, and 60 wt % of the ceramic powder. Also shown for comparison are specific heat data for the bulk SC-1C ceramic.	81

# List of Figures (continued)

	<u>Page</u>
Figure 37. Specific heat data for the SC-1C powders <u>alone</u> in the composites with 7052 glass. Note that below about 7 K the powders in the 7052 glass matrix have <u>larger</u> specific heats than the bulk ceramic, indicating a solid-state reaction.	82
Figure 38. Specific heat data for the SC-1C + 7570 composites at 30, 45, and 60 wt % of the ceramic powder. Also shown for comparison are specific heat data for the bulk SC-1C ceramic, and note that the 60% composite has a larger specific heat than the bulk ceramic below 6.5 K.	83
Figure 39. Repeatability of the specific heat data for the 60% SC-1C + 7570 composite.	85
Figure 40. Specific heat data for the SC-1C powders <u>alone</u> in the composites with 7570 glass. Note that below about 7 K the powders in the 7570 glass matrix have <u>larger</u> specific heats than the bulk ceramic, indicating a solid-state reaction.	86
Figure 41. Thermal conductivities of the composites of SC-1C and 7570 glass (upper plot) and 7052 glass (lower plot).	89
Figure 42. Thermal conductivities of the composites with 7570 glass at the lowest temperatures. The $K \propto T^2$ trend in all the data suggests that Kapitza resistance may play a dominant role in the phonon transport through these composites.	91
Figure 43. Photographs of short sections of NbTi wire (0.012" diam) coated with SC-2B (0.0015" thick): (a) Straight section; (b) 1" bend.	93
Figure 44. Photographs of a 16-ft section of NbTi wire (0.012" diam) coated continuously with SC-2B (0.019" thick) by a hot-extrusion process: (a) Entire 16-ft coil; (b) Approx. $\frac{1}{2}$ " bend test.	95
Figure 45. Plot of thermal relaxation time <u>versus</u> enthalpy per unit length for a 0.127 mm thick coating for all the materials studied (taken from Table 14). The materials fall into two categories: "Pb-like" and "resin-like."	104

# List of Tables

	<u>Page</u>
Table 1. Densities of the SC Dielectric Materials	10
Table 2. Volumetric Enthalpies of the SC-1 Materials Relative to 4.2 K at 7.5 T (in units of $\text{mJ cm}^{-3}$ )	36
Table 3. Geometric Phonon Scattering Limits (SC-2)	44
Table 4. Volumetric Enthalpies for the SC-2 Materials Relative to 4.2 K (in units of $\text{mJ cm}^{-3}$ )	50
Table 5. Geometric Phonon Scattering Limits (SC-3)	57
Table 6. Volumetric Enthalpies of the SC-3 Materials Relative to 4.2 K (in units of $\text{mJ cm}^{-3}$ )	60
Table 7. Volumetric Enthalpies of the SC-1C + 7031 Composite Relative to 4.2 K (in units of $\text{mJ cm}^{-3}$ )	67
Table 8. Calibration Data for the CIPG Heat Transfer Sample	68
Table 9. Densities and Porosities of the SC-1B + Glass Composite Materials	71
Table 10. Volumetric Enthalpies of the SC-1B + Glass Composites Relative to 4.2 K (in units of $\text{mJ cm}^{-3}$ )	74
Table 11. Densities and Porosities of the SC-1C + Glass Composite Materials	79
Table 12. Volumetric Enthalpies of the SC-1C + Glass Composites Relative to 4.2 K (in units of $\text{mJ cm}^{-3}$ )	87
Table 13. Volumetric Enthalpies ( $\text{mJ cm}^{-3}$ ) Relative to 4.2 K	97
Table 14. Thermal Parameters for a Hypothetical Coating 0.127 mm (0.005") thick	102

### List of Symbols and Abbreviations

$C$	Specific heat
$K$	Thermal conductivity
$k$	Thermal diffusivity
$\rho$	Density
$\tau$	Thermal relaxation time
$\lambda$	Phonon mean-free path
7031	General Electric 7031 transformer varnish
7570	Glass composition code 7570
7052	Glass composition code 7052
CIPG	Carbon-impregnated porous glass

## 1. SUMMARY

The objective of this investigation was to characterize the low-temperature thermal properties of several new, inorganic, dielectric materials which offer favorable enthalpy-stabilization advantages as dielectric insulators for superconductors.

Specific heat and thermal conductivity measurements are reported on four classes of materials: (1) SC-1 materials, which are refractory ceramics; (2) SC-2 materials, which can be hot-extruded onto NbTi at  $\approx 350^\circ\text{C}$ ; (3) SC-3 materials, which might be hot-extruded onto NbSn at  $\approx 600^\circ\text{C}$ ; and (4) Composites of powders of the SC-1 ceramics cast into glass and varnish matrices. Thermal properties' measurements at low temperatures are reported both in zero field and in intense magnetic fields up to 15 T, and a total of eighteen materials were studied.

A broad range of thermal properties are possible with these dielectric materials: Enthalpies (4.2  $\rightarrow$  6 K) range from 7.2 to 121  $\text{mJ cm}^{-3}$  (for comparison, the corresponding enthalpy for Pb is 30.3  $\text{mJ cm}^{-3}$ ), and thermal diffusivities (at 5 K) range from 0.005 to 375  $\text{cm}^2/\text{s}$  (the corresponding value for Pb is 42  $\text{cm}^2/\text{s}$ ). For the most favorable materials, the specific heat and thermal conductivity are unaffected by intense magnetic fields.

The ceramic + glass composites (Class 4 above) were chosen to be compatible with the 600-750°C reaction temperature range of NbSn, and it was found that a favorable solid-state reaction occurs between the ceramic



## II. INTRODUCTION

The stability of superconducting magnets, motors, and generators depends, among other things, on providing means for stabilizing "hot spots" in the wire. Whatever their cause (wire defects, trapped flux, etc.), these hot spots can cause local normalization of the wire which can propagate catastrophically. Commonly, a copper cladding is provided so that the current can skirt around the normal region.

The problem of dissipating the heat generated by a hot spot (or any source of heating) has received considerable attention, and this field of superconductivity technology is generally referred to as enthalpy stabilization(1). All previous suggestions for improving the enthalpy stabilization of superconductors have dealt exclusively with metallic approaches(2), such as adding a coating of Pb to gain the added specific heat offered by Pb [this metal has the largest specific heat of any convenient material at low temperatures due to its low Debye temperature (108 K) and large density ( $11.3 \text{ g/cm}^3$ ) -- see below, also]. A clever suggestion was recently made by a group at Los Alamos(3) to add  $\text{GdAlO}_3$  powders to the copper cladding to gain a specific heat increase at  $\sim 4 \text{ K}$ .

-- > The purpose of this study was to investigate for the first time dielectric materials for enthalpy stabilization, the broad picture being that these materials would also serve as the dielectric-insulation coating. These new, inorganic materials resulted from basic research by the author into the specific heats of ferroelectric-type materials at low

and glass which leads to enhanced specific-heat properties in several cases. In a particularly noteworthy case (60% SC-1C ceramic + 40% 7570 glass), the composite has a much larger specific heat ( $\approx 0.07 \text{ J cm}^{-3} \text{ K}^{-1}$ ) than the bulk ceramic alone below 7 K. There is evidence that the low thermal conductivities of all the composites are due to Kapitza resistance, and suggestions are made for improving these conductivities.

The SC-2 and SC-3 type materials have near-metallic thermal conductivities near 4.2 K (i.e.,  $K \lesssim 7 \text{ W cm}^{-1} \text{ K}^{-1}$ ), and in the case of SC-2 materials it is shown that boundary scattering does not degrade the thermal conductivity for coating thicknesses  $\gtrsim 0.1\text{-}0.2 \text{ }\mu\text{m}$ . Neither the SC-2 nor -3 materials contain paramagnetic ions, yet an expected dependence of the thermal conductivity on intense magnetic fields was found in these materials. The case of SC-3A is particularly dramatic: The thermal conductivity at 10.5 K has a large maximum at  $\approx 9 \text{ T}$ .

Attempts to coat a NbTi wire (0.012" diam) with the SC-2B material by a hot-extrusion process ( $\sim 350^\circ\text{C}$ ) met with some success: A 16-ft section of wire was coated, and demanding bend tests ( $\sim \frac{1}{2}$ " radius) showed that the coating remained intact. This coating, however, was impractically thick, 0.019", due to the available extrusion die used, and a gap developed between the wire and the coating (seen in corona-discharge studies). Much thinner coatings on short sections (inches) of the wire showed no evidence of a gap.

Recommendations are made for future studies of these dielectric coating materials, in areas of both applied and basic research.

temperatures(4). There it was found that these materials universally contain low-lying vibrational modes which often dominate the specific heat at low temperatures; that is, the specific heats of these materials can be an order of magnitude larger than one would expect from the Debye temperature alone (as determined, say, from elastic constant data). During the course of this research, the author also discovered a family of ferroelectric-ferromagnetic materials which have an additional specific-heat contribution from a magnetic transition (as will be seen below, some of these latter materials achieve low-temperature specific heat values which are almost as large as that of water at room temperature).

We remark at the outset that these materials are not well understood, from a basic-physics viewpoint, in particular, the ferroelectric-ferromagnetics. Nor was it the purpose of the investigations reported here to address the solid-state physics of these materials. Rather, the spirit of these studies was to provide a broad range of low-temperature experimental data on these materials which will be needed to judge their practical significance as potential dielectric coatings for superconducting wires. Certainly, the data reported here deserve deeper study. Some of the evidence measured recently(5) actually suggests that the thermal and dielectric (but not mechanical) properties of ferroelectrics are similar to those of glasses at low and ultra-low temperatures.

To illustrate and introduce the attractive low-temperature thermal properties of these potential dielectric insulation materials, some

preliminary specific heat and thermal conductivity data are shown in Figs. 1 and 2, respectively. The specific heats of the new ceramics SC-1C and SC-2B are shown plotted volumetrically in Fig. 1 compared to published data on resins(6) (We shall describe these materials' designations in the next section.). The resin data in Fig. 1 are representative of the specific heats of conventional organic dielectric insulations (e.g., Formvar), and, as seen, the SC-1C and SC-2B dielectric materials offer specific heat values  $\sim 10$ -50 times larger than those of organic insulations. In Fig. 2 are shown thermal conductivity data for the dielectrics SC-2B, SC-1A, SC-1B, SC-1D, and SC-1C compared to representative data for epoxies (6) at low temperatures. The preliminary data in Fig. 2 indicate that the SC-2B material has a near-metallic thermal conductivity,  $\sim 500$  times larger than that of the epoxies.

Consequently, these new, inorganic dielectrics offer considerable enthalpy-stabilization advantages compared to conventional dielectrics. Both specific heat and thermal conductivity considerations enter enthalpy stabilization: A very large specific heat is desirable to minimize the temperature rise associated with a hot spot, and a large thermal conductivity is desirable to transmit the heat generated to a helium bath. This is a complex problem, as one must consider film-boiling versus nucleate-boiling in the helium bath, and it is beyond the scope of the study here to investigate transient heating phenomena through these potential dielectric coatings. One intuitively anticipates, however, that a material with a very large specific heat should also have a

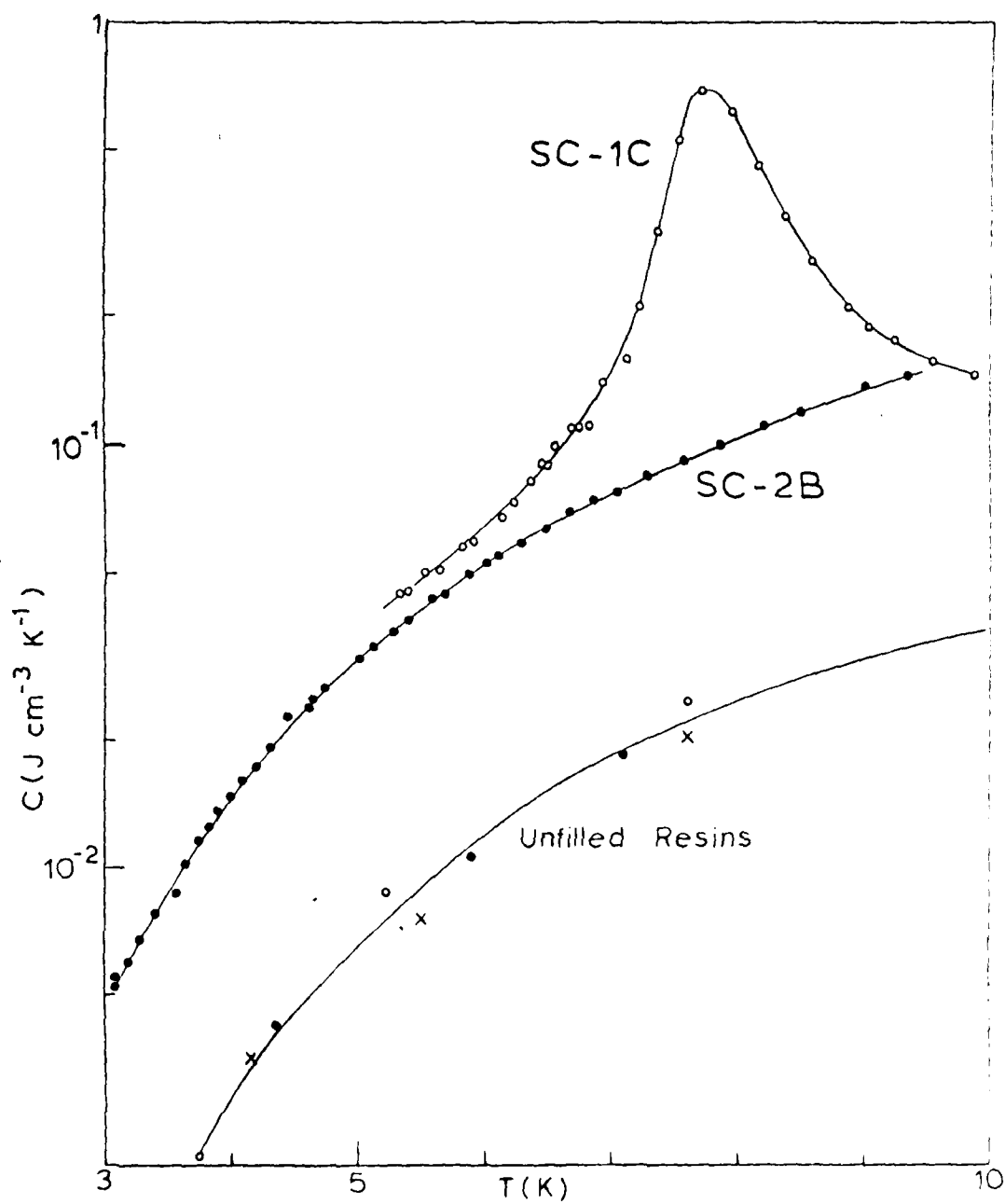


**Figure 1.** Volumetric specific heats below 10 K for two dielectrics, SC-1C and SC-2B, compared to data on unfilled resins (Ref. 6).

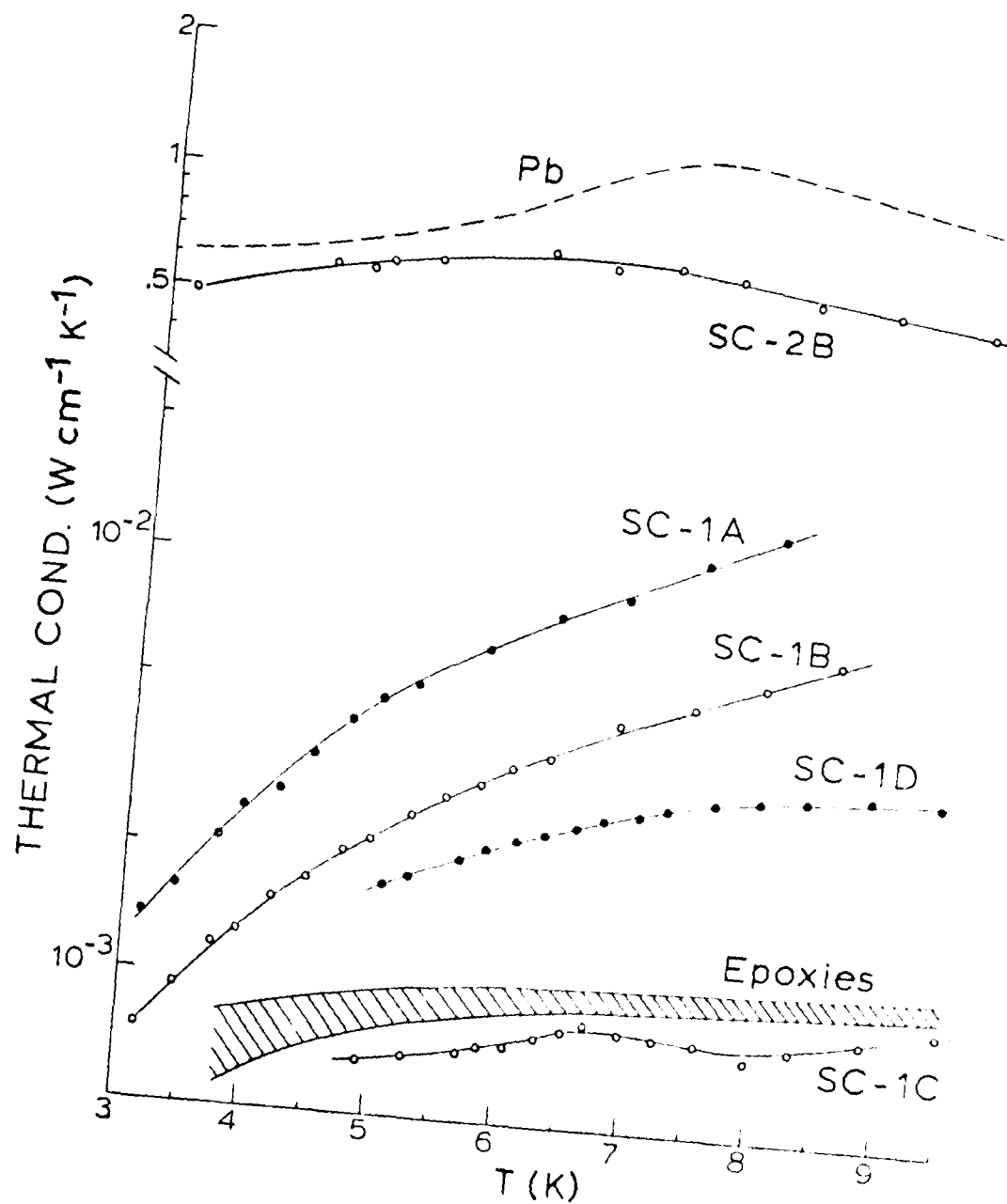


**Figure 2.** Preliminary thermal conductivity data below 10 K for SC-2B compared to Pb and for the SC-1 class of materials compared to epoxies.

reasonably large thermal conductivity, since the thermal diffusivity is probably the most important parameter.

The purpose of this study at the outset was to measure the low-temperature thermal properties (including the effects of intense magnetic fields) of three classes of new, inorganic dielectrics (so-called SC-1, SC-2, and SC-3 materials, see below). This involved developing new methods for measuring thermal properties in intense magnetic fields. As the program evolved, thirteen composite materials were included which were mixtures of the SC-1 materials with glasses and with a varnish. Initial attempts to coat a NbTi wire with one of the pure materials by a hot extrusion process met with some success as a 16-ft section of wire was uniformly coated. And lastly, a heat-transfer sample consisting of a rod of carbon-impregnated-porous-glass coated with an SC-1C + varnish composite was assembled and the thermal properties of the constituent materials measured.

This report is organized as follows: Section III describes the dielectric materials studied; Section IV describes the experimental methods used; Sections V, VI, and VII describe the thermal properties in zero field and in intense H-fields of the SC-1, SC-2, and SC-3 classes of materials, respectively; Section VIII describes the SC-1C + varnish composite and the heat transfer sample; Sections IX and X describe the zero-field thermal properties of the SC-1B + glass and SC-1C + glass composites, respectively; Section XI describes some initial studies of coating NbTi wire with SC-2B; and Sections XII and XIII are the Conclusions and Recommendations, respectively.

### III. DIELECTRIC MATERIALS STUDIED

#### Pure Materials

The SC-1 class of materials are refractory ceramics which sinter to dense bodies in the temperature range 1250-1350°C. The SC-1A and SC-1B ceramics have the columbite crystal structure and have specific heat maxima at 4.2 and 5.3 K, respectively, (see Fig. 3 below). The SC-1C and SC-1D ceramics are two-phase, spinel + columbite structures and have specific heat maxima at 8 and 10.5 K, respectively. Because of the refractory nature of these SC-1 materials, it is probable that the only viable approach for using these materials as coatings would be to mix powders of these ceramics into a suitable vehicle (e.g., varnish, glass, epoxy, etc.).

The SC-2 class of materials are plastic-like materials which can be hot-extruded at about 350°C without an organic binder and therefore seem ideal candidates for coating NbTi (In fact, our successful wire-coating attempt involved extruding SC-2B directly onto NbTi wire.). These ferroelectric-type materials do not contain paramagnetic ions and so do not have magnetic anomalies in the specific heat.

The SC-3 class of materials are similar to the SC-2 materials except that the hot-extrusion temperature is about 600°C. For this reason, these SC-3 materials were considered possible coating materials for NbSn.

Broadly speaking, these three classes of new, inorganic dielectrics



can also be categorized along the lines of their low-temperature thermal properties, as follows: The SC-1 materials have enormous specific heats ( $\sim 0.2$ - $1.0 \text{ J cm}^{-3} \text{ K}^{-1}$ ) but rather small thermal conductivities ( $\sim 10^{-3}$ - $10^{-2} \text{ W cm}^{-1} \text{ K}^{-1}$ ). The SC-2 materials have very large specific heats ( $\sim 0.5 \text{ J cm}^{-3} \text{ K}^{-1}$ ) and large thermal conductivities ( $\sim 1 \text{ W cm}^{-1} \text{ K}^{-1}$ ). Finally, the SC-3 materials have modest specific heats ( $\sim 0.02 \text{ J cm}^{-3} \text{ K}^{-1}$ ) and very large thermal conductivities ( $\sim 4 \text{ W cm}^{-1} \text{ K}^{-1}$ ).

A contributing factor to the large volumetric specific heats of these materials is their rather large densities which are summarized in Table 1 below.

Table 1

Densities of the SC Dielectric Materials

Material	Density( $\text{g/cm}^3$ )
SC-1A	5.163
-1B	5.495
-1C	5.912
-1D	5.321
SC-2A	7.557
-2B	7.003
-2C	7.092
SC-3A	4.440
-3B	4.526

### Composite Materials

Thirteen composite materials were investigated. The first composite was formed by mixing fine powders of ceramic SC-1C into a transformer varnish, G.E. 7031. This varnish is known to have excellent low-temperature properties and is widely used by experimentalists. The primary purpose of studying this composite was in connection with fabricating a heat-transfer sample.

The remaining twelve composites were mixtures of fine powders of SC-1C and SC-1B and the glasses 7570 and 7052 in three mixing ratios each: 30, 45, and 60% by weight of ceramic powders. The solidification temperatures for these glass + ceramic composites are in the 600-750°C temperature range, chosen to correspond to the NbSn reaction range. The purpose of including these composites in the program was to explore the formability and thermal properties of these materials as possible candidates for the glass + ceramic wire coating facility at the Westinghouse R&D Center.

Finally, this dielectric coating program ran in parallel with a program sponsored by the National Bureau of Standards (NBC Contract NB81RAC10007) to investigate various ceramic modifications in the SC-1C and SC-1D materials. There it was found that the SC-1C material could be improved significantly compared to the data shown in Fig. 1(7), and this improved version of SC-1C was used exclusively in this coating program. We shall return to this point in detail in Section V.

#### IV. EXPERIMENTAL METHODS

In this section, we will describe the methods for measuring specific heat and thermal conductivity, both in zero-field and in intense magnetic fields. The methods used to prepare the dielectric samples will be described separately under the materials sections below (i.e., Sections V through XI).

##### Zero Field Measurements

The specific heat and thermal conductivity measurements in zero magnetic field were made in the adiabatic calorimeter which has been described in the literature(4,8). Briefly, a specific heat sample was suspended within a temperature-controlled adiabatic shield on a thermal link, and the time constant of this link was designed to be  $\geq 100$  s by varying the length and metal of the link. The sample was outfitted with a heater ( $\sim 300\Omega$ ) and carbon-chip thermometer, and addenda weights were determined by cumulative weighings. The carbon-chip thermometer was calibrated in situ during the run against a calibrated germanium thermometer(9). The sample was pulsed with the heater, and  $\Delta T/T$  values were maintained at 2-4%. For large specific heat samples, the addenda corrections were typically  $\leq 0.5\%$ , and the overall uncertainty of the method is  $\approx \pm 2\%$ .

Thermal conductivity measurements were made in the same calorimeter, and two different methods were used depending on the thermal conductivity

of the sample. For samples with  $K \lesssim 0.1 \text{ W cm}^{-1} \text{ K}^{-1}$ , a "one heater, two thermometers" linear-heat-flow method was used wherein a temperature difference  $\Delta T$  was measured at steady-state with the heater activated. For samples with  $K \gtrsim 0.1 \text{ W cm}^{-1} \text{ K}^{-1}$ , a "two heater, one thermometer" linear-heat-flow method was used wherein the two heaters were independently activated to the same power level and  $\Delta T$  was measured. The reason for these two methods is that for low-thermal-conductivity samples, a significant  $\Delta T$  (e.g.,  $\Delta T/T \approx 3\%$ ) can be established with modest heater-power levels, and so small uncertainties in the calibrations of the two thermometers are not significant. On the other hand, for a high-thermal-conductivity sample, the  $\Delta T$ 's can be quite small even at large heater-power levels. In this latter case, the use of one thermometer has the advantage that  $\Delta T$ 's can be determined very accurately despite uncertainties in the absolute calibration; the disadvantage of the method is the requirement to have matched heaters.

In both of these thermal conductivity methods, the carbon-chip thermometer(s) was calibrated in situ (9), the sample heater(s) was fine manganin wire ( $\sim 300 \Omega$ ), and the "reservoir" end of the sample was silver-epoxied to a copper stud which bolted into the adiabatic shield. The largest source of error is determining the spacing between the two thermometers or the two heaters, and this translates into an uncertainty  $\lesssim \pm 5\%$  for both methods.

In both the specific heat and thermal conductivity measurements,

the calorimeter was evacuated at room temperature, and no helium exchange gas was used. Also, activated charcoal granules placed in the bottom of the calorimeter assured extremely high vacuum conditions at helium temperatures. These vacuum conditions meant long cooldown times, typically  $\sim 4$  h for a thermal conductivity run,  $\sim 8$  h for a specific heat run.

#### Measurements in Intense Magnetic Fields

Measurements in intense magnetic fields were complicated by three factors: (1) The space limitation imposed by the tailpiece of the insert dewar (3.81 cm diam); (2) The effect of intense magnetic fields on the thermometry; and (3) The remoteness of the intense H-field facilities (MIT and Purdue) combined with the need to transport the experiment to the facility. The third complication also meant that the logistics of the experiments had to be carefully pre-arranged (i.e., magnet time, He availability, etc.), and there was little room for error or misjudgment.

The space limitation of the dewar dictated a single-can cryostat; that is, there was no room for a temperature-controlled adiabatic shield. The concern here is the radiation load on the sample. This was solved by lining the can with aluminized Mylar, and estimates of the radiation load indicated power levels  $< 1 \mu\text{W}$ , assuming worst conditions. Since the planned measurements involved samples with large specific heats or large thermal conductivities, this radiation power was insignificant. The cryostat that was designed and built could accommodate three specific heat samples or

two thermal conductivity samples per run. The specific details of this cryostat are given in Appendix A1.

The problem of measuring low temperatures in intense magnetic fields is solved either of two ways: (1) Calibrating the magnetoresistive effect in resistance thermometers; or (2) Using capacitance thermometry. The capacitance thermometer(10) has the advantage of being unaffected by intense magnetic fields(11), and was adopted for the measurements here. This thermometer has the disadvantage of poor reproducibility from run to run, complicated by a transient drift ( $\sim 30$  min) after reaching He temperatures(12). These problems seemed far less formidable than calibrating a magnetoresistive thermometer because our long cooldown times ( $\sim 3-6$  h) effectively eliminated the transient drift, and the capacitance thermometer could be easily calibrated each run in zero field [This thermometer is nearly linear, 2-20 K, and easily curve-fitted(13).]. Unencapsulated capacitance thermometers were used in all the measurements here in H-fields.

Finally, three trips were made to the Francis Bitter National Magnet Laboratory (MIT) and one trip to the Physics Dept. at Purdue University. A 14 T Bitter magnet was used at MIT, and a 13 T superconducting magnet at Purdue.

Specific Heat Measurements. The decision to use capacitance thermometry meant that the addendum contribution of this thermometer to the

total heat capacity of the sample had to be known. This thermometer element is somewhat large (81 mg) and so could constitute a significant addendum, especially if the effect of an intense H-field were to seriously depress the sample's specific heat. Consequently, the heat capacity of a capacitor element was measured(14).

The specific heat method adopted was a version of the so-called "calibrated-wire" technique wherein the sample slowly ( $\leq 10$  mK/s) drifted in temperature from 20 K to 3 K in the presence of an intense H-field. The resulting T-t data record was computer-processed to yield specific heat data, and it was estimated that the uncertainty in the method was  $\sim \pm 7\%$ . The details of this method were prepared for publication(15), and this writeup is given in Appendix A1.

The specific heat sample drifted slowly by being connected to a 3 K reservoir through a thermal-link wire. This wire was calibrated by first drifting the sample in zero field, provided the thermal conductivity of the wire is H-field independent (see Appendix A1). Unfortunately, our large-specific-heat dielectric materials required the use of a copper link wire, and copper has a significant magneto-thermal conductivity effect. Therefore, the thermal conductivity of this copper wire in intense H-fields was measured(16), and a summary of these data is given in Appendix A1.

The specific heat measurement technique in intense fields used here required knowing the zero-field specific heat (see Appendix A1). In all

the H-field specific heat data reported below, these measurements were made on the same samples on which the zero-field measurements had been made.

Thermal Conductivity Measurements. A decision was made to measure thermal conductivity data in intense H-fields only on the dielectric materials with large zero-field thermal conductivities. This choice was dictated by magnet availability and by the belief that in the dielectrics with relatively small conductivities, phonon scattering was probably dominated by phenomena that are H-field independent.

Consequently, the "two heater, one thermometer" linear-heat-flow method discussed above was employed involving capacitance thermometry. These measurements were done using the same cryostat described above for the specific heat measurements.

#### V. SC-1 MATERIALS

As mentioned above, the SC-1 dielectrics are ceramics which sinter easily in the 1250-1350°C temperature range, so the pellets and bars needed for thermal properties' measurements were prepared by conventional ceramic methods. The densities obtained in the ceramic processing were  $\geq$  95% of theoretical density.

#### Zero-Field Measurements

Volumetric specific heat data on the original SC-1 materials are



shown plotted in Fig. 3 compared to Pb. Note the logarithmic scale in Fig. 3. This volumetric plot is the most demanding for making comparisons with Pb, because this metal has a very large density. The Fig. 3 data show the enormity of these specific heat maxima in the SC-1 materials; for example, the SC-1D ceramic has a maximum  $\approx 1.5 \text{ J cm}^{-3} \text{ K}^{-1}$  at 10.5 K (at room temperature, water has a specific heat of  $4.2 \text{ J cm}^{-3} \text{ K}^{-1}$ ).

As mentioned above, an NBS-sponsored program(7) had the goal of investigating ceramic modifications in SC-1C and SC-1D. These ceramics are two-phase, spinel + columbite materials, and the columbite phase mineralizes the spinel phase. It was found that the spinel:columbite ratio plays a significant role in determining the specific-heat properties of the SC-1C material(7), and these data are shown in Fig. 4. The 9:1, spinel:columbite ratio results in the largest specific heat values for SC-1C, as seen in Fig. 4. For SC-1D, the specific heat values were somewhat insensitive to the spinel:columbite ratio. Consequently, in all the data reported below, the SC-1C and SC-1D ceramics with 9:1 ratios were measured.

The zero-field thermal conductivity data on the SC-1 materials are shown in Fig. 5, where the arrows indicate the temperatures of the specific heat maxima. There appears to be some structure in the thermal conductivity of the SC-1C and SC-1D materials associated with the specific heat maxima (i.e., magnetic transitions), but the data in Fig. 5 for SC-1A and SC-1B vary smoothly and monotonically through the temperature region of the specific heat maxima.

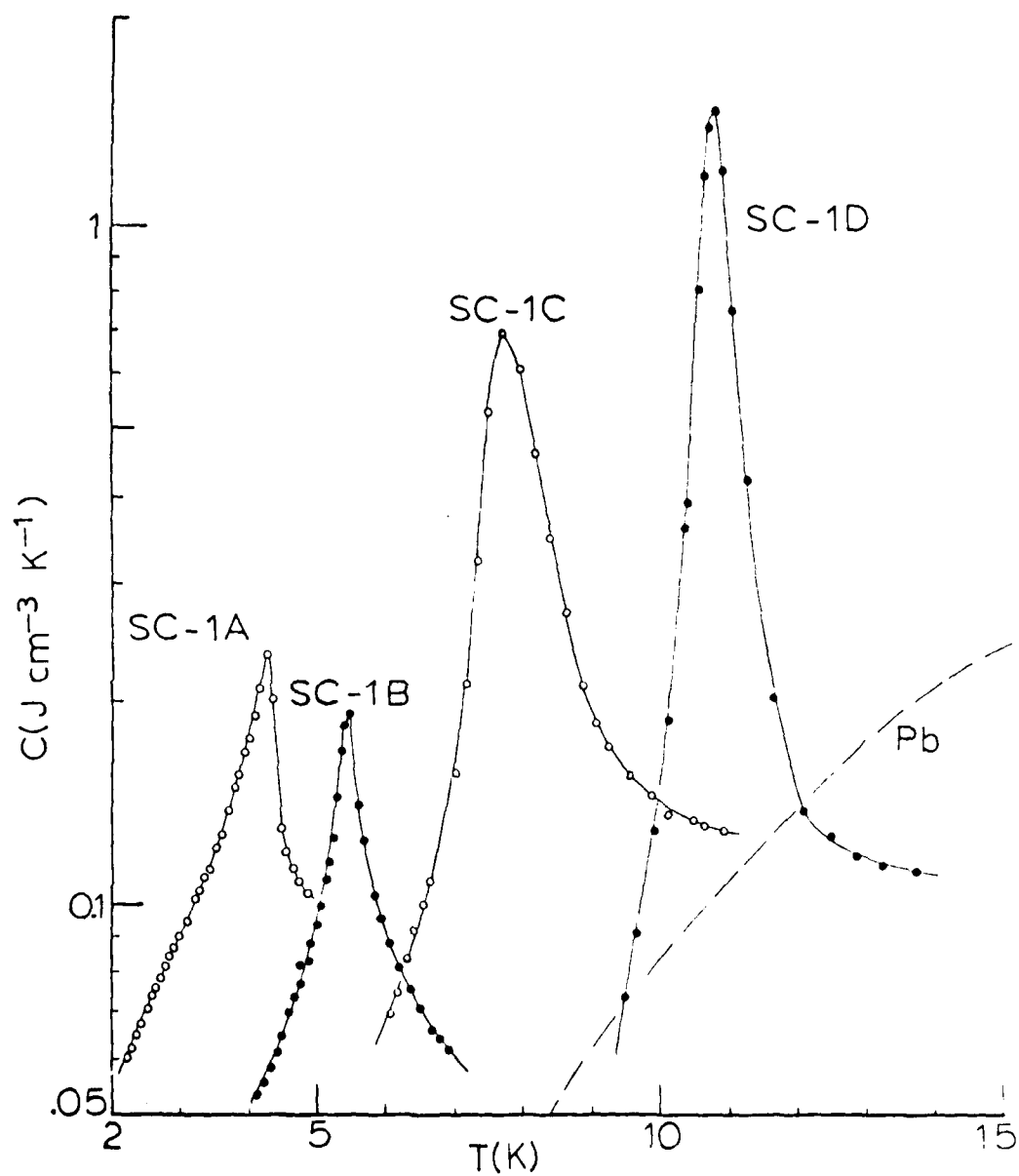


**Figure 3.** Volumetric specific heat data below 15 K for the SC-1 class of materials compared to Pb. The SC-1C material shown has a spinel:columbite ratio of 3:1 (see text).

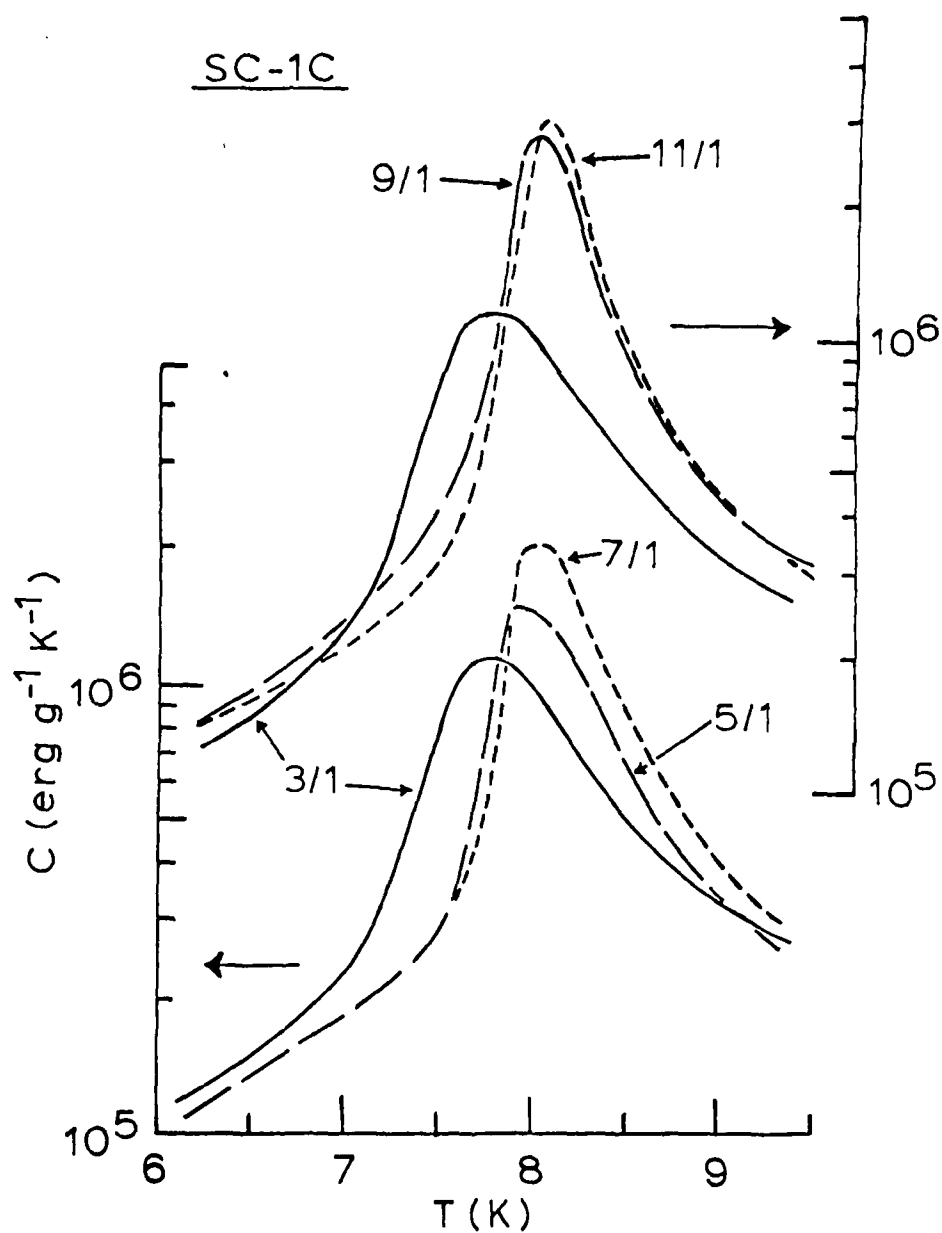
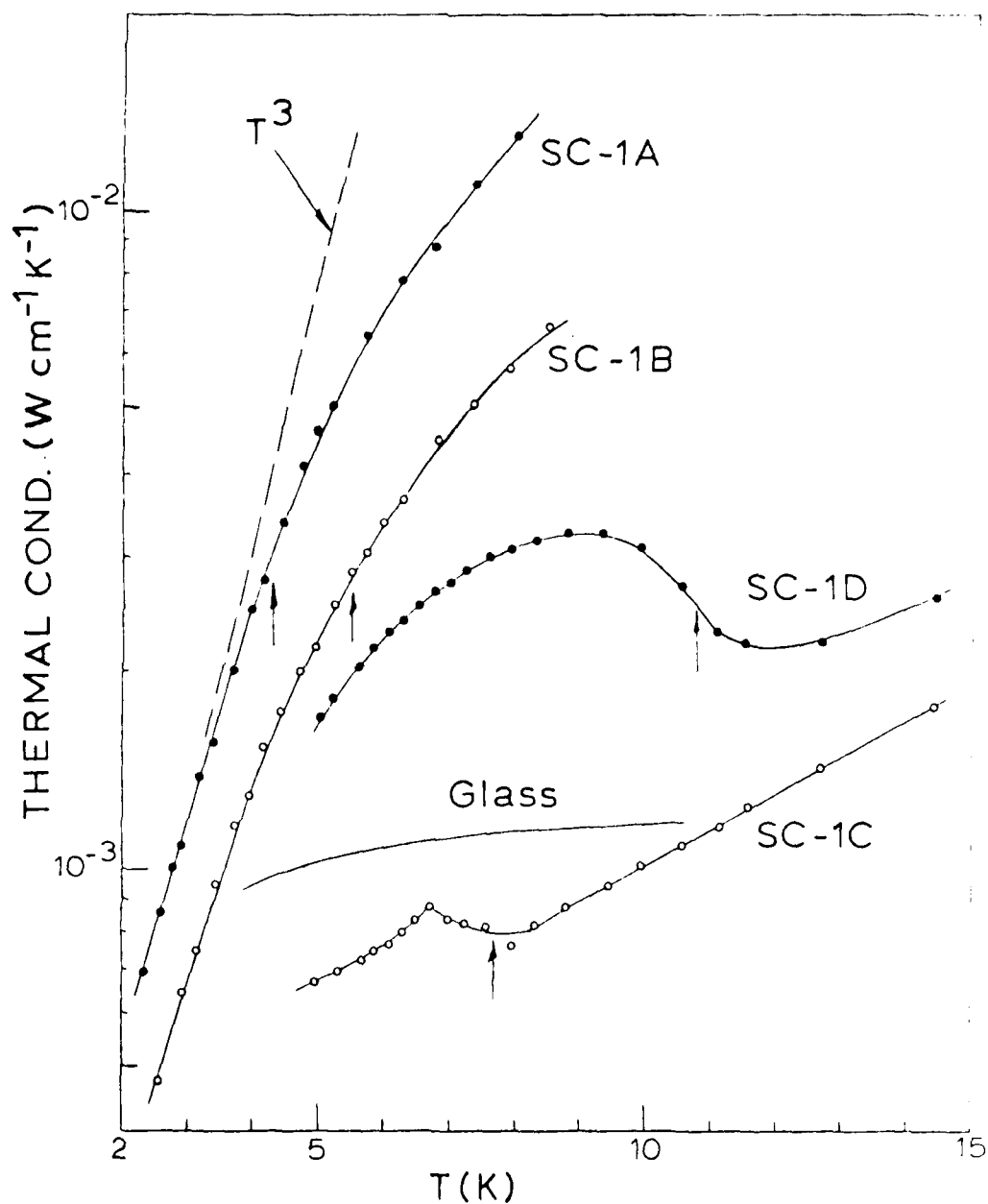


Figure 4. Dependence of the specific heat of SC-1C on the spinel:columbite ratio (from Ref. 7). The 9/1-ratio material was used exclusively in the studies here.



**Figure 5.** Thermal conductivity data below 15 K for the SC-1 class of materials. Arrows indicate the temperatures of the specific heat maxima (Fig. 3), and data for glass (vitreous silica) are shown for comparison.

The thermal conductivities of these SC-1 materials are generally quite small in the temperature range of interest (the conductivity of glass is shown for comparison in Fig. 5). The single-phase columbite materials, SC-1A and -1B, approach the  $T^3$  boundary-scattering limit as indicated by the dashed line in Fig. 5. The two-phase, spinel + columbite materials, SC-1C and -1D, have much lower thermal conductivities, as expected for two-phase ceramics.

#### Magnetic Field Measurements

A decision was made to measure only the specific heats of the SC-1 materials in intense magnetic fields. The reason for this was that the refractory nature of these ceramics virtually dictates that these materials be used as "fillers" in glasses, varnishes, etc., and the thermal conductivity of such composites is often not dominated by the thermal conductivity of the ceramic filler(17).

SC-1A. The specific heat data for SC-1A measured at 2.5, 5.0, and 7.5 T are shown in Fig. 6 compared to the zero-field specific heat data. The zero-field data have a maximum at 4.35 K, and the effect of a magnetic field is to lower this transition temperature and to suppress somewhat the height of the maximum. At 7.5 T, the transition temperature is  $\leq 3.9$  K.

The specific heat of SC-1A at 4.2 K is actually increased by fields up to to 5 T due to the lowering of the transition temperature, as seen in Fig. 6. However, above 5 T, the 4.2 K specific heat decreases rapidly

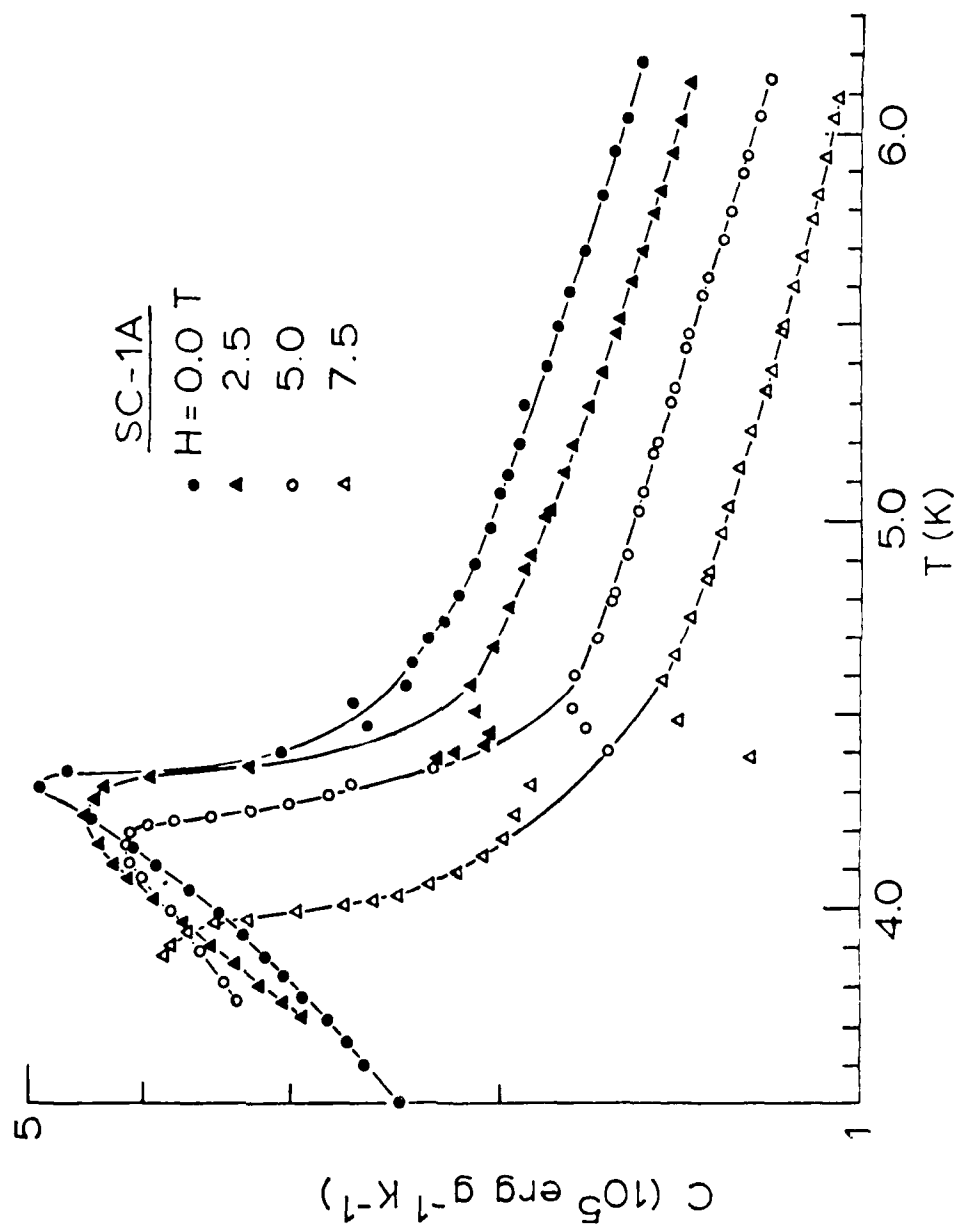


Figure 6. Magnetic-field dependence of the specific heat of SC-1A below 6.5 K at 2.5, 5.0, and 7.5 T. Zero-field data are shown for comparison.

with field and has dropped by  $\approx 50\%$  at 7.5 T.

The data in Fig. 6 were numerically integrated to obtain the enthalpy of SC-1A as a function of temperature relative to 3.87 K. In computing these enthalpy data from the data in Fig. 6, the lowest common temperature from the 0, 2.5, 5.0, and 7.5 specific-heat data sets was chosen as the reference temperature, in this case, 3.87 K. This same procedure was employed in all the enthalpy plots below. The density given in Table 1 was used to calculate these quantities on a volumetric basis, and these enthalpy data are shown in Fig. 7. Zero-field data are also shown for comparison.

The enthalpy corresponds to the heat energy stored in the material, and the Fig. 7 data reveal a disadvantage of SC-1A; namely, the enthalpy decreases with the magnetic field strength (note the logarithmic scale in Fig. 7). This is due to the lowering of the transition temperature with increasing magnetic field strength.

SC-1B. The H-field dependence of the specific heat of the SC-1B material is shown in Fig. 8 for H-fields up to 7.5 T. Although both SC-1A and SC-1B are single-phase, columbite-structure materials, an H-field depresses the specific heat of SC-1B more dramatically than that of SC-1A (Fig. 6). The dominant effect of an H-field is to "flatten" the specific heat of SC-1B, leaving some small structure at  $\approx 5.4$  K, the transition temperature in zero field.

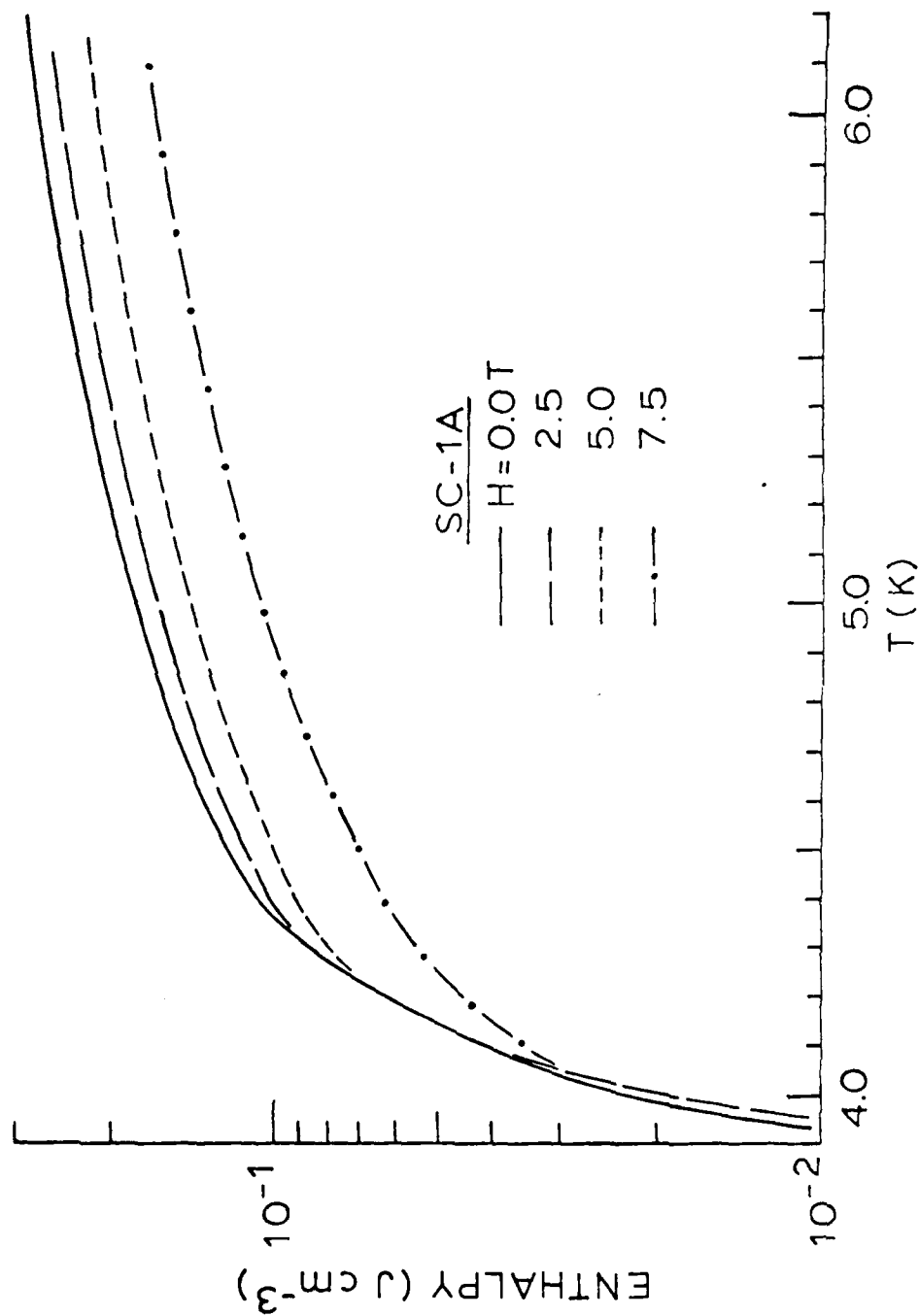


Figure 7. Volumetric enthalpy of SC-1A relative to 3.87 K at 0, 2.5, 5.0, and 7.5 T.



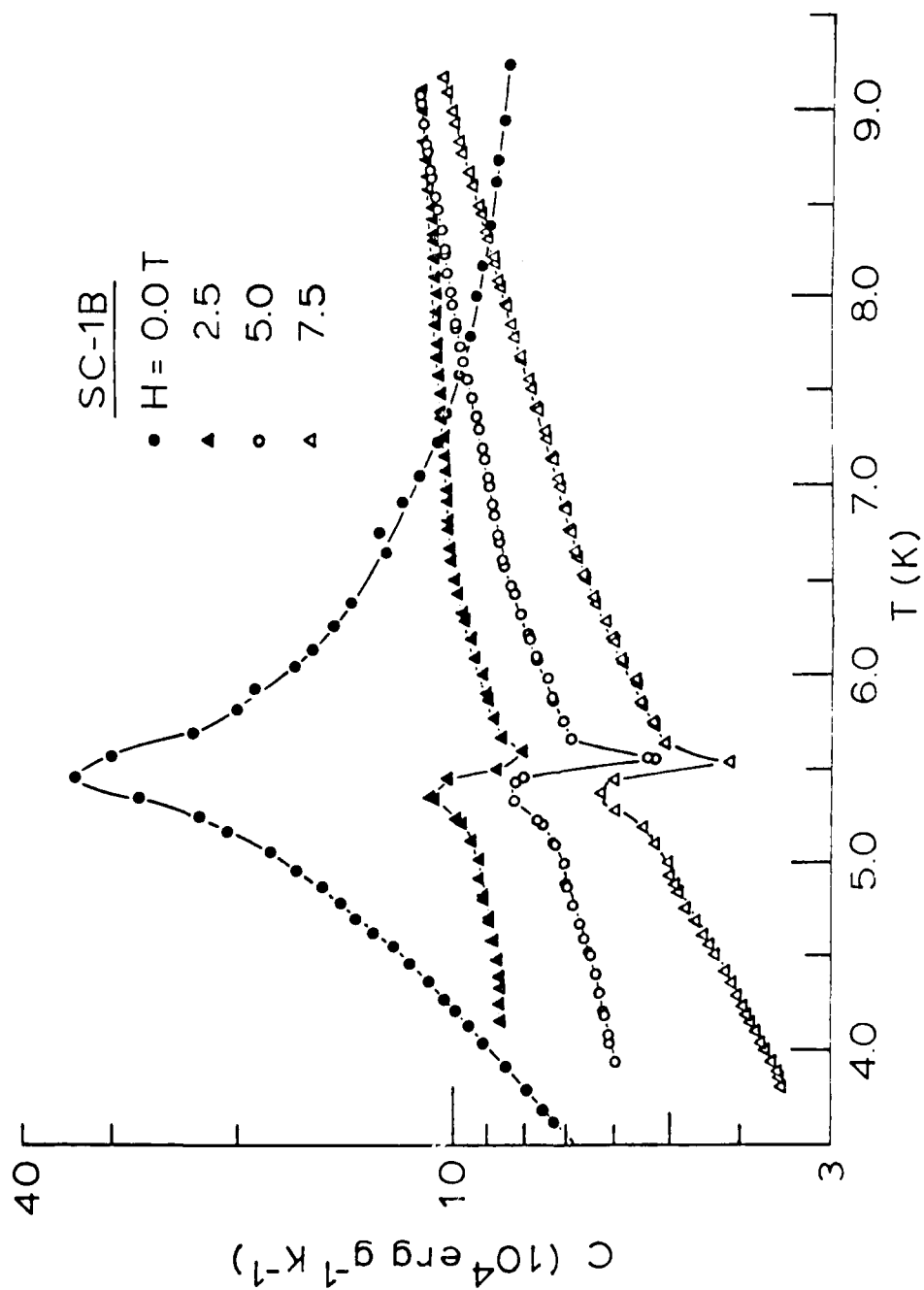


Figure 8. Magnetic-field dependence of the specific heat of SC-1B below 9.5 K at 2.5, 5.0, and 7.5 T. Zero-field data are shown for comparison.

The corresponding volumetric enthalpy data relative to 4.13 K, calculated from the specific heat data of Fig. 8, are shown in Fig. 9. The H-field suppression of the specific heat of SC-1B also results in a significant suppression of the enthalpy of this material.

SC-1C. The magnetic field dependence of the specific heat of this material was pursued more extensively than those of the other SC-1 materials for three reasons: (1) The specific heat maximum at 8 K, Fig. 3, suggested that this material might be the most attractive coating material of the SC-1 series, especially as the specific heat of the SC-1B material is depressed so markedly by an H-field (Fig. 8); (2) The initial measurements suggested that an H-field may actually increase the specific heat of SC-1C; and (3) It was found early on that a considerable amount of structure appeared in the specific heat of this material in an intense H-field (see Fig. 6 in Appendix A1).

The specific heat of SC-1C at 0, 7.5, and 15 T is shown in Fig. 10, and at these intense H-fields the specific heat displays a great deal of structure in the form of satellite peaks but is not depressed. This was one of the most significant findings in this study.

The specific heat data at 7.5, 10, 12.5, and 15 T are shown in Fig. 11 (note that the data scales are the same). Structure appears in the specific heat at 7.5 and 15 T but is noticeably missing at 10 and 12.5 T. We can only speculate about the level splittings responsible for these phenomena

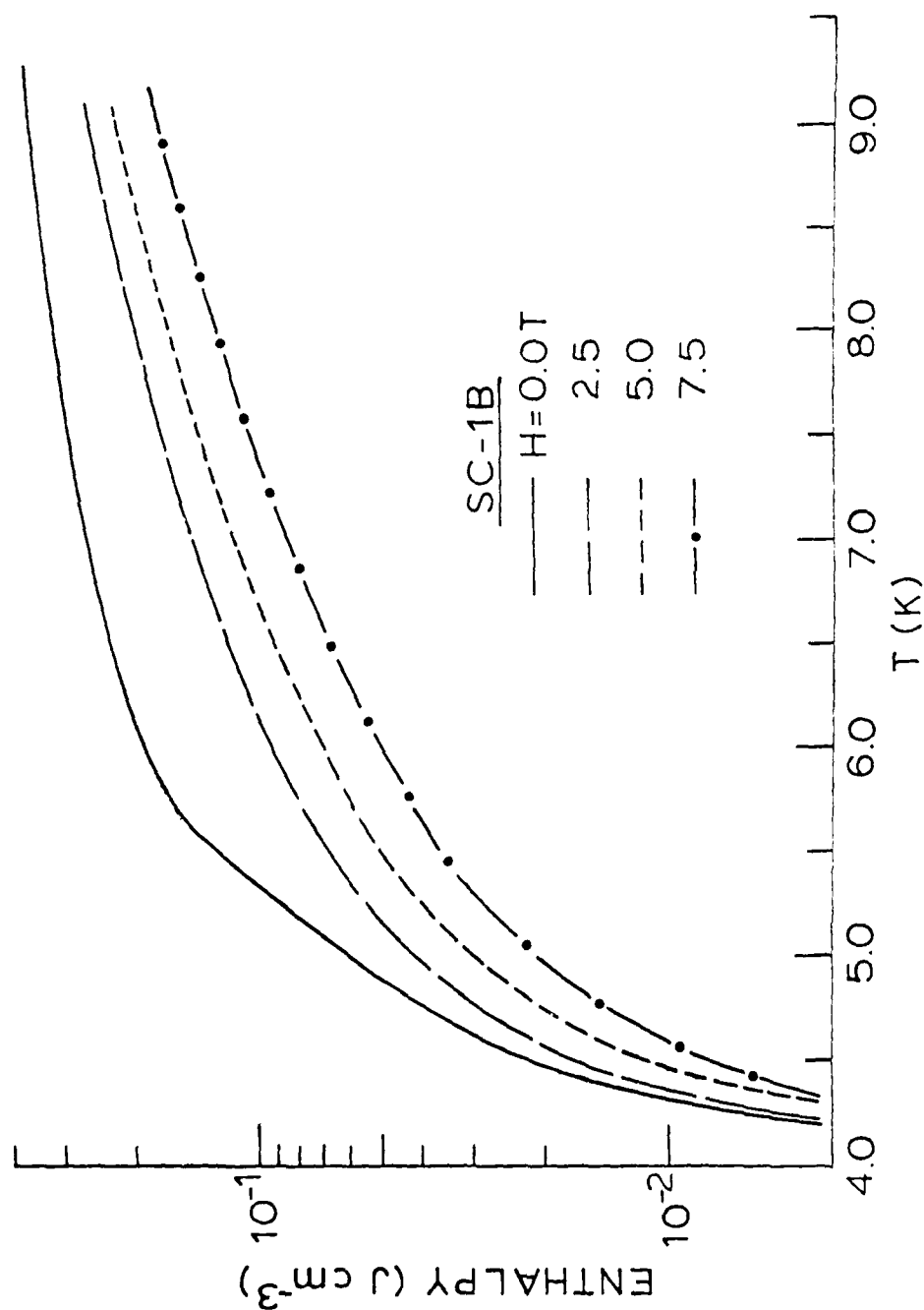


Figure 9. Volumetric enthalpy of SC-1B relative to 5.13 K at 0, 2.5, 5.0, and 7.5 T.

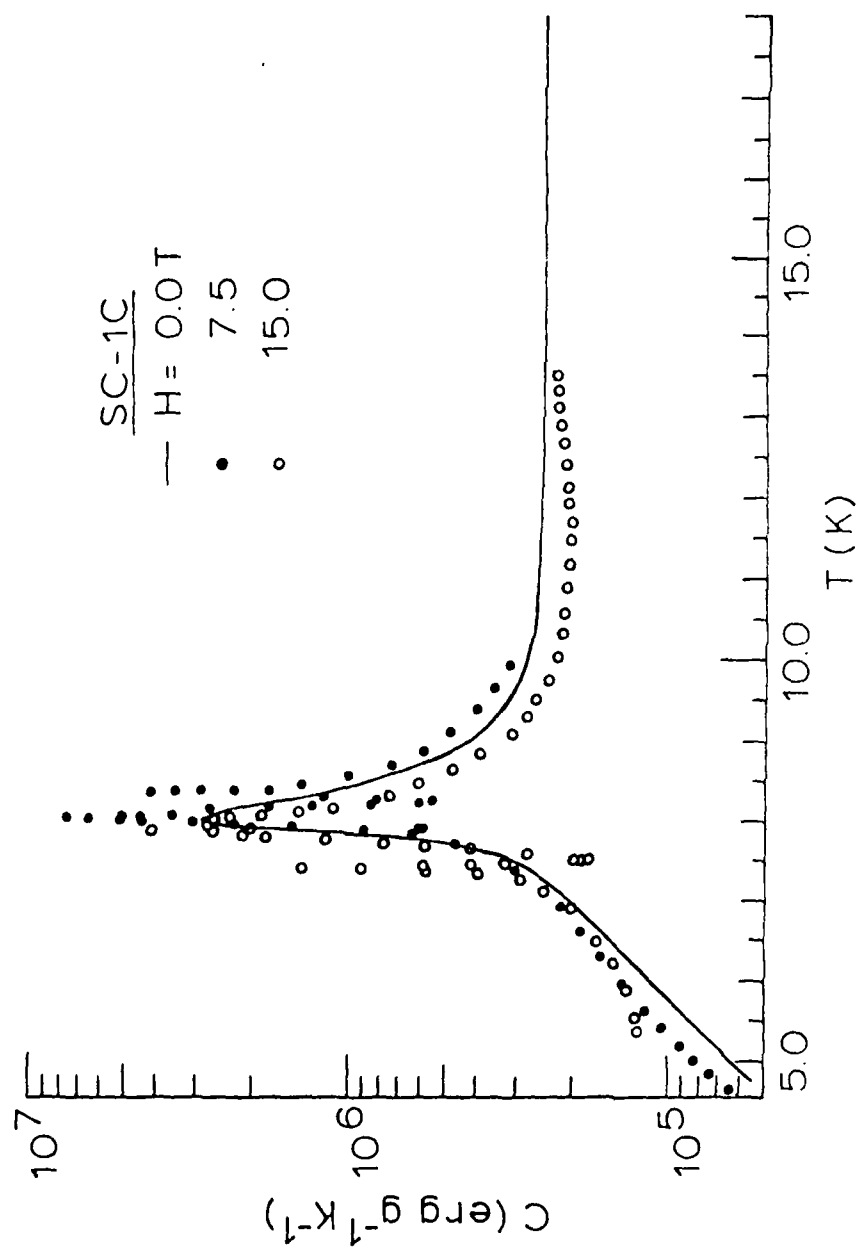
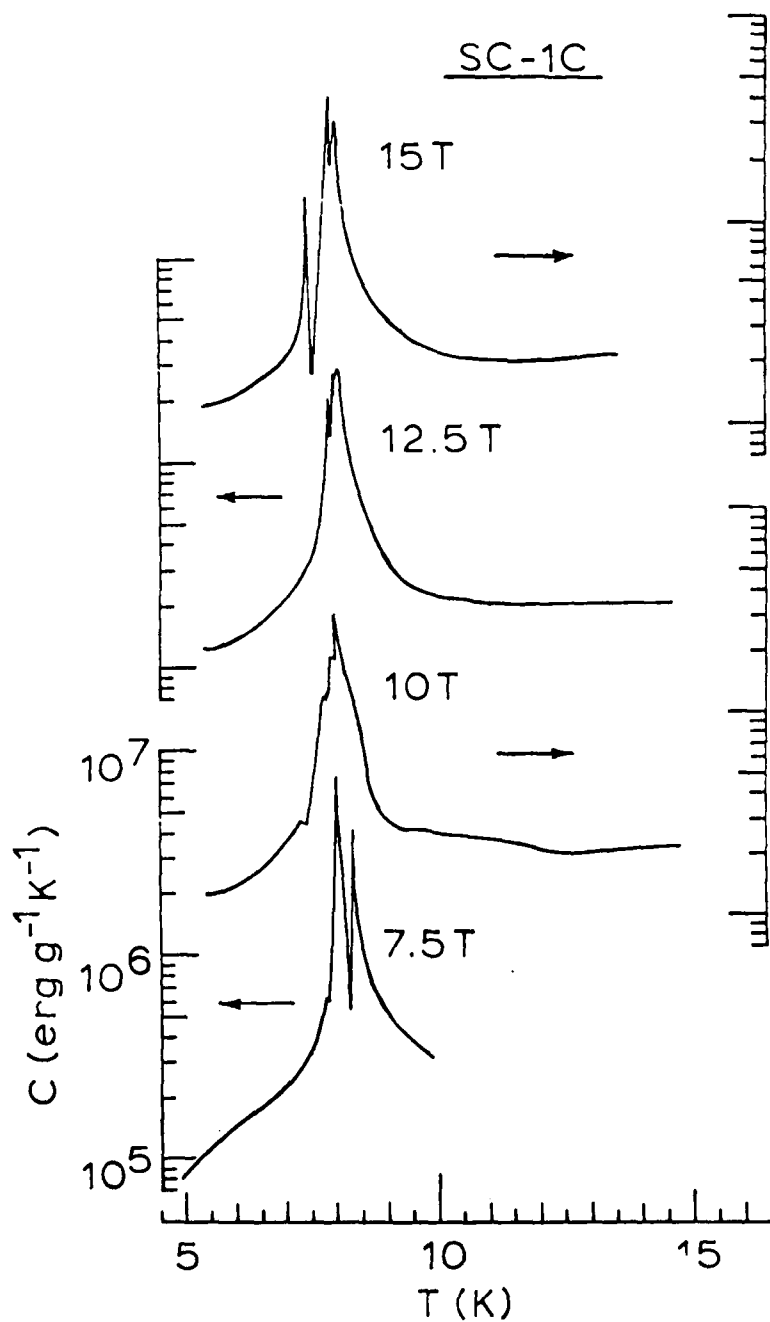


Figure 10. Magnetic-field dependence of the specific heat of SC-1C below 18 K at 7.5 and 15 T. Zero-field data are shown for comparison. Intense magnetic fields induce considerable structure in the specific heat in the neighborhood of the dominant 8 K peak.



**Figure 11.** Specific heat of SC-1C at 7.5, 10.0, 12.5, and 15.0 T. Note the structure at 7.5 and 15.0 T.

at this time. These results are not believed to be dependent upon the experimental method because the central, dominant peak at 8 K is reproduced almost identically at all H-fields.

The specific heat data in Fig. 10 were numerically integrated using the density of SC-1C in Table 1 to obtain the volumetric enthalpy at 7.5 and 15 T, relative to 4.91 K, and these data are shown in Fig. 12. These data show a remarkable experimental result: The enthalpy is increased by these intense H-fields, and these results appear to be much larger than the experimental uncertainty in the original specific heat data (note the logarithmic scales). These results, which are of considerable thermodynamic significance, are due to the appearance of the satellite structure in the specific heat of SC-1C at intense H-field levels (Recall that the zero-field specific heat of Fig. 10 was measured on the same sample, and these zero-field data enter the analyses of the H-field data, as explained in Appendix A1.).

SC-1D. Specific heat data measured on SC-1D at 5, 7.5, and 15 T are shown in Fig. 13, compared to the zero-field specific heat. As seen above with the columbite structure materials SC-1A and -1B, there is a considerable difference also between the spinel + columbite materials SC-1C and -1D: The effect of intense H-fields on the specific heat of SC-1D is to depress somewhat the central peak at 10.5 K, but there is no indication of the satellite structure that appears in the SC-1C data (compare Figs. 10 and 13). The H-field data on SC-1C and -1D were measured under identical

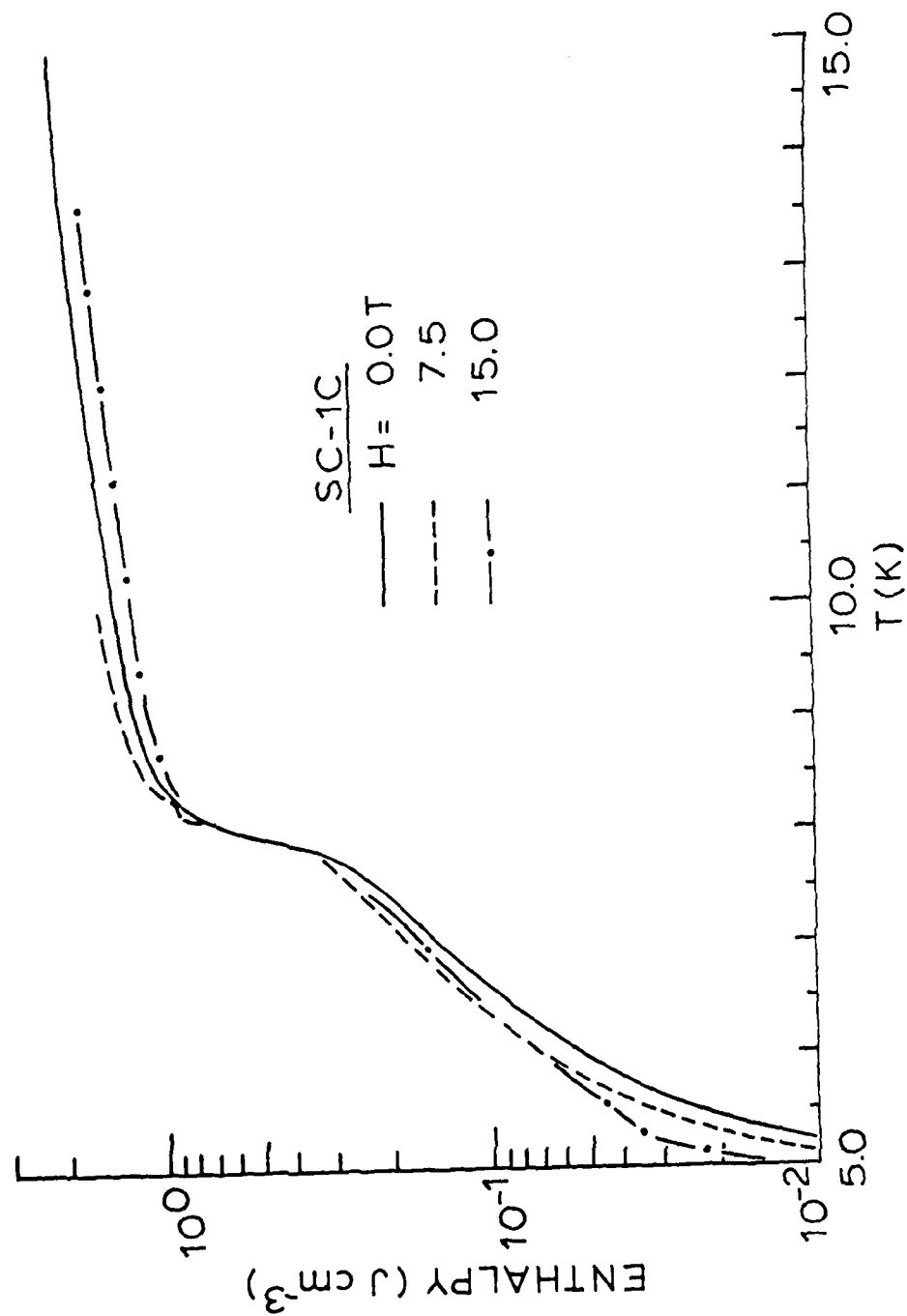


Figure 12. Volumetric enthalpy of SC-1C relative to 4.91 K at 0, 7.5, and 15.0 T. At temperatures below about 7.5 K, the enthalpy is increased by intense magnetic fields.

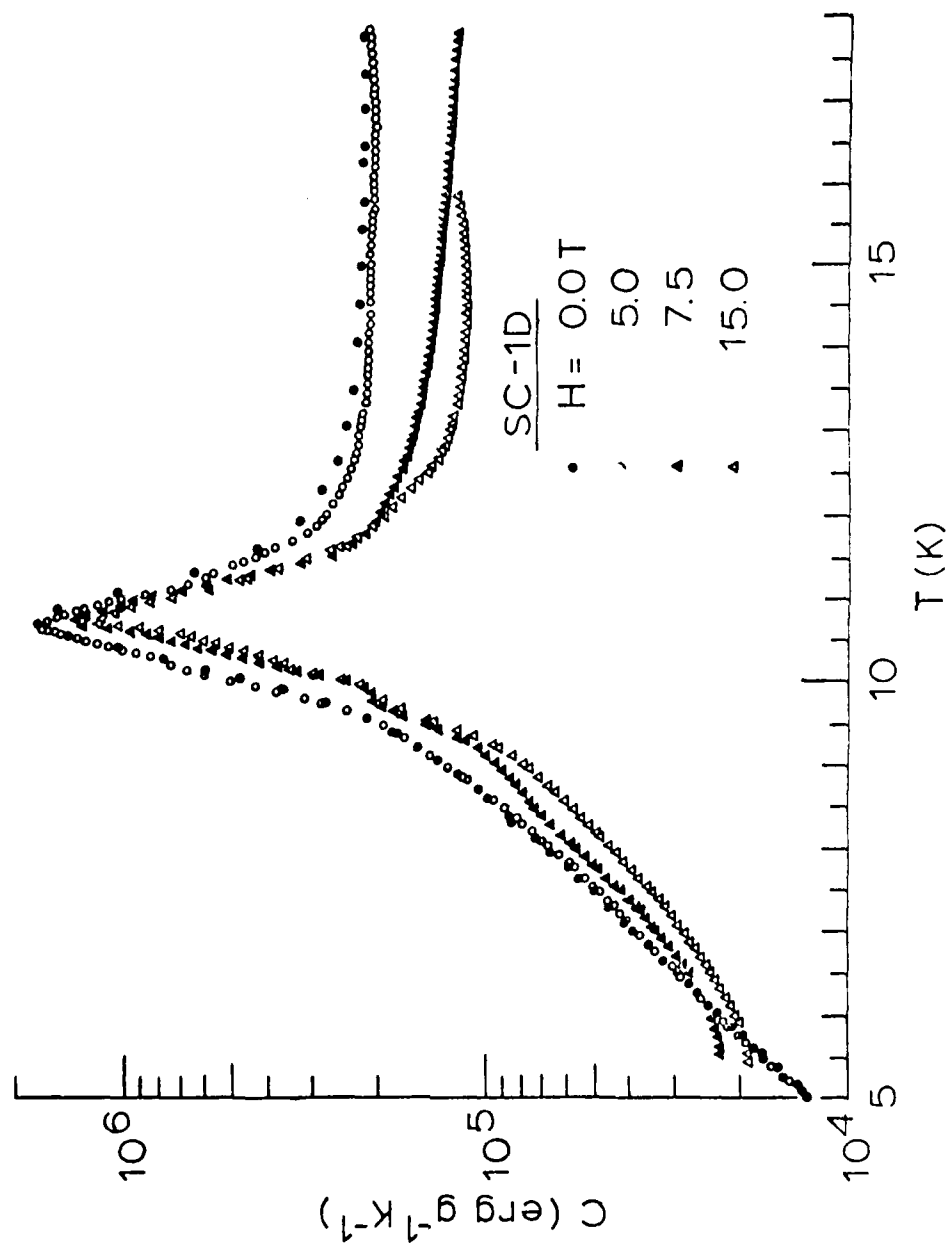


Figure 13. Magnetic-field dependence of the specific heat of SC-1D below 19 K at 5.0, 7.5, and 15.0 T. Zero-field data are shown for comparison.



conditions, which lends additional support to the satellite structure in the specific heat data of SC-1C.

The specific heat data for SC-1D in Fig. 13 in the neighborhood of the dominant peak are apparently H-field independent between 0 and 5 T and again between 7.5 and 15 T, as there are basically only two specific heat curves in Fig. 13 in the neighborhood of the peak. At 7.5 and 15 T, there is an increase in the specific heat with decreasing temperature below ~6 K. This effect is also evident in SC-1C (Fig. 10), but for this latter material the effect occurs only at 15 T and for temperatures below ~5.5 K. At these intense H-field levels, a second specific heat anomaly is apparently induced in the spinel phases of SC-1C and -1D at temperatures below 4 K.

The Fig. 13 data were numerically integrated to obtain volumetric enthalpy data relative to 4.71 K, and these data are shown in Fig. 14. The enthalpy data are H-field independent between 0 and 5 T, as implied by the specific heat data of Fig. 13. However, at 7.5 T, the enthalpy is larger than the zero-field enthalpy for temperatures below 8 K, and this is due to the specific heat increase shown in Fig. 13 below 6 K. At 15 T, this effect is less pronounced than at 7.5 T.

We can summarize these H-field data on the SC-1 class of materials by considering the enthalpy of a hypothetical coating at various temperatures above 4.2 K. This is equivalent to asking what heat energy would be required to raise the temperature of the coating above 4.2 K, and we select

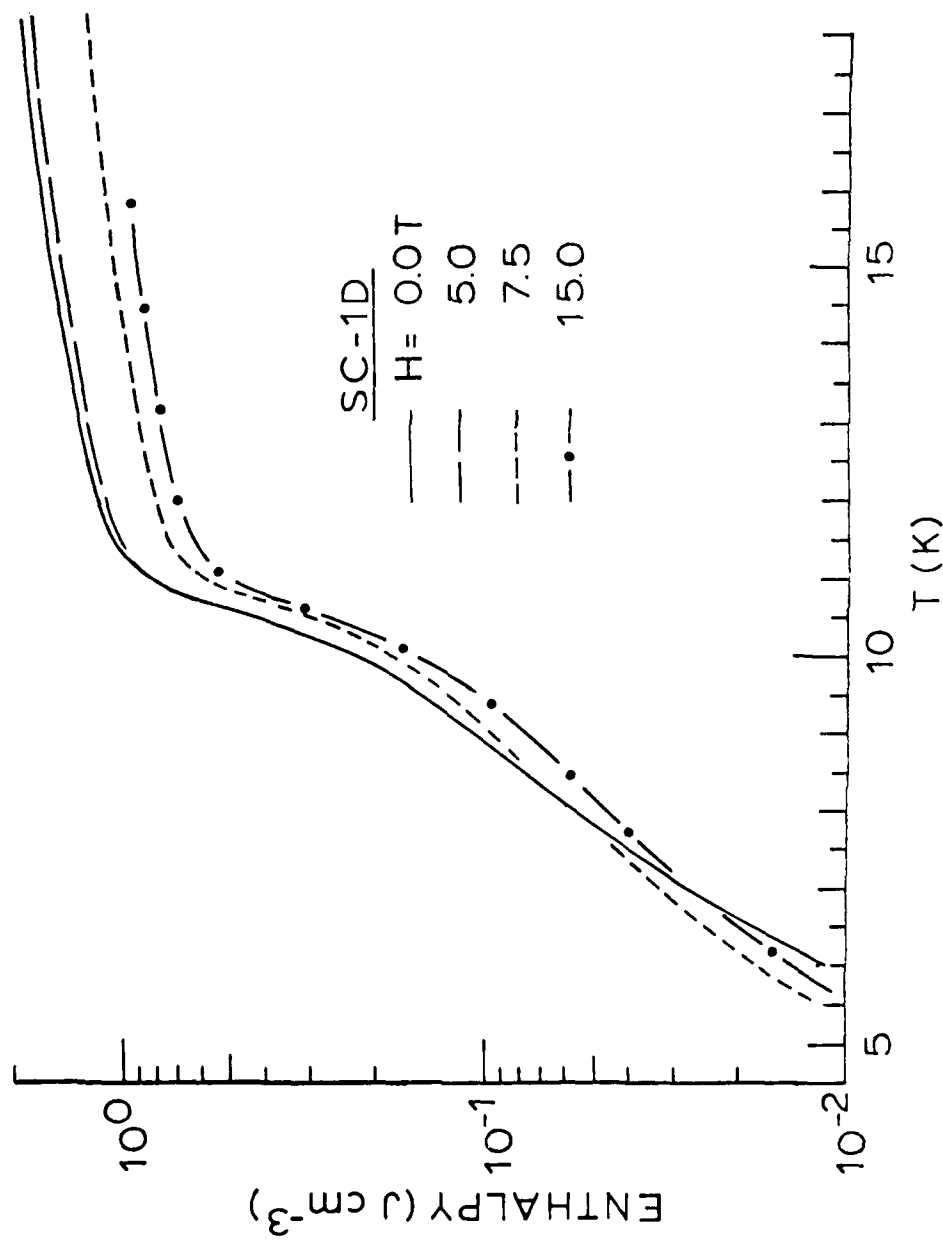


Figure 14. Volumetric enthalpy of SC-1D relative to 4.71 K at 0, 5.0, 7.5, and 15.0 T. At the two highest magnetic-field levels, the enthalpy is increased over the zero-field enthalpy for temperatures below 7 K.

H = 7.5 T. These summary data are given in Table 2.

Table 2

Volumetric Enthalpies of the SC-1 Materials  
Relative to 4.2 K at 7.5 T (in units of  $\text{mJ}/\text{cm}^3$ )

T(K)	SC-1A	SC-1B	SC-1C	SC-1D
5	60.94	19.75	28.45	9.69
6	121.1	49.38	94.12	22.77
7	--	84.97	201.8	38.27
8	--	127.9	590.0	62.24
9	--	179.0	1374.3	102.6
10	--	--	1597.7	187.4

The data for SC-1A and SC-1B in Table 2 are limited to temperatures below 6 and 9 K, respectively, because the specific heat data for these materials at 7.5 T did not extend to higher temperatures.

#### VI. SC-2 MATERIALS

These materials are inorganic, simple-cubic structures with melting points at  $\approx 450^\circ\text{C}$ . The test samples used here were single crystals supplied by Harshaw Chemical Co., Solon, Ohio. These crystals were cut into appropriate shapes using a diamond saw, and after the cutting operations, the samples were annealed overnight at  $100\text{--}150^\circ\text{C}$ .

#### Zero-Field Measurements

The zero-field specific heat data for SC-2A, -2B, and -2C are shown in

Figure 15. Also shown, for convenience, are the zero-field data for SC-3A and -3B. Neither the SC-2 nor the SC-3 materials contain paramagnetic ions, and the data in Fig. 15 are plotted (volumetrically) as  $CT^{-3}$  to illustrate the strongly non-Debye nature of the SC-2 specific heat data. That is, for a Debye solid,  $CT^{-3} = \text{constant}$  at these low temperatures, and, as seen in Fig. 15, the SC-3 materials are very nearly Debye-like. However, the SC-2 materials have large, broad maxima in  $CT^{-3}$ , and this means that in these ferroelectric-type materials there are low-lying vibrational modes which contribute to the specific heat at low temperatures and give rise to these  $CT^{-3}$  maxima. These low-lying modes in ferroelectrics have been universally found(4) to follow a single-Einstein-oscillator model,

$$C = C_D(\theta_D/T) + 3Rrx^2e^x/(e^x-1)^2, \quad x = \theta_E/T, \quad (1)$$

where  $C_D$  is the Debye function ( $C_D \propto T^3$  for  $T \ll \theta_D$ ),  $\theta_D$  is the Debye temperature,  $\theta_E$  is the Einstein temperature, and  $r$  is the number of Einstein oscillators per formula weight. It is easily shown from Eq.(1) that  $C/T^3$  has a maximum at a temperature  $T_{\text{max}} \cong 0.23 \theta_E$ , and it is interesting to observe in Fig. 15 that both the SC-2 and the SC-3 materials approach about the same Debye limit,  $(C/T^3)_0 \cong 0.05 \text{ mJ cm}^{-3} \text{ K}^{-4}$  at the lowest temperatures. However, due to the low-lying mode in SC-2B,  $(C/T^3)_{\text{max}}$  is about four times larger than the Debye background, and this maximum occurs in the very useful temperature range of  $\sim 4$  to 7 K. These findings in the SC-2 class of materials were the original impetus for proposing them for dielectric coatings.

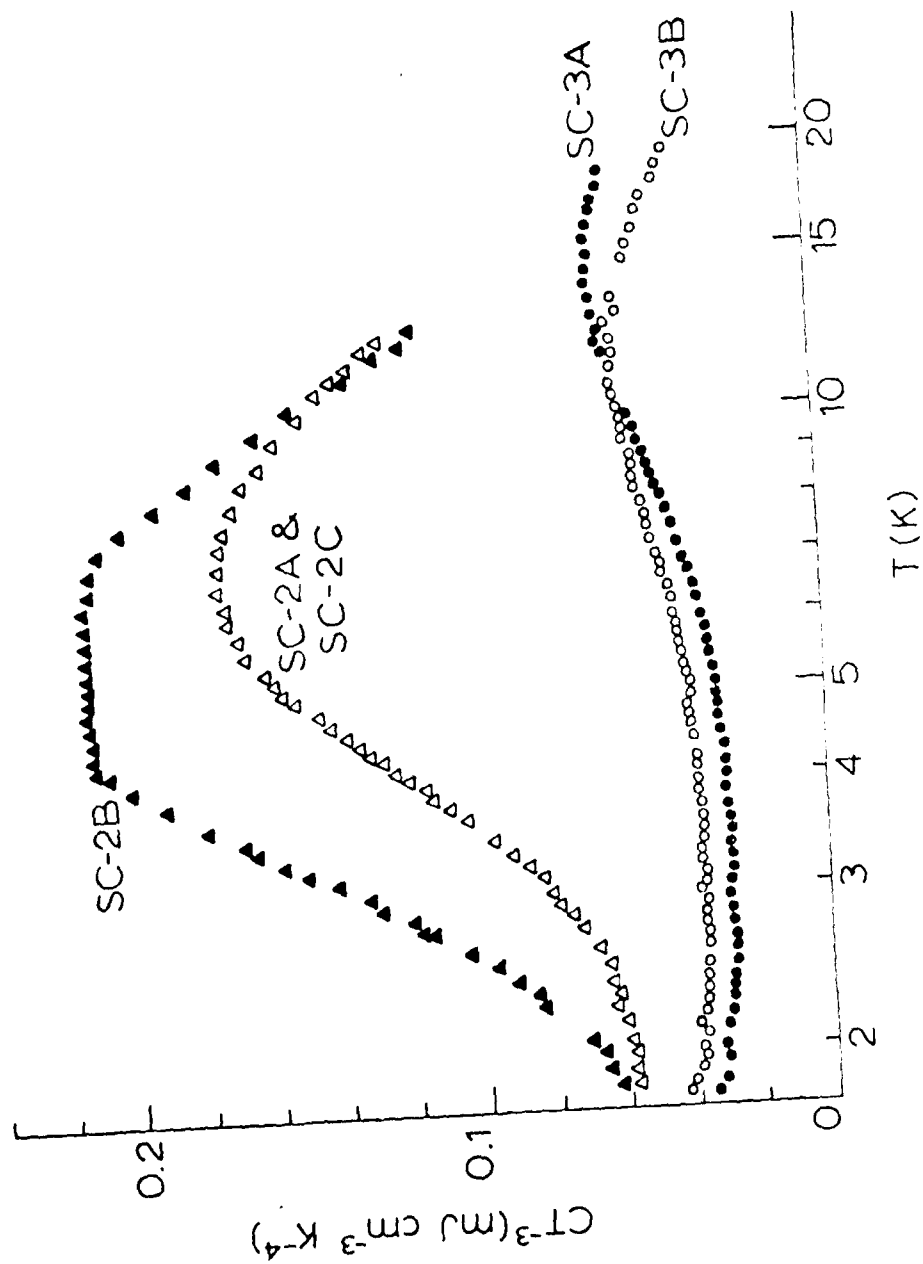


Figure 15. Volumetric specific heat data for the SC-2 and SC-3 materials plotted as  $CT^3$  to emphasize the non-Fermi, "ferroelectric" modes in the SC-2 materials (see text).

The first thermal-conductivity measurements on the SC-2 materials were made on samples with relatively large cross-sectional areas ( $\sim 0.2 \text{ cm}^2$ ). These data are shown in Fig. 16, and two features are apparent: Thermal conductivity (K) values in the "metallic" range are present (i.e.,  $\geq 1 \text{ W cm}^{-1} \text{ K}^{-1}$ ), and all three materials display the  $K \propto T^3$  boundary scattering limit at the lowest temperatures (shown by the dashed lines in Fig. 16).

The  $K \propto T^3$  boundary scattering limit comes about as follows. Elementary theory predicts that

$$K \cong (1/3)Cv\lambda \quad (2)$$

where C is the volumetric specific heat, v is the average sound velocity, and  $\lambda$  is the phonon mean-free path (in the dominant phonon approximation). The mean-free path becomes very large at low temperatures, and when  $\lambda$  becomes equal to the sample dimension (or some other characteristic dimension within the sample, see below), then, since  $\lambda$  cannot increase further,  $K \propto C \propto T^3$  for a Debye solid. Thus,  $K \propto T^3$  signals phonon scattering from some characteristic geometric boundary.

This discussion reveals that boundary scattering is a very important consideration in designing a dielectric coating, since in principle the coating thinness could seriously reduce the thermal conductivity.

For the above reasons, thermal conductivity measurements were made on bundles of thin rods of SC-2A and SC-2B, and these data are shown in

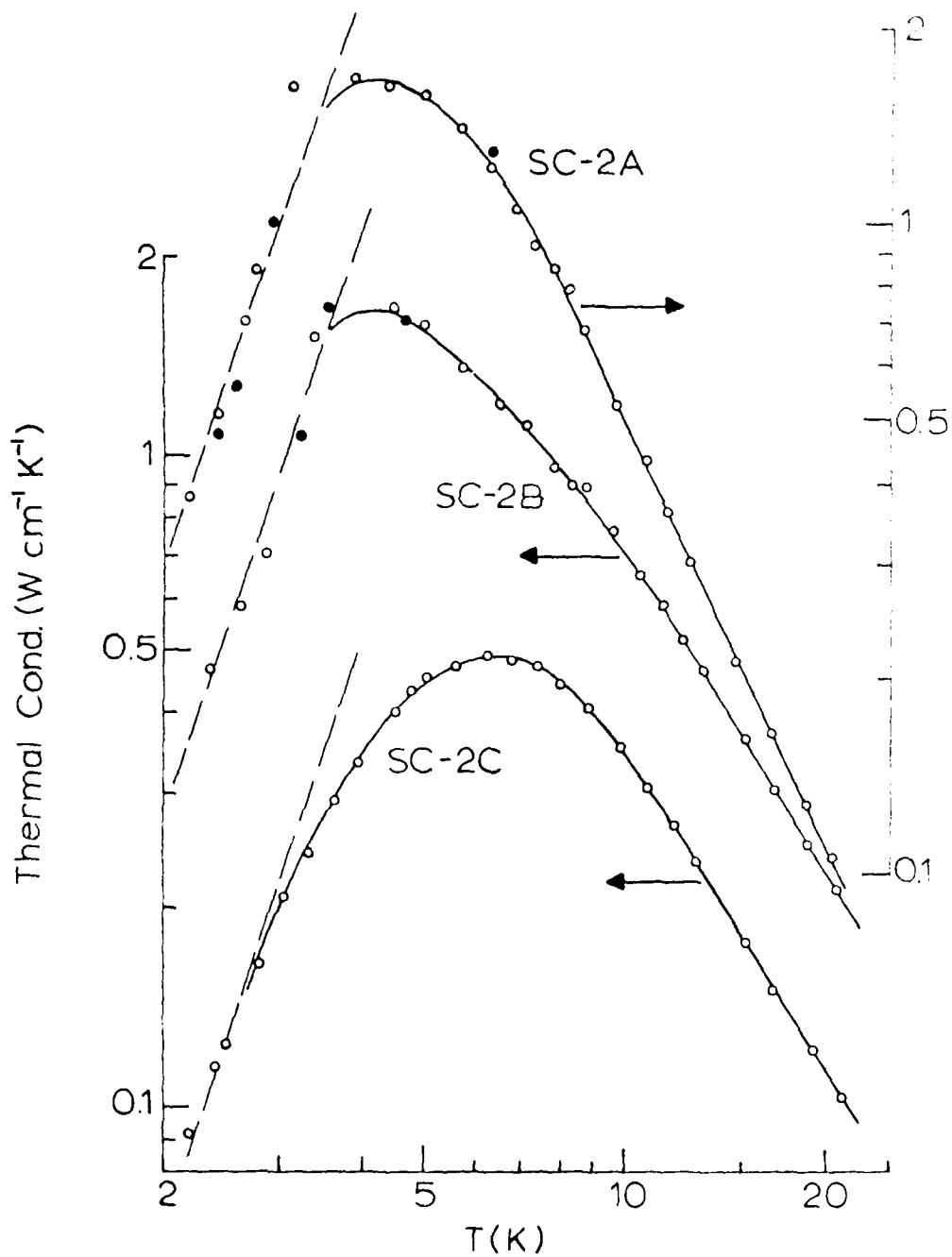


Figure 16. Thermal conductivities of the SC-2 materials showing near-metallic thermal-conductivity values with maxima near 5 K.

Figs. 17 and 18, respectively. Thin-rod measurements were not made on SC-2C because, from Fig. 16, this material has a much smaller thermal conductivity than either SC-2A or -2B. Also shown for comparison in Figs. 17 and 18 are thermal conductivity data for commercial copper(18) and for the bulk samples of SC-2A and -2B from Fig. 16.

The data in Figs. 17 and 18 reveal that the thermal conductivity is not significantly degraded in going to thin samples and approximately the same  $T^3$  limit is reached. These data clearly demonstrate that boundary scattering is occurring from some entity within the material whose characteristic dimension is considerably smaller than the sample dimensions involved in the measurements.

Pursuing this further, we can make use of the thermal data in Figs. 15-18 to estimate the characteristic dimensions responsible for boundary scattering in these SC-2 materials. Referring to Eq.(2), a knowledge of the sound velocity is required for the analysis, and we shall adopt  $v = 2 \times 10^5$  cm/s as a representative value for cubic structures such as the SC-2 materials (also, sound velocities in a wide range of solids cluster about this value).

The specific heat data in Fig. 15 show strong, non-Debye contributions for the SC-2 materials, as discussed above, and we have to decide whether these contributions should be included in  $C$  in Eq.(2). That is, do these low-lying modes carry heat and therefore contribute to  $K$ ? These modes are



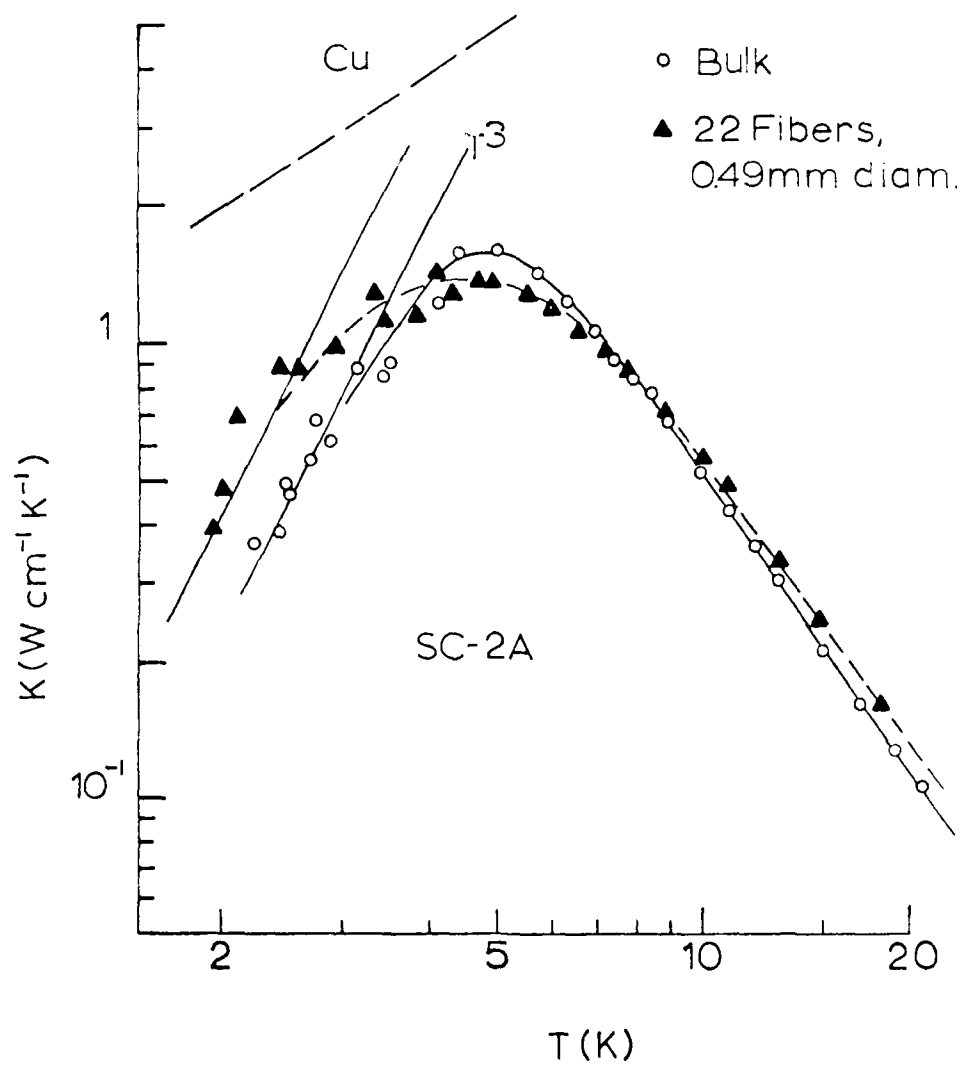
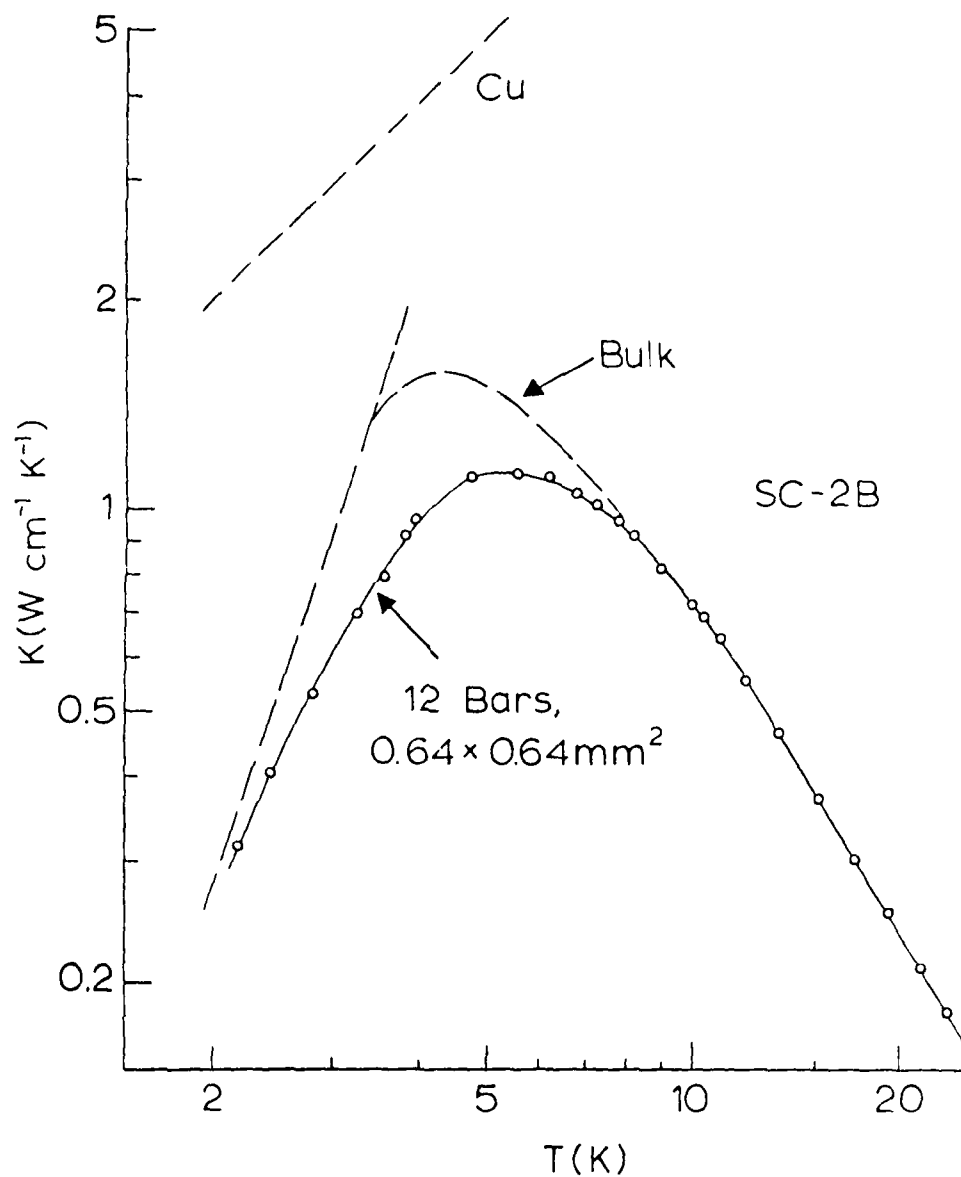


Figure 17. Thermal conductivity data measured on thin (0.49 mm) fibers of Sc-2A. Shown for comparison are data on bulk SC-2A and on commercial copper.



**Figure 18.** Thermal conductivity data measured on thin (0.64 mm) bars of SC-2B. Shown for comparison are data on bulk SC-2B and on commercial copper.

electric-field-independent(19), implying acoustic modes, and we will here assume that they do carry heat. This assumption, if incorrect, will not seriously affect the results below because the non-Debye modes are mostly frozen out in that temperature range where  $T^3$  boundary scattering is clearly defined.

The procedure is straightforward for applying Eq.(2): At the lowest temperature in the  $K \propto T^3$  limit,  $C$  is taken from Fig. 15,  $K$  is taken from Figs. 16-18, and Eq.(2) is solved for  $\lambda_b$ , the limiting mean free path. These results are summarized in Table 3.

Table 3

Geometric Phonon Scattering Limits		
Material	Smallest Sample Dimension(cm)	$\lambda_b$ (cm)
SC-2A	0.145 (Fig. 20)	0.018
-2A	0.048 (Fig. 21)	0.018
-2B	0.155 (Fig. 20)	0.009
-2B	0.064 (Fig. 22)	0.009
-2C	0.169 (Fig. 20)	0.002

It is interesting to observe that the  $\lambda_b$ -values in Table 3 are much smaller than the sample dimensions, and these results imply that the "metallic" thermal conductivities shown in Fig. 16 should be retained by these SC-2 materials for dielectric-coating thicknesses greater than, or equal to, these characteristic  $\lambda_b$ -values.

### Magnetic-Field Measurements

Although the SC-2 materials contain no paramagnetic ions ( $\text{Fe}^{3+}$ ,  $\text{Ni}^{2+}$ , etc.), it was not considered safe to assume that there would be no effects on the thermal properties in intense magnetic fields. Therefore, it was decided to investigate the effects of intense magnetic fields on these SC-2 materials.

The specific heat data for SC-2A at 2.5 and 5 T are shown in Fig. 19, compared to the zero-field data. These data indicate that up to 5 T, there is no apparent H-field dependence of the specific heat of SC-2A, at least within the uncertainty of the measurement ( $\leq \pm 10\%$ ). The corresponding volumetric enthalpy data relative to 4.40 K for SC-2A are shown in Fig. 20 for 0 and 5 T.

The specific heat data for SC-2B at 2.5 and 5 T are shown in Fig. 21, compared to the zero-field specific heat. In contrast to SC-2A, there appears to be an H-field dependence to the specific heat of SC-2B, the effect being to uniformly suppress the entire curve as seen in Fig. 21. The effect appears to be real because the 5 T curve is below the 2.5 T curve; however, the effect is small:  $C_H/C_0 \geq 90\%$  at 2.5 T, and  $C_H/C_0 \geq 86\%$  at 5 T.

The volumetric enthalpy data relative to 4.29 K for SC-2B are shown in Fig. 22 for 0 and 5 T.

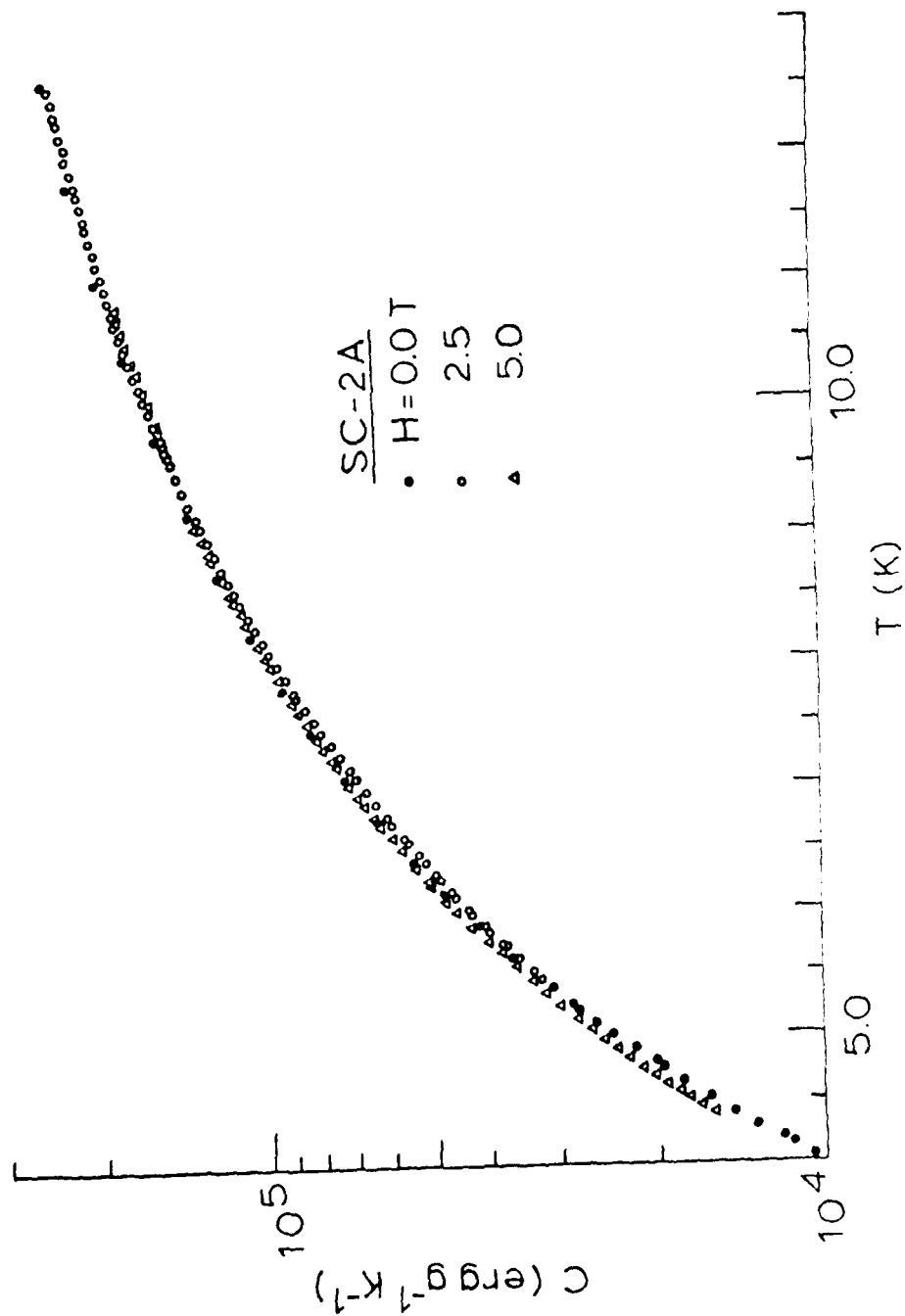


Figure 19. Magnetic-field dependence of the specific heat of SC-2A below 13 K at 2.5 and 5.0 T. Zero-field specific heat data are shown for comparison.

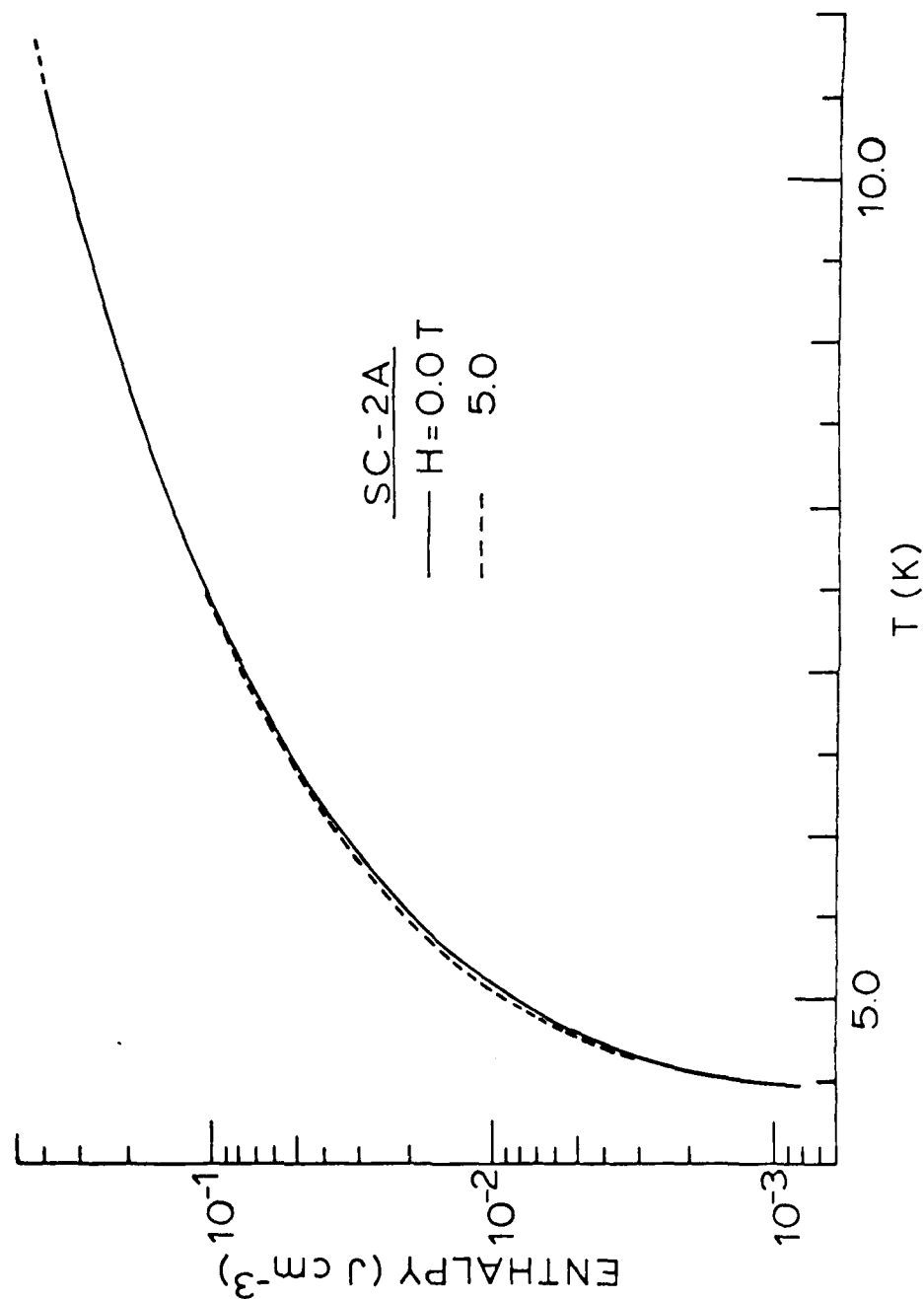


Figure 20. Volumetric enthalpy of SC-2A relative to 4.40 K at 0 and 5 T. The enthalpy of SC-2A is unaffected by intense magnetic fields.

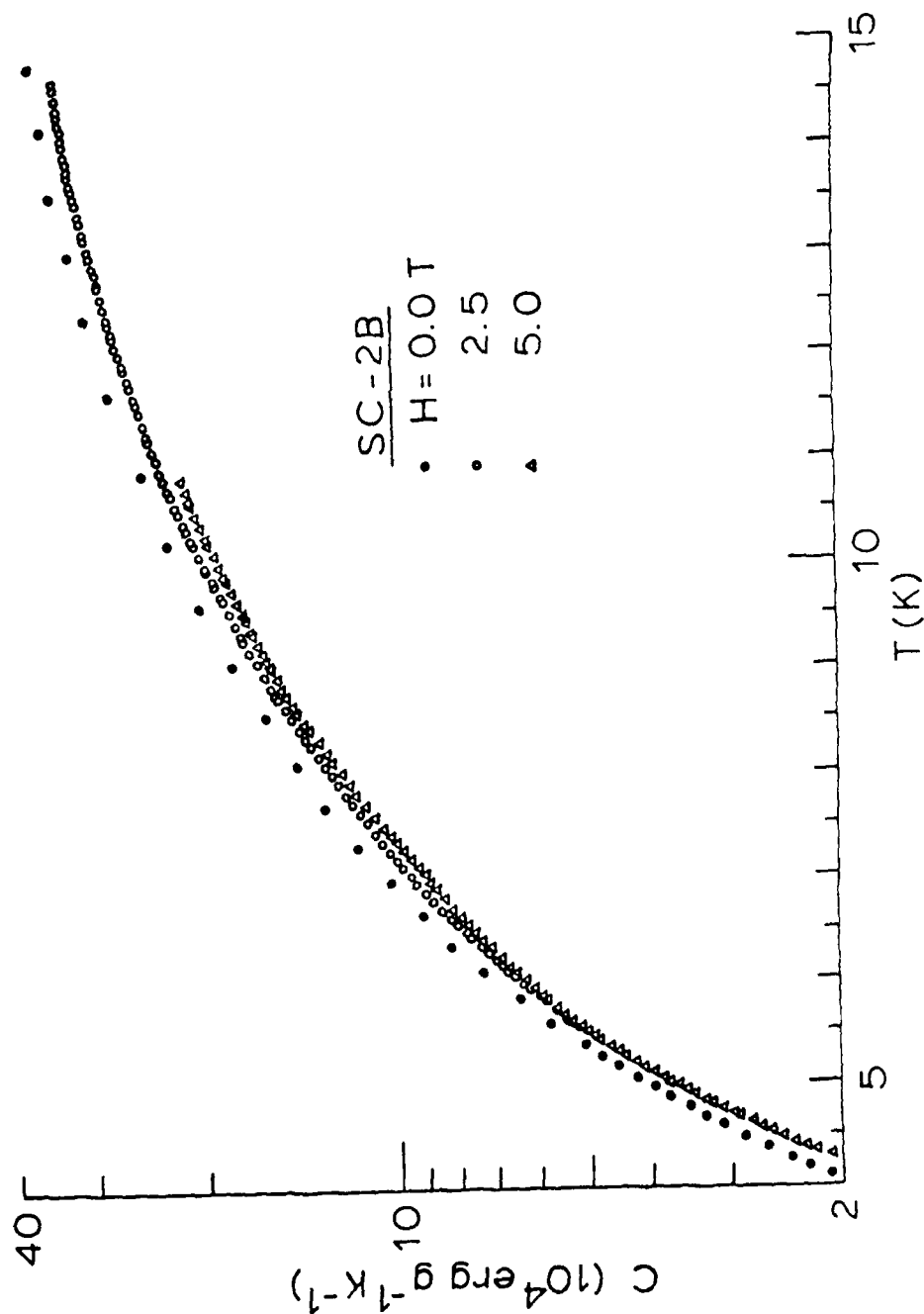


Figure 21. Magnetic-field dependence of the specific heat of SC-2B below 15 K at 2.5 and 5.0 T. Zero-field specific heat data are shown for comparison.

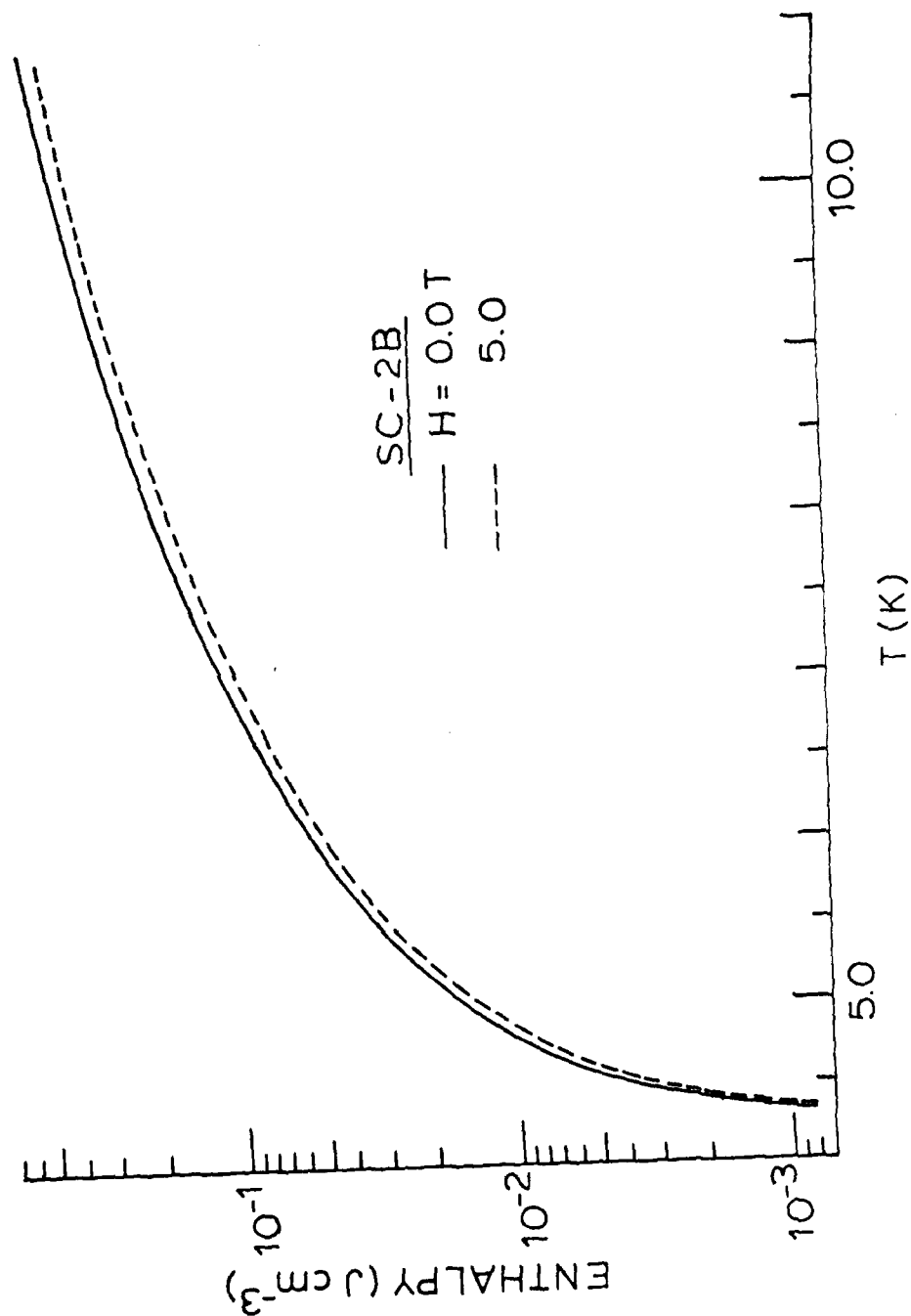


Figure 22. Volumetric enthalpy of SC-2B relative to 4.29 K at 0 and 5 T. The enthalpy of SC-2B is slightly depressed by an intense magnetic field.



No measurements were made on the SC-2C material in intense magnetic fields. Priorities had to be set in these H-field measurements, and SC-2C was not selected because both the specific heat (Fig. 15) and thermal conductivity (Fig. 16) of this material are inferior to those of SC-2A and -2B. Nonetheless, it can probably be concluded from the H-field results on SC-2A and -2B that the specific heat of SC-2C is no more affected by intense H-fields than the specific heats of SC-2A or SC-2B.

As was done above in Table 2 for the SC-1 materials, the volumetric enthalpies for the SC-2 materials are given in Table 4 relative to 4.2 K. The zero-field data for SC-2A and SC-2C were used in Table 4, but because of the slight H-field dependence found for the specific heat of SC-2B (Fig. 21), the enthalpy data in Table 4 for this material are taken at 5 T.

Table 4

Volumetric Enthalpies for the SC-2 Materials  
Relative to 4.2 K (in units of  $\text{mJ cm}^{-3}$ )

T (K)	SC-2A <sup>(a)</sup>	SC-2B <sup>(b)</sup>	SC-2C <sup>(a)</sup>
5	10.65	15.32	10.83
6	36.47	50.53	39.58
7	79.86	104.1	84.35
8	144.6	178.6	154.7
9	232.1	277.4	253.1
10	344.3	400.0	382.4

(a) Zero-field

(b)  $H = 5 \text{ T}$

The thermal conductivities of SC-2A and -2B were also investigated in intense magnetic fields in order to attempt to demonstrate that the thermal properties of this class of dielectric materials are H-field insensitive at low temperatures. That is, one can generalize Eq.(2) to an integral over the density of states showing that if the specific heat is H-field independent, then the thermal conductivity should also be H-field independent. Note in this regard that a specific heat measurement samples all vibrational modes in the Brillouin zone, whereas only those modes that carry heat contribute to the thermal conductivity.

The first experiments here consisted of measuring  $K$  vs.  $T$  at one field level (5 T) on the thin-bars samples of SC-2A and -2B, and it was found that these data matched the zero-field data of Figs. 17 and 18 within experimental error ( $\leq \pm 10\%$ ).

A second set of measurements were made which were more convincing, since they were relative rather than absolute measurements. These measurements, which were something of a tour de force, were made using the "one thermometer, two-heater" method, and the procedure was as follows: At zero field, a certain heater power level was determined to give a favorable  $\Delta T$ , and the capacitance thermometer reading with the lower heater activated was recorded. Under an applied H-field, the set point of the controller was adjusted to give the same thermometer reading with the same power applied to the lower heater. With the same power level applied to the upper heater, the  $\Delta T$  was measured. In this fashion, thermal conductivity data were

measured under essentially isothermal conditions relative to the zero-field thermal conductivity, and these data are shown in Fig. 23 for SC-2A and -2B for H-fields up to 12.5 T. At each field level, between 4 and 8 points were taken, and the error bars in Fig. 23 reflect the spread in the data. The uncertainty in the absolute temperature for each sample is also shown. The zero-field measurements in Fig. 23 have the smallest uncertainty because there is usually an unavoidable noise associated with the "field-on" measurements.

The Fig. 23 data suggest a small decrease in the thermal conductivity of SC-2A with applied magnetic field, and, contrastingly, a small increase in the thermal conductivity of SC-2B. These may very well be real effects, since the data were measured under identical conditions on essentially identical samples, and the samples behave oppositely. Moreover, the uncertainties in the temperatures in Fig. 23 (0.01-0.02 K) translate into uncertainties in the thermal conductivities of only  $\sim 0.1\%$  (as deduced from the temperature dependence of  $K$  in the neighborhood of the temperature involved). What is clear, however, is that the thermal conductivities of these materials retain their "metallic" values in intense magnetic fields.

## VII. SC-3 MATERIALS

The SC-3 materials are inorganic, simple-cubic structures similar to the SC-2 materials; the melting points of the SC-3 materials, however, are  $\sim 630^\circ\text{C}$ . Single crystals of the two SC-3 materials were obtained from

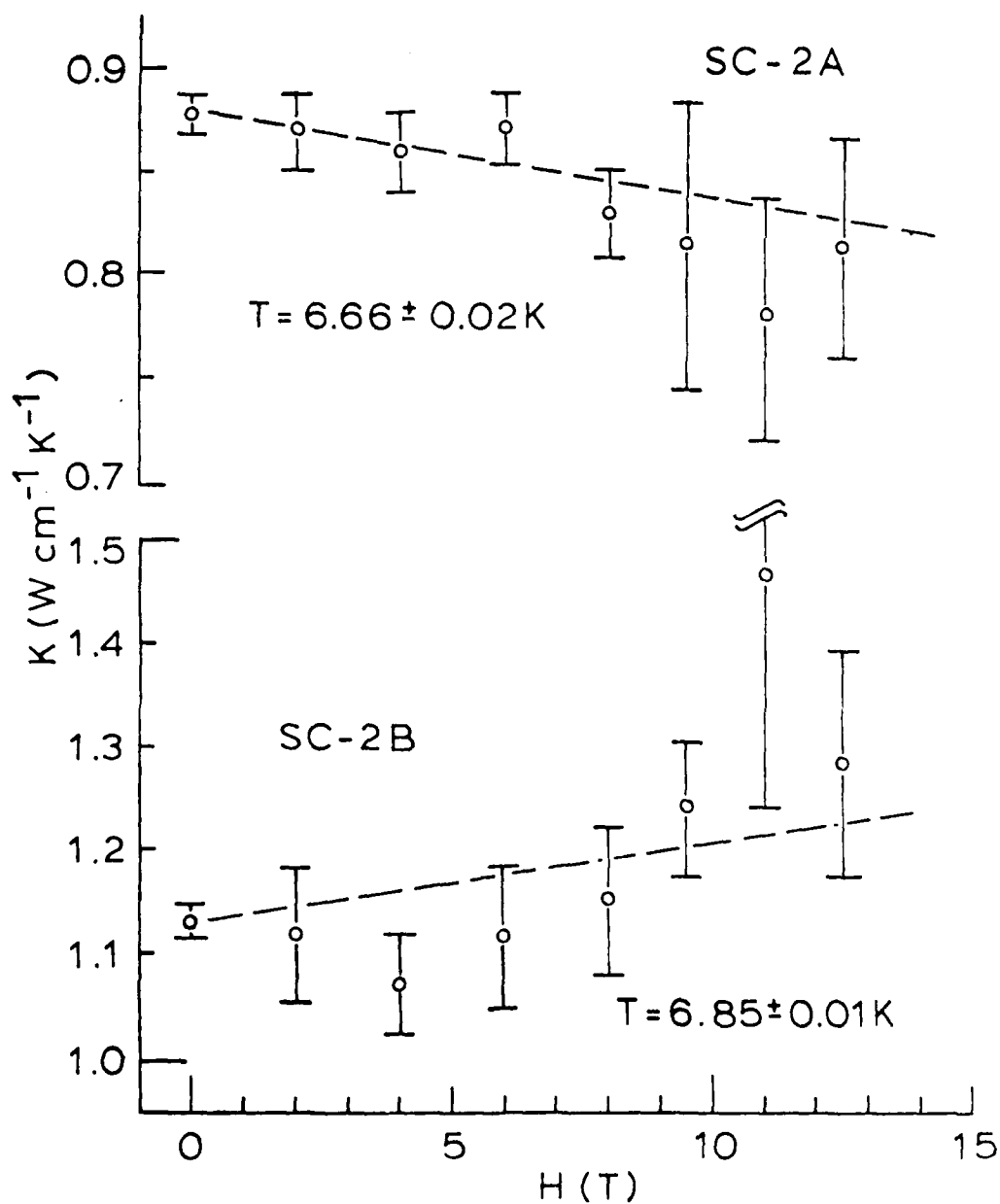


**Figure 23.** Magnetic-field dependence of the thermal conductivities of SC-2A and -2B at constant temperature. A field-sweep method was used, and the two samples were measured under identical conditions. Four to eight points were measured at each field level.

the Harshaw Chemical Co., and the appropriate specific heat and thermal conductivity samples were cut from the crystals using a diamond saw.

#### Zero-Field Measurements

The zero-field specific heat data for SC-3A and -3B are shown in Fig. 15 and have been discussed above.

The zero-field thermal conductivity of SC-3A and -3B measured on relatively large bars are shown in Fig. 24. Shown for comparison in Fig. 24 are thermal conductivity data for commercial copper(18). These SC-3 materials have the largest thermal conductivities of any of the materials studied in this program.

As with the SC-2 materials in Fig. 16, the SC-3 materials display the  $T^3$  boundary scattering limit at the lowest temperatures in Fig. 24. This boundary scattering was investigated further by measuring the thermal conductivity of a bundle of small bars of SC-3A, and these data are shown in Fig. 25 (see, also, the discussion above in Section VI).

The Fig. 25 data show that the thermal conductivity of SC-3A is much more size-dependent than the thermal conductivities of the SC-2 materials (compare with Figs. 17 and 18). Following the same analyses discussed in Section VI, the limiting mean free path,  $\lambda_b$ , can be estimated for the SC-3 materials, and these data are summarized in Table 5.

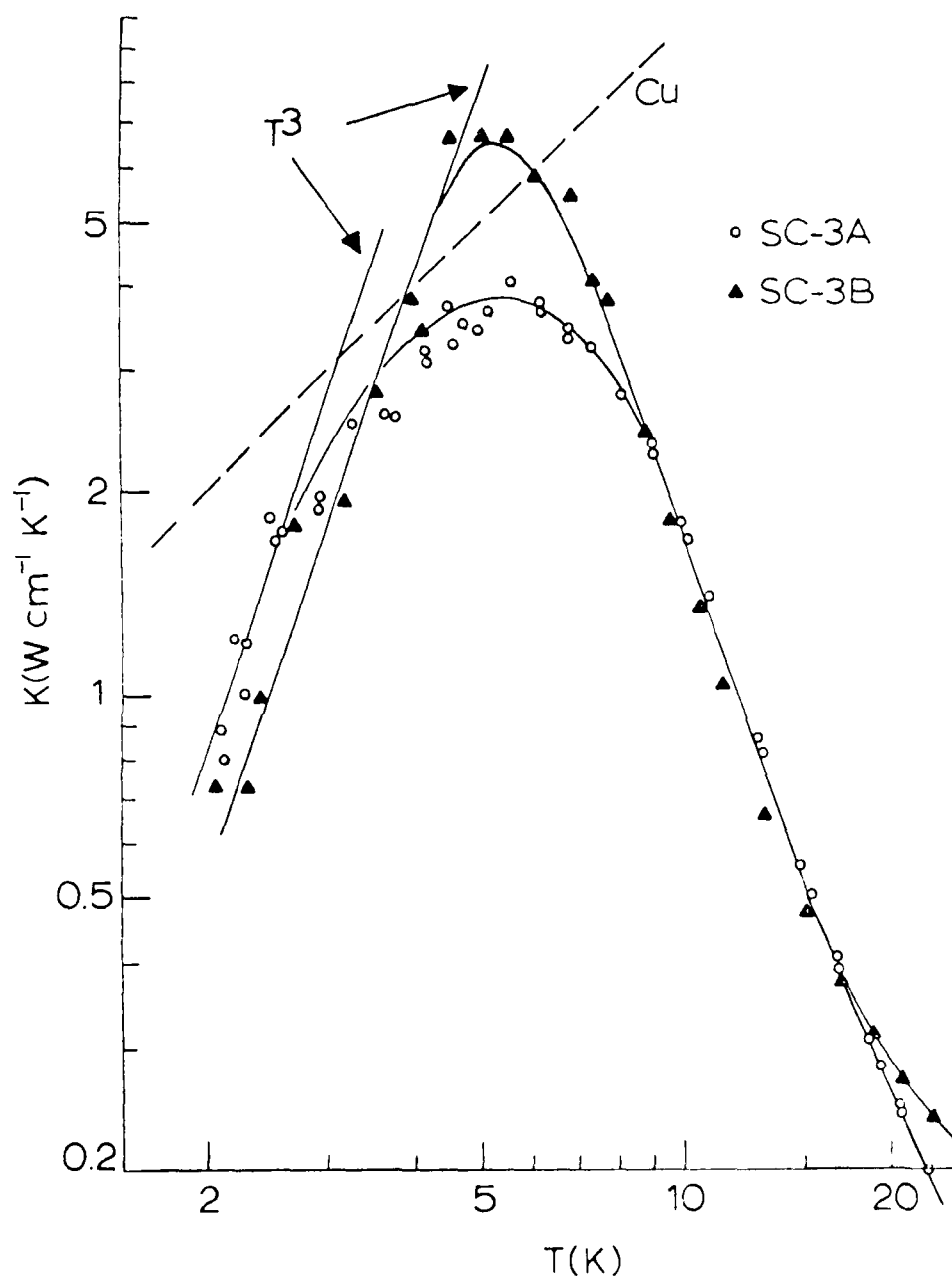
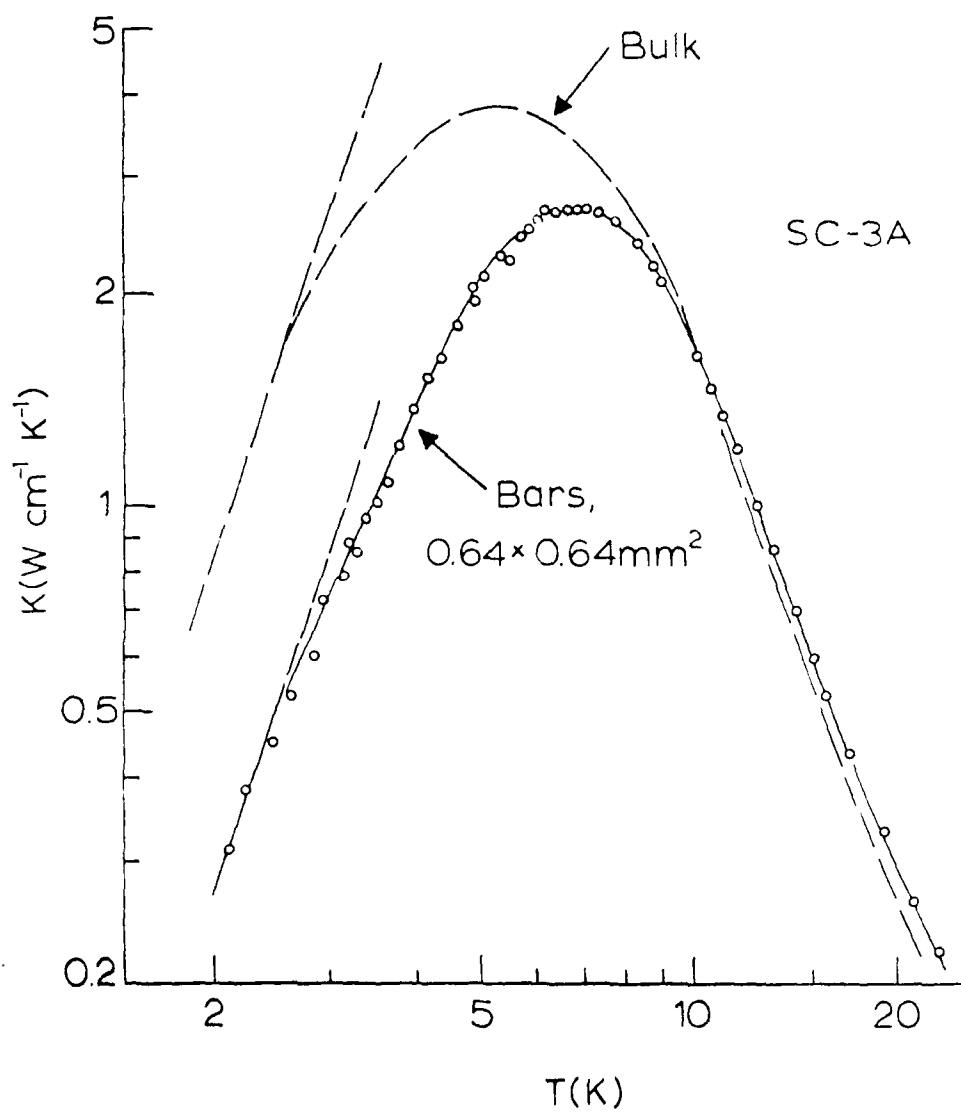


Figure 24. Thermal conductivities of the SC-3 materials (bulk samples, zero field). Data for commercial copper are shown for comparison, and these SC-3 materials have the largest thermal conductivities of any of the materials studied.



**Figure 25.** Thermal conductivity data measured on thin (0.64 mm) bars of SC-3A. These data reveal stronger boundary-scattering effects than the data for SC-2A (Fig. 17) or SC-2B (Fig. 18).

Table 5

Geometric Phonon Scattering Limits		
Material	Smallest Sample Dimension (cm)	$\lambda_b$ (cm)
SC-3A	0.414	0.056
SC-3A	0.064	0.019
SC-3B	0.406	0.030

Comparing the  $\lambda_b$ -data in Tables 3 and 5, it is seen that, in general, the characteristic scattering lengths in the SC-3 materials are considerably larger than in the SC-2 materials. This finding may limit the ultimate utility of these SC-3 materials because, as seen in Fig. 25, on going to ever thinner sections of SC-3A, the thermal conductivity progressively decreases. We shall return to this point in detail below.

#### Magnetic-Field Measurements

The SC-3 materials, like the SC-2 materials, contain no paramagnetic ions. Nonetheless, the thermal properties of SC-3B were measured in intense magnetic fields.

The specific heat data for SC-3B at 2.5, 5, and 7.5 T are shown in Fig. 26, compared to the zero-field data. As with SC-2B (Fig. 21), there is a small but progressive decrease in the specific heat with magnetic field. The corresponding volumetric enthalpy data relative to 3.94 K are shown in Fig. 27. The enthalpy data for SC-3B in Fig. 27 are practically H-field independent up to 6.5 K.



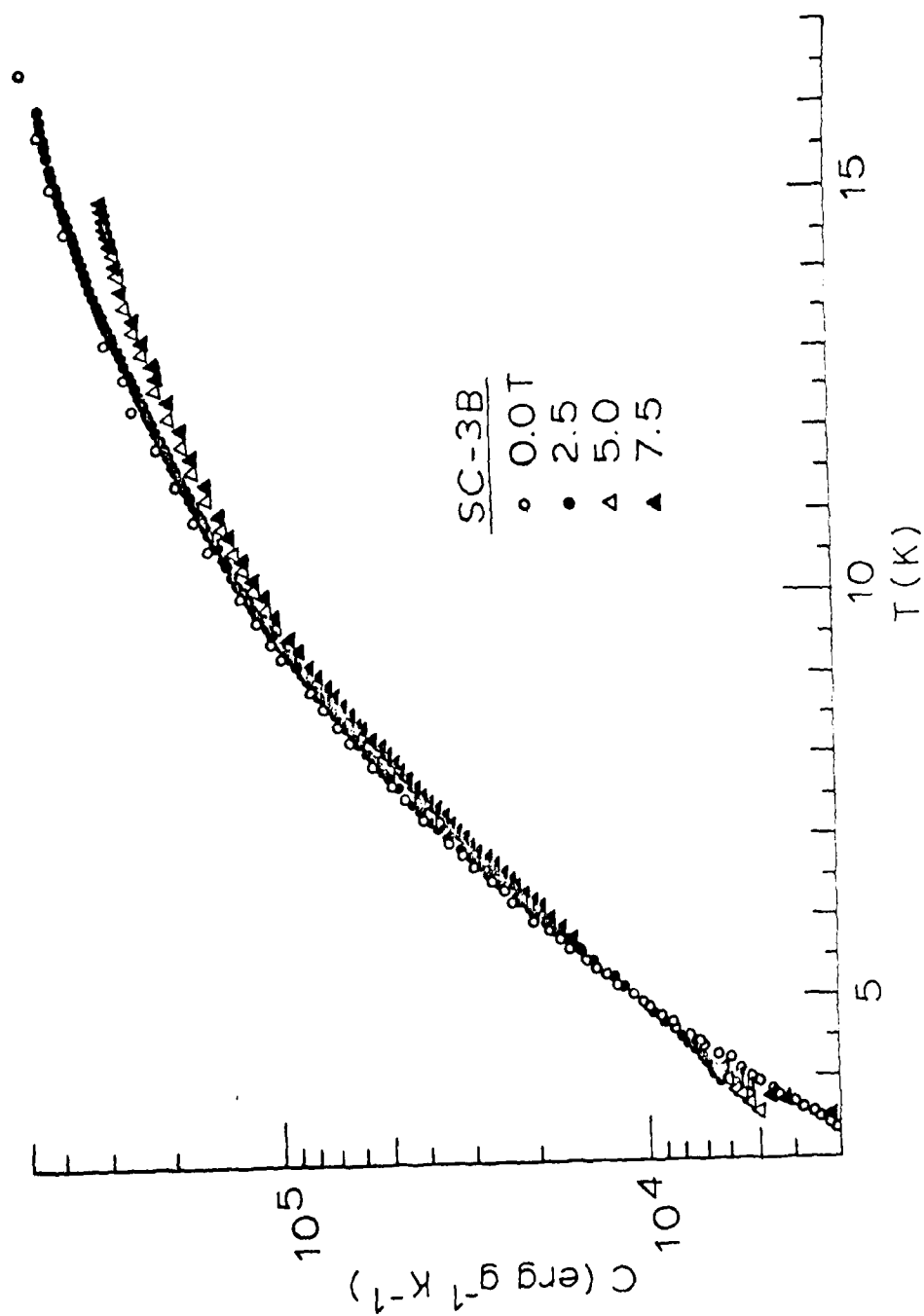


Figure 26. Magnetic-field dependence of the specific heat of SC-3B below 17 K at 2.5, 5.0, and 7.5 T. Zero-field data are shown for comparison.

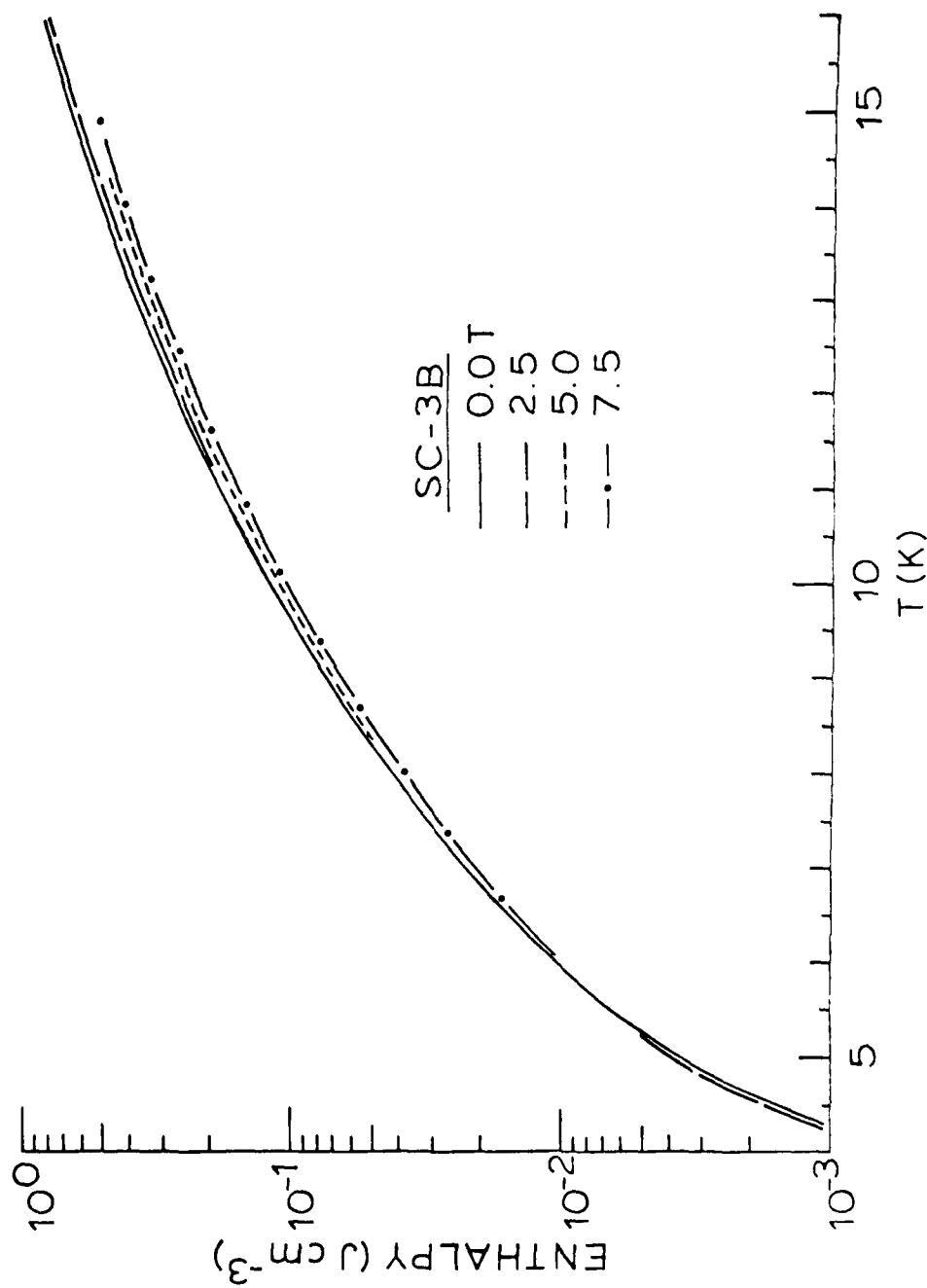


Figure 27. Volumetric enthalpy of SC-3B relative to 3.94 K at 0, 2.5, 5.0, and 7.5 T. The enthalpy of SC-3B is depressed slightly by intense magnetic fields at temperatures above 6 K.

As was done above for the SC-1 and SC-2 materials, the volumetric enthalpies for the SC-3 materials are given in Table 6 relative to 4.2 K. The zero-field specific heat data for SC-3A were used (Fig. 15) to compute the enthalpies for this material. For SC-3B, the enthalpies at 5 T are given.

Table 6  
Volumetric Enthalpies of the SC-3 Materials  
Relative to 4.2 K (in units of  $\text{mJ cm}^{-3}$ )

T (K)	SC-3A(a)	SC-3B(b)
5	2.10	3.15
6	7.20	9.77
7	16.37	21.42
8	31.80	40.96
9	56.04	71.02
10	92.12	114.3

(a) At zero field.

(b) At 5 T.

Finally, the thermal conductivity of SC-3A was measured in intense magnetic fields by the isothermal, field-sweep method described above (Section VI). These data are shown in Fig. 28 and represent one of the most intriguing findings in this program; namely, the thermal conductivity of SC-3A goes through a maximum at  $\sim 8-9$  T. In judging these data, recall that the measurement here is a relative method and that at each H-field level several measurements were made. The error bars in Fig. 28 reflect the spread in the data at each H-field level, and the noise conditions in

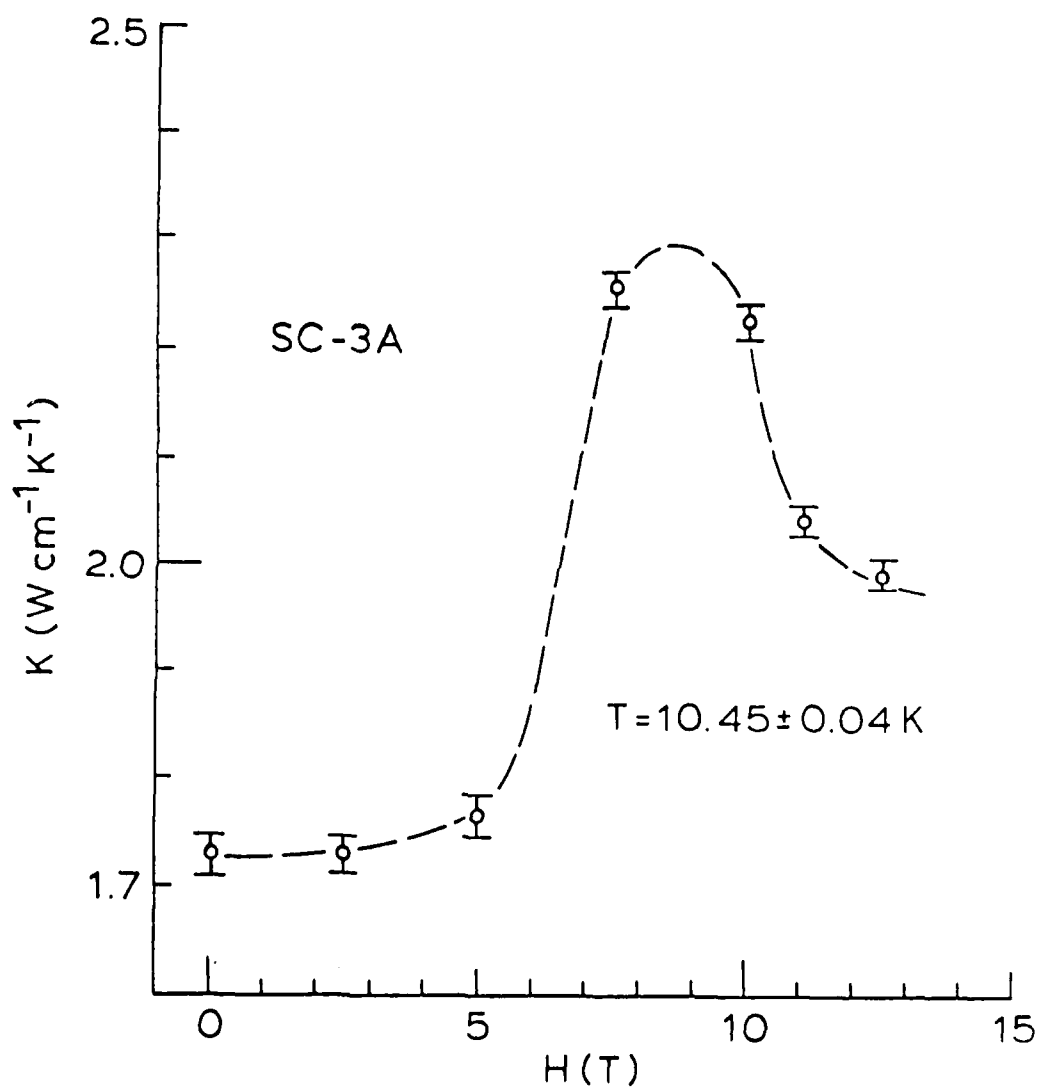


**Figure 28.** Magnetic-field dependence of the thermal conductivity of SC-3A at 10.45 K. Several points were measured at each field level, and a large maximum appears in the thermal conductivity at about 9 T.

these measurements were very favorable (compare with Fig. 23). The temperature of the data set is given in Fig. 28, and the uncertainty in the temperature ( $\pm 0.04$  K) is far too small to explain the anomaly in the thermal conductivity data.

Because there are so many measurements involved in the data of Fig. 28, we believe this thermal conductivity maximum in SC-3A is real. The effect is large,  $\approx 35\%$  increase in K between 0 and 8 T, and it is difficult to reconcile this effect with the rather small dependence of the specific heat of SC-3B on H-fields (Fig. 26). However, central to this argument is the assumption that SC-3A and SC-3B behave the same. Specific heat data on SC-3A in intense H-fields are needed to pursue this unusual effect further.

#### VIII. SC-1C + VARNISH COMPOSITE

The first composite studied was also the most straightforward, namely, a mixture of SC-1C powder in a common transformer varnish. The varnish here was General Electric 7031 (abbreviated "7031" below) which is a viscous, orange liquid that air-cures in 24 h. This varnish is well-known to low-temperature experimentalists for its adhesion and durability at low temperatures. Although our original purpose for studying this simple composite was in connection with fabricating a transient-heat-transfer test sample (see below), the potential of this composite as a coating material should not be dismissed lightly because this composite lends itself readily to a dip-coating process.

A dip-coating mixture of 7031 and SC-1C was prepared as follows: Ceramic powders of SC-1C were first prepared by conventional processes (i.e., mixing, calcining, grinding, re-calcining, grinding, sintering, and grinding), and subsequent scanning-electron-micrographs revealed a grain size  $\approx 1-2 \mu\text{m}$ . This powder was slowly added to the 7031 to form an initial, viscous mixture, the condition being that the powder remained in suspension. The solvent for the 7031 is a 50:50 mixture of alcohol and toluene, and this solvent was slowly added to the 7031 + SC-1C mixture until a sufficiently low viscosity was obtained such that no bubbles would form on a dipped glass capillary tube. The resulting viscosity was such that an approximately 0.0005" layer was coated per dip, and 30-60 min were allowed for air curing between dips. Coated capillary tubes had final thicknesses ranging from 0.003 to 0.015 in, and subsequent scanning-electron-micrographs showed that uniform, pore-free coatings were obtained. These cured coatings had a rubbery texture, appeared hard enough to be scratch-resistant, and appeared flexible enough to withstand bend tests (no quantitative data were measured on these mechanical properties). The final mixture was kept tightly sealed and refrigerated between dippings.

A sample of this composite material for thermal properties measurements was prepared as follows: A 1/8" diam section of a candy cane was repeatedly dipped in the mixture to form a 1/4" diam rod. The center cane was dissolved in water, and a sample 1" long was cut from the center of the tube for the thermal properties sample. Specific heat and thermal conductivity data measured on this sample are shown in Figs. 29 and 30,

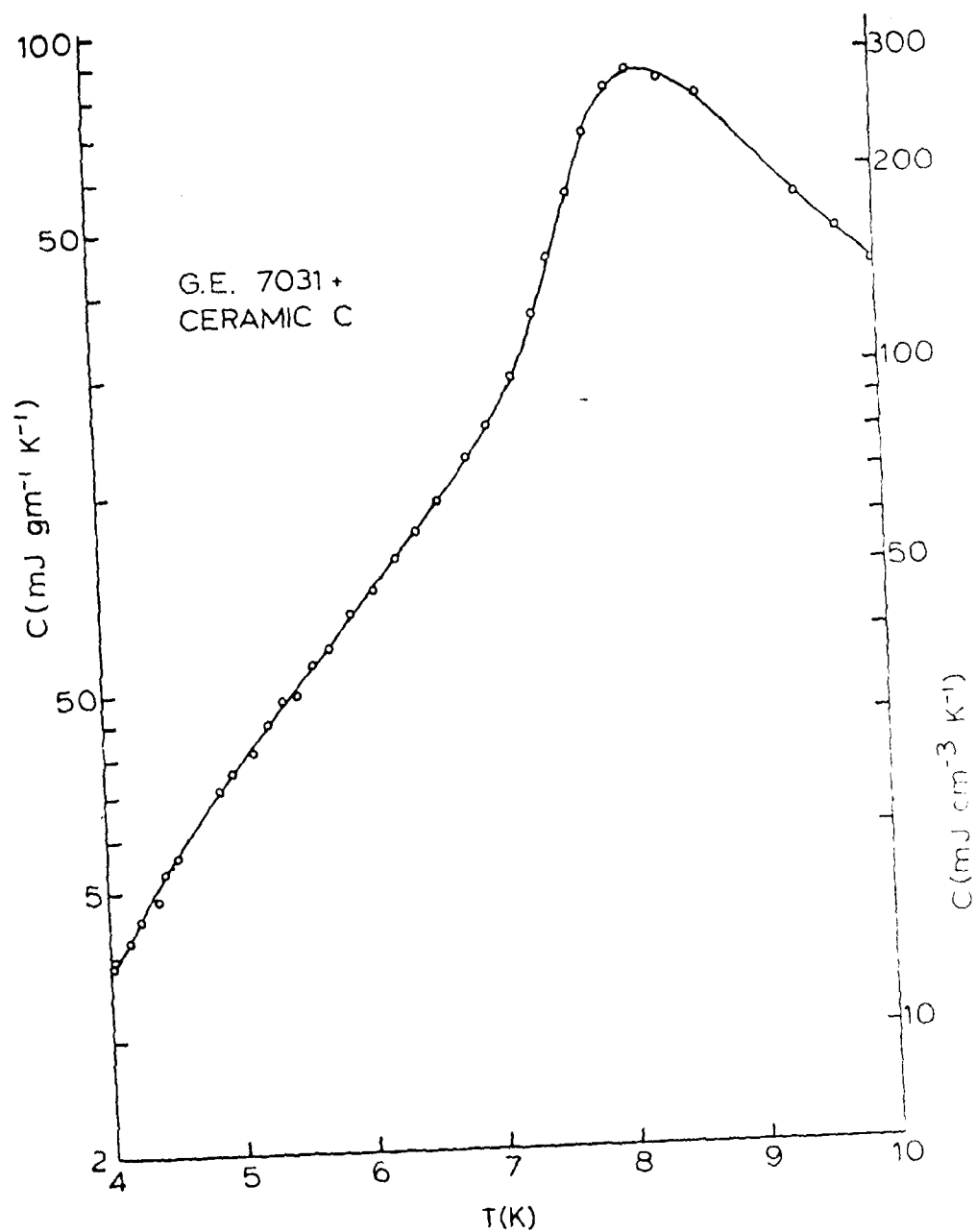
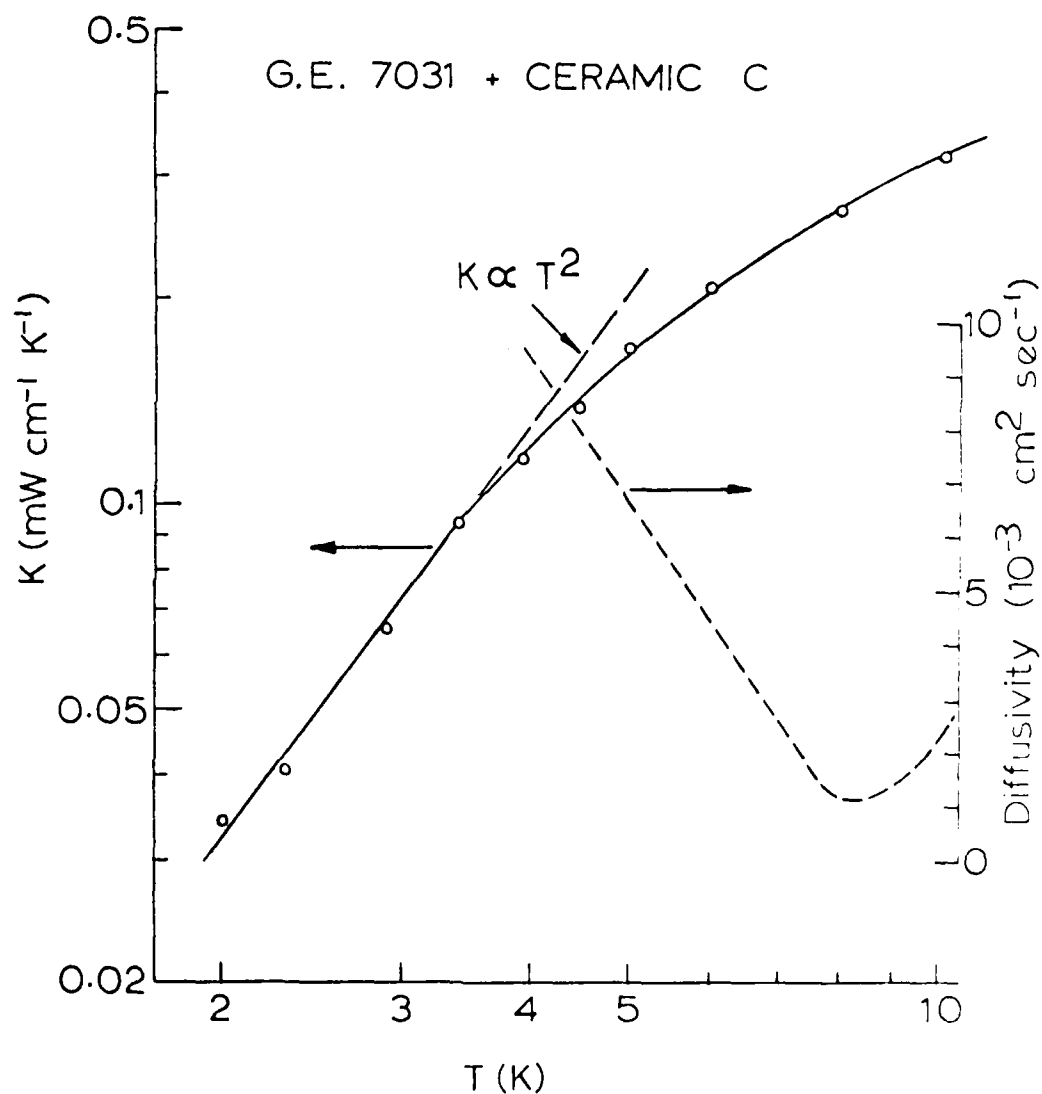


Figure 29. Specific heat of the SC-1C + G.E. 7031 composite (zero field). The density of the composite is estimated to be 3.3 g/cm<sup>3</sup>, and the volumetric scale shown is based on this density.



**Figure 30.** Thermal conductivity of the SC-1C + 7031 composite (zero field). The conductivity data follow a  $T^2$  law at the lowest temperatures, and thermal diffusivity data are also shown [estimated using Eq. (9) and the data in Fig. 29].



respectively. Also shown in Fig. 30 are thermal diffusivity data for this material, calculated according to

$$k = K/C\rho \quad (3)$$

where  $K$  is the thermal conductivity,  $C$  is the gravimetric specific heat, and  $\rho$  is the density (taken here to be  $3.3 \text{ g/cm}^3$ , see below).

The Fig. 29 data show that this composite has a broad specific heat maximum at 8.2 K of  $86 \text{ mJ g}^{-1} \text{ K}^{-1}$  ( $280 \text{ mJ cm}^{-3} \text{ K}^{-1}$ , note accompanying volumetric scale in Fig. 29). The thermal conductivity data in Fig. 30 approach the glassy  $T^2$  limit at the lowest temperatures, as one would expect for amorphous materials, and it is significant to observe that the thermal conductivity of this composite is much smaller than the thermal conductivities of the two constituents (i.e., compare with Figs. 1 and 5, where the thermal conductivity of the 7031 can be assumed equivalent to that of unfilled resins). This effect has been observed on other composites and attributed to a Kapitza resistance between the ceramic grains and the resin matrix(17).

The density of the coating was estimated from the dimensions of the tube sample and the weight of the sample, with the result that  $\rho = 3.3 \text{ g/cm}^3$  (used to determine the volumetric scale in Fig. 29). The mixing ratio achieved in the composite was estimated as follows: At 8 K, the specific heat of the ceramic powder is  $2.5 \times 10^6 \text{ erg g}^{-1} \text{ K}^{-1}$  (from Fig. 4, note that

the 9:1 ratio ceramic was used), and the literature value(20) for the specific heat of 7031 at this temperature is  $1.53 \times 10^5 \text{ erg g}^{-1} \text{ K}^{-1}$ . Consequently, the weight ratio of the ceramic in the composite is 27.5%.

Finally, using the specific heat data in Fig. 29, the volumetric enthalpy of this composite relative to 4.2 K is determined, and these data are summarized in Table 7.

Table 7  
Volumetric Enthalpies<sup>(a)</sup> of the SC-1C + 7031 Composite  
Relative to 4.2 K (in units of  $\text{mJ cm}^{-3}$ )

T (K)	Enthalpy
5	18.80
6	54.58
7	116.9
8	310.9
9	617.7
10	719.4

(a) Zero magnetic field

#### Heat Transfer Sample

The goal here was to fabricate a heat transfer sample which would simulate a coated superconducting wire. The requirements for the "wire" are that it act both as a heater and a thermometer. A carbon-impregnated-porous-glass rod (CIPG) was selected as the "wire" because of the favorable resistance-temperature characteristic of this material which forms the basis of the so-called carbon-glass cryogenic thermometer(21). The coating

on this CIPG rod was, of course, the SC-1C + 7031 composite discussed above.

The CIPG rod (1/8" diam x 5" long) was obtained from Corning Glass Works and cut into three sections: one short section (~1/2") for resistance calibration, and two long sections (~2 1/2") for dip-coating. The short section was calibrated 4-24 K, and these calibration data are given in Table 8.

Table 8

Calibration Data for the CIPG Heat Transfer Sample

T (K)	R ( $\Omega$ )	T (K)	R ( $\Omega$ )	T (K)	R ( $\Omega$ )
4.0	36.324	7.5	15.021	15.0	8.5491
4.2	33.298	8.0	14.042	16.0	8.2333
4.4	30.751	8.5	13.222	17.0	7.9600
4.6	28.586	9.0	12.524	18.0	7.7222
4.8	26.725	9.5	11.926	19.0	7.5147
5.0	25.113	10.0	11.407	20.0	7.3375
5.5	21.898	11.0	10.557	21.0	7.1767
6.0	19.507	12.0	9.8911	22.0	7.0289
6.5	17.664	13.0	9.3571	23.0	6.8867
7.0	16.204	14.0	8.9180	24.0	6.7497

These calibration data in Table 8 for the short section of the rod can be transferred to the long sections by scaling the 4.2 K dip values. A more accurate procedure for calibration transfer is described in Ref. 21; namely, at each temperature,  $R_L = kR_S^m$ , where  $R_L$  and  $R_S$  are the resistances of the long and short sections and k and m are constants. Thus, if  $R_L$  is

measured at two temperatures,  $k$  and  $m$  can be determined (the 4.2 K dip-value transfer mentioned above corresponds to  $m = 1$ , and, in practice, it is generally found that  $m$  is very nearly unity).

For modelling purposes, the specific heat and thermal conductivity of the CIPG material are required. These thermal data on this material were measured on the short section (specific heat) and on one of the long sections (thermal conductivity) of the rod. These data are of broad interest because the CIPG material is widely used for cryogenic thermometry and for cryogenic bolometry; consequently, these thermal data were published in the open literature(22).

Nichrome-gold electrodes were evaporated on the ends of the two CIPG rods, and copper leads were attached with silver epoxy. The rods were then dip-coated with the SC-1C + 7031 composite as described above (i.e., 0.0005" layers per dip, 30-60 min, air curing between dips). The final rods had composite coating thicknesses of 0.003" and 0.015", and these rods were delivered to Wright-Patterson Air Force Base for testing.

#### IX. SC-1B + GLASS COMPOSITES

The goal in performing some exploratory research on composites of SC-1B (and SC-1C) powders dispersed in glass matrices was to lay some groundwork for potentially coating NbSn wire using the glass-on-wire coating facilities of the Westinghouse R&D Center. That is, these facilities were established

to coat conventional wires with glass + alumina composites, so little imagination was required to consider replacing the alumina powders with the SC-1 type powders to gain enthalpy stabilization.

The composites here were prepared by Dr. T. P. Gupta of the Westinghouse R&D Center under subcontract to Lake Shore Cryotronics, and the initial studies were aimed at identifying glasses which would densify in the NbSn-reaction temperature range, 600-750°C. A review of the glass literature suggested two candidate glass compositions, Codes 7052 and 7570, and these glasses were selected for the composite studies with SC-1B (and SC-1C).

The SC-1B refractory ceramic was selected because of the favorable maximum in this material at 5.4 K, Fig. 3. At the time this selection was made, the results were not available on the effect of intense magnetic fields on the specific heat (Fig. 8) and enthalpy (Fig. 9) of SC-1B.

Three mixing ratios of powders of SC-1B in the two glasses were chosen: 30, 45, and 60 wt % of the SC-1B powders. The starting powders of SC-1B were in the particle size range of 1-5  $\mu\text{m}$ . In Table 9 below are given the measured densities of the composites and the estimated porosities of these composites (based upon literature densities of 2.28 and 5.42  $\text{g/cm}^3$  for the 7052 and 7570 glasses, respectively). Also given in Table 9 are the volume %'s of the SC-1B powders in the composites.

Table 9

Densities and Porosities of the  
SC-1B + Glass Composite Materials

Glass	Wt.% of SC-1B	Vol.% of SC-1B	Actual Density(g/cm <sup>3</sup> )	Porosity <sup>(a)</sup> (%)
7570	30	29.7	4.513	17.1
	45	44.7	3.878	28.9
	60	59.7	4.133	24.4
7052	30	15.1	2.339	15.4
	45	25.3	2.733	11.7
	60	38.4	2.244	36.1

(a) Estimated based on the measured density

The Table 9 data indicate considerable porosity levels in these composites which is somewhat surprising since no organic binders were used (i.e., powders of the ceramic and glass were simply mixed and fired).

#### Specific Heat Measurements (Zero-Field)

The specific heat measurements on these six composites are shown in Figs. 31 and 32 for the 7570 and 7052 glasses, respectively. Also shown for comparison are specific heat data on the bulk ceramic. As expected, the larger the SC-1B content, the larger the specific heats of these composites. However, whereas the SC-1B + 7052 data in Fig. 32 appear to scale uniformly with the ceramic content, the SC-1B + 7570 data in Fig. 31 tell another story: At 30 wt % SC-1B in 7570, the specific heat maximum at 5.3 K is noticeably missing. This seems to imply a solid-state reaction between SC-1B and 7570, even though at the higher mixing ratios the specific heat maxima do develop.

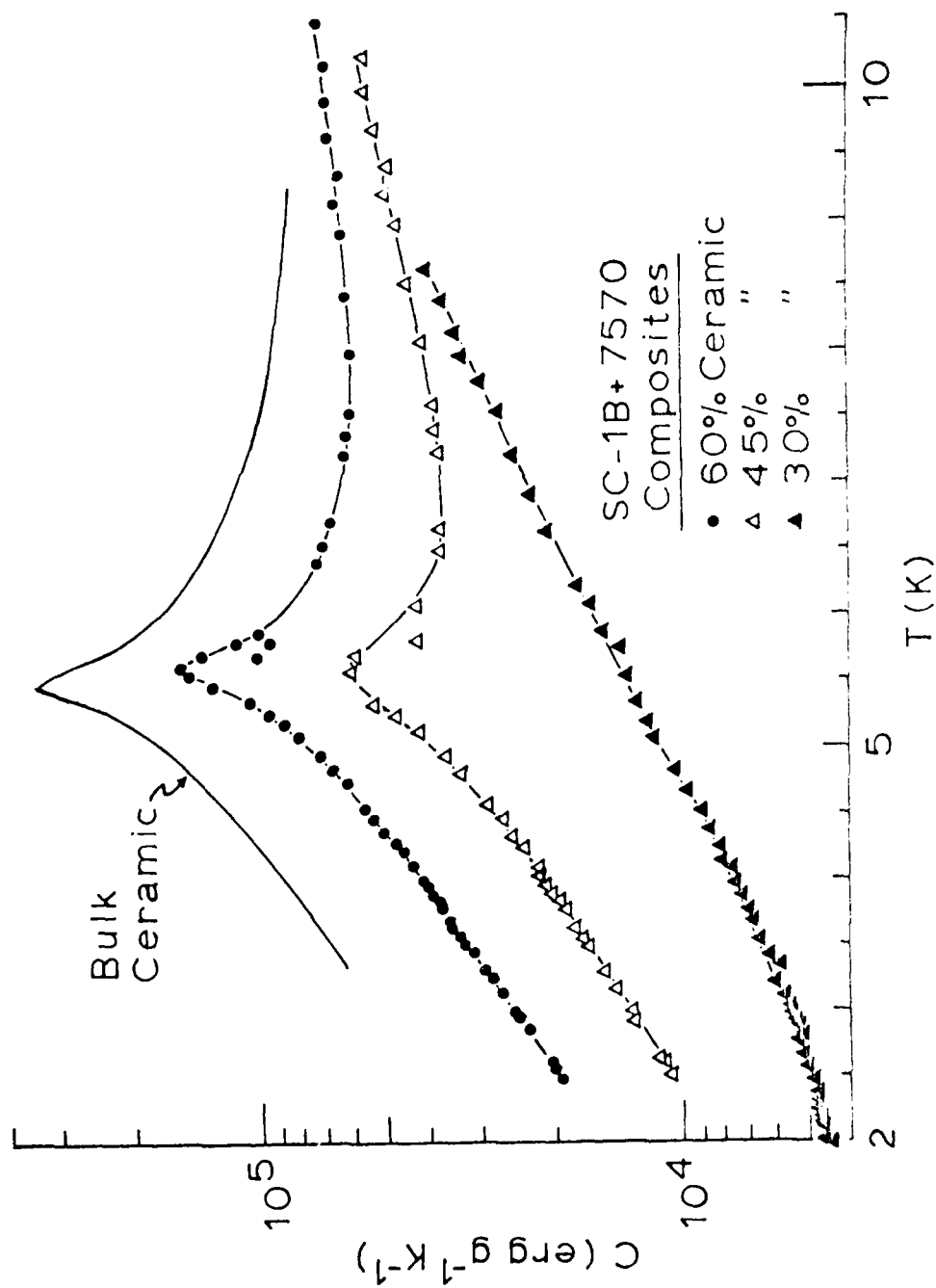


Figure 31. Specific heat data for the SC-1B + 7570 composites with 30, 45, and 60 wt % of the ceramic powder. Also shown for comparison are specific heat data for the bulk ceramic.

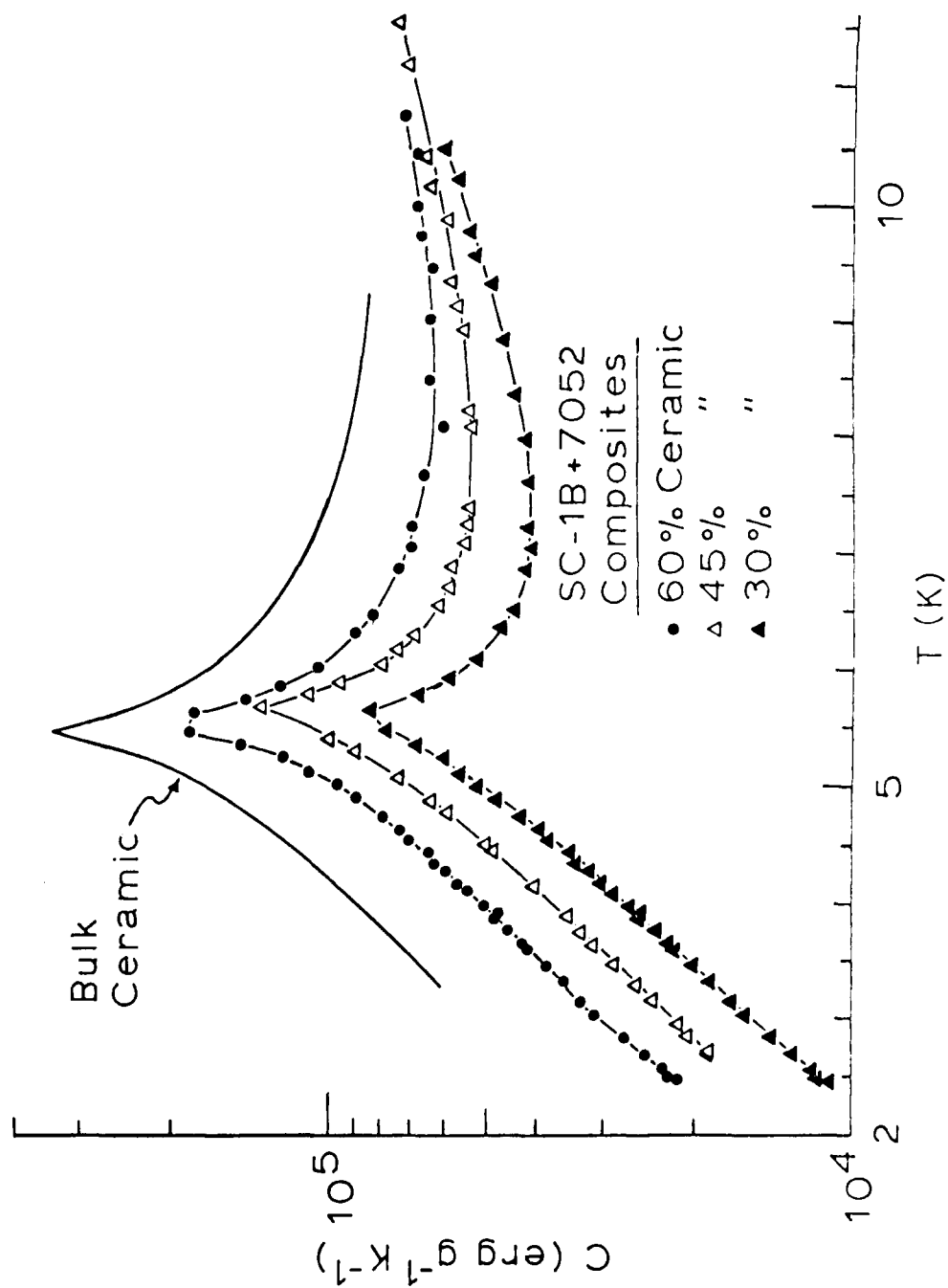


Figure 32. Specific heat data for the SC-1B + 7052 composites at 30, 45, and 60 wt % of the ceramic powder. Also shown for comparison are specific heat data for the bulk ceramic.



Pursuing this further, the specific heat of the ceramic portion alone can be deduced from the mixing ratio (note that the contribution from the glass phase to the specific heat is negligible), and these specific heats of the ceramic powders in the composites are shown in Figs. 33 and 34. These data clearly show that the specific heat of SC-1B is degraded when the ceramic powders are mixed into the 7570 glass (Fig. 33), whereas there is essentially no change in the SC-1B material upon mixing into the 7052 glass (Fig. 34). It is interesting to note that in all of these composites, there is an enhancement of the specific heat of the SC-1B at temperatures  $\geq 7$  K.

Volumetric enthalpies relative to 4.2 K were calculated using the specific heat data in Figs. 31 and 32 and density data from Table 9. Only the 45 and 60% composites were considered, and these enthalpy data are given in Table 10.

Table 10

Volumetric Enthalpies of the SC-1B + Glass Composites  
Relative to 4.2 K (in units of  $\text{mJ cm}^{-3}$ ) (a)

T (K)	7570 Glass +		7052 Glass +	
	45% Powder	60% Powder	45% Powder	60% Powder
5	8.93	19.30	12.12	13.23
6	28.18	64.88	39.50	44.65
7	43.24	96.20	57.56	63.80
8	58.22	121.9	72.38	78.79
9	75.25	147.8	87.28	93.01
10	95.18	175.3	102.7	107.7

(a) Zero magnetic field

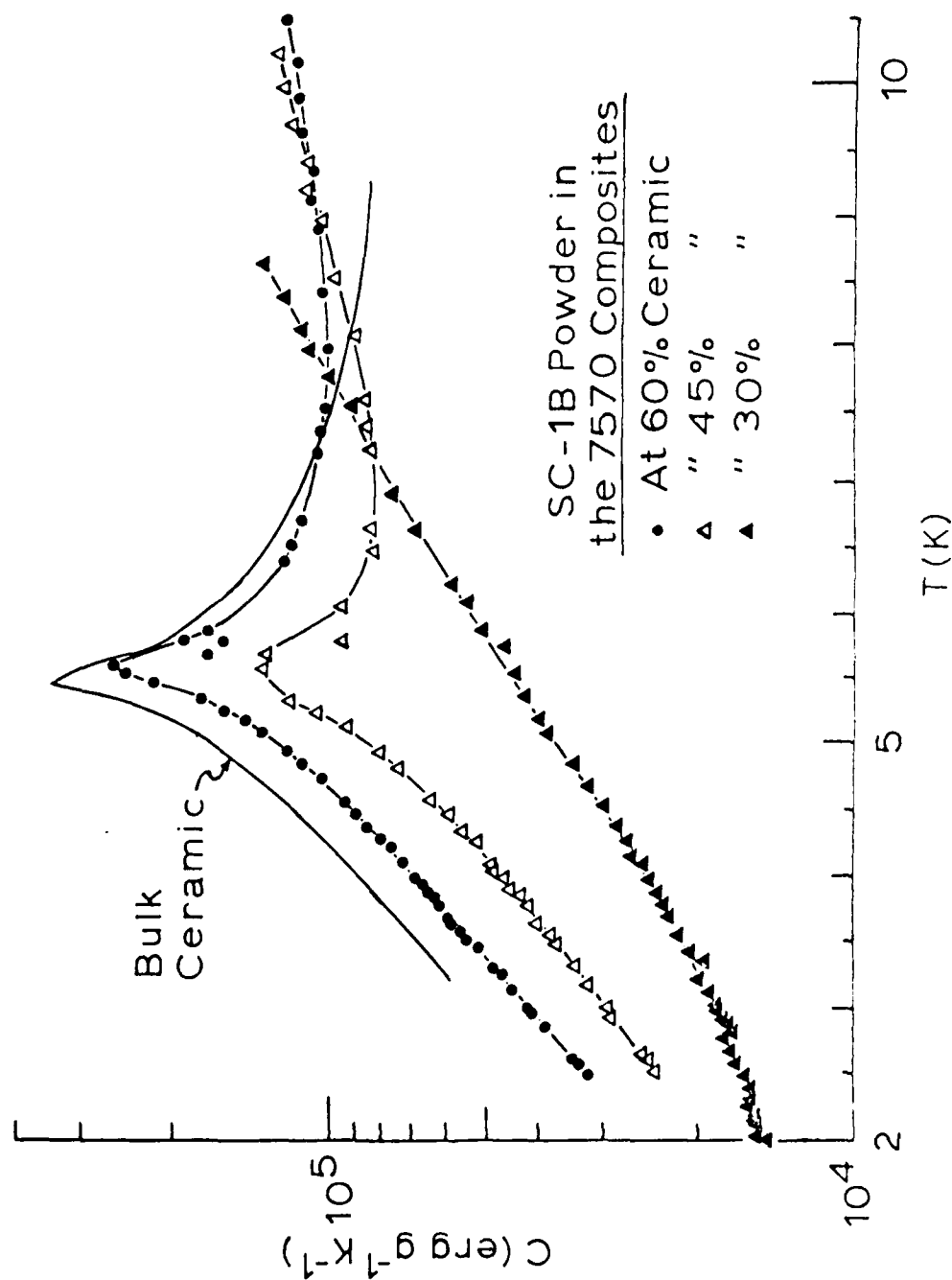


Figure 33. Specific heat data for the SC-1B powders alone in the composites with 7570 glass. Specific heat data for bulk SC-1B are also shown, and note that the SC-1B powders in the composites have reduced specific heats, indicating a solid-state reaction between the ceramic and the glass.

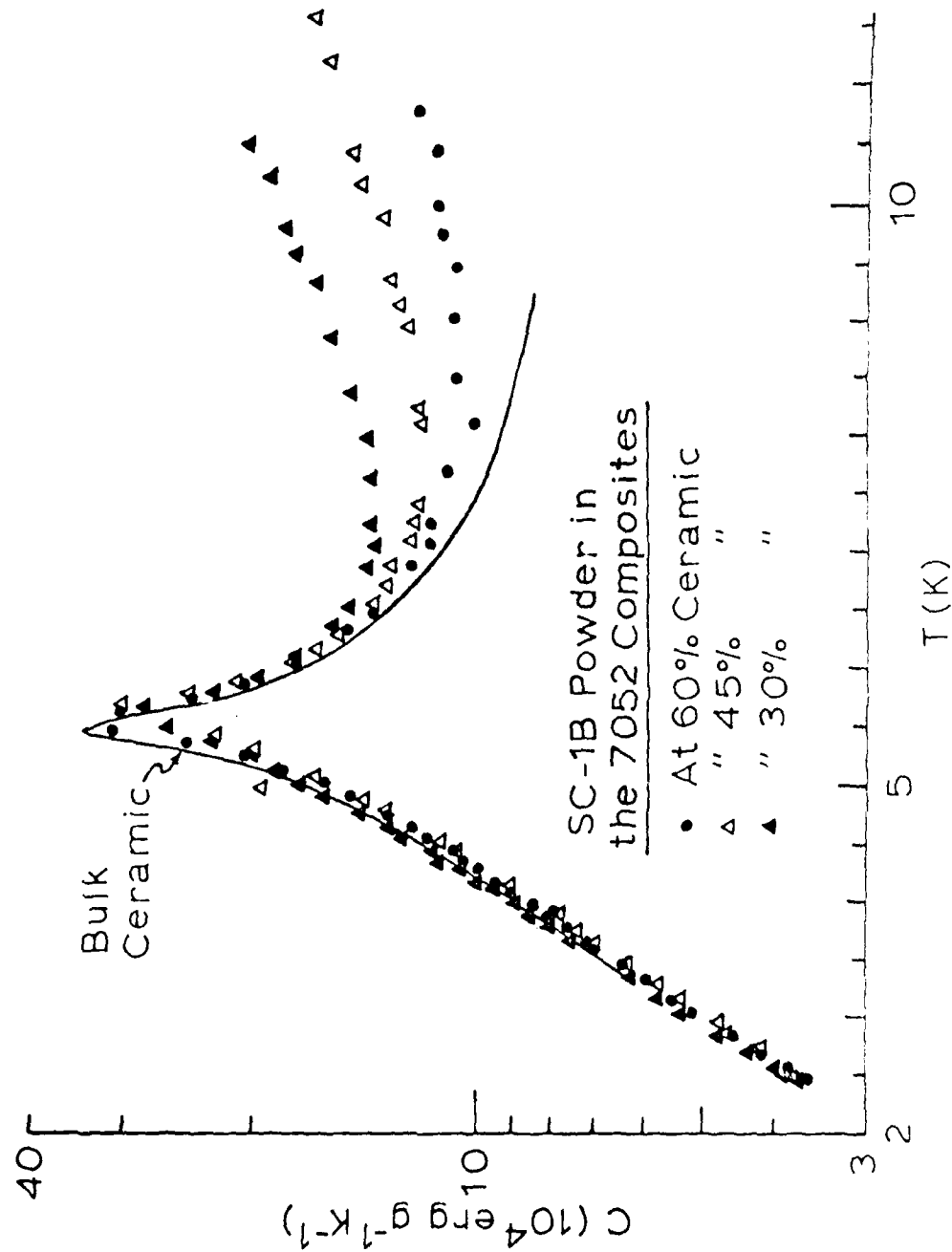


Figure 34. Specific heat data for the SC-1B powder alone in the composites with 7052 glass. In contrast to the case of the 7570 glass (Fig. 33), there is apparently no solid-state reaction between the SC-1B powder and the 7052 glass.

The Table 10 data indicate that the composite of 60% SC-1B in 7570 has the largest volumetric enthalpy of the composites in this series, irrespective of the demonstrated solid-state reaction between 7570 and SC-1B (Fig. 33). A major contribution to this result is the density of this composite (Table 9).

#### Thermal Conductivity Measurements (Zero-Field)

Thermal conductivity data measured on the six SC-1B + glass composites in the range 2-13 K are shown in Fig. 35. The data for the 7052 composites are generally larger than for the 7570 composites. The thermal conductivity data for all the composites are glasslike (i.e.,  $\leq 1 \text{ mW cm}^{-1} \text{ K}^{-1}$ ), whereas the thermal conductivity of the SC-1B ceramic is  $\approx 10 \text{ mW cm}^{-1} \text{ K}^{-1}$  at, say, 10 K (see Fig. 5).

In Fig. 35, the data for the 7052 composites show a small dependence on the powder content, and, in fact, the thermal conductivity decreases somewhat as the powder content increases. Conversely, for the 7570 composites, the thermal conductivity increases as the powder content increases. These phenomena are due to connectivity between the ceramic grains: From Table 9, the volume %'s of SC-1B in 7570 are considerably larger than in 7052, and one expects that connectivity occurs for volume %'s  $\geq 33\%$ . Therefore, more thermal-connection paths are established in the 7570 composites than in the 7052 composites.

These are complex phenomena, however, and involve more than connectivity

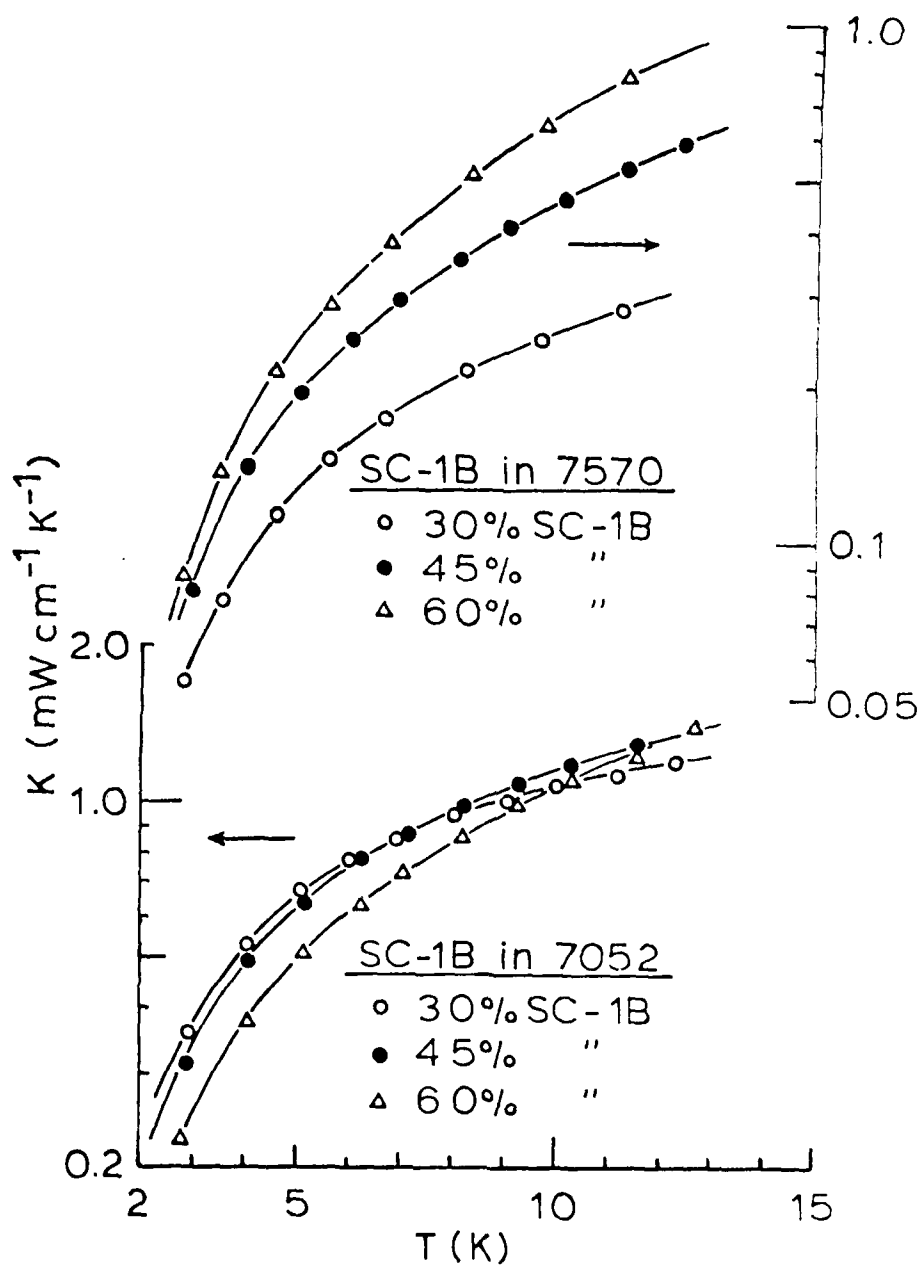


Figure 35. Thermal conductivities of the composites of SC-1B and 7570 glass (upper plot) and 7052 glass (lower plot).

between grains. One must also take into account the Kapitza resistance between the grains and the glass matrix and the phonon scattering from the pores (note the large porosity levels in Table 9). Also, there is evidence in Fig. 33 of a solid-state reaction between SC-1B and the 7570 glass, whereas there is apparently no reaction with the 7052 glass (Fig. 34).

#### X. SC-1C + GLASS COMPOSITES

As with the SC-1B + glass composites above, three mixing ratios of SC-1C powders in the 7570 and 7052 glasses were studied: 30, 45, and 60 wt %. The measured densities, porosities, and volume %'s of these SC-1C + glass composites are summarized in Table 11 below.

Table 11

Densities and Porosities of the  
SC-1C + Glass Composite Materials

Glass	Wt.% of SC-1C	Vol.% of SC-1C	Actual Density(g/cm <sup>3</sup> )	Porosity <sup>(a)</sup> (%)
7570	30	28.2	5.337	3.99
	45	42.9	4.486	20.33
	60	57.9	4.688	17.82
7052	30	14.2	2.609	6.66
	45	24.0	2.737	13.14
	60	36.6	2.502	30.71

(a) Estimated based on the measured density

Comparing with the SC-1B + glass composites in Table 9, it is seen that the composites with SC-1C have somewhat smaller porosities, particularly

at the lower powder contents.

#### Specific Heat Measurements (Zero-Field)

The specific heat data for the SC-1C + 7052 composites are shown in Fig. 36 compared to the bulk specific heat. At 30% SC-1C, a slight maximum develops which becomes well developed at 45 and 60%. The temperature of these latter maxima is  $\approx 7$  K compared to the bulk maximum, 8 K.

The specific heat data for the SC-1C powders only in the glass are shown in Fig. 37, and it is seen that below about 7.5 K the powders all have larger specific heats than the bulk ceramic. An interaction takes place between SC-1C and 7052 which shifts the transition to lower temperatures in the composites and results in these increased specific heat values (Contrast these Fig. 37 results with the results in Fig. 34 for SC-1B powders in 7052.).

The specific heat data measured on the SC-1C + 7570 composites are shown in Fig. 38 compared to the bulk-ceramic data. At the 60%-powder level, the composite has a much larger specific heat than the bulk ceramic below 6 K, and this was one of the most significant findings in this study. To underscore the importance of this finding, the Fig. 38 data are plotted on a volumetric basis, which is the most demanding basis for making comparisons. The 30 and 45% composites in Fig. 38 appear to scale with the respective mixing ratios and have maxima at  $\approx 8$  K.

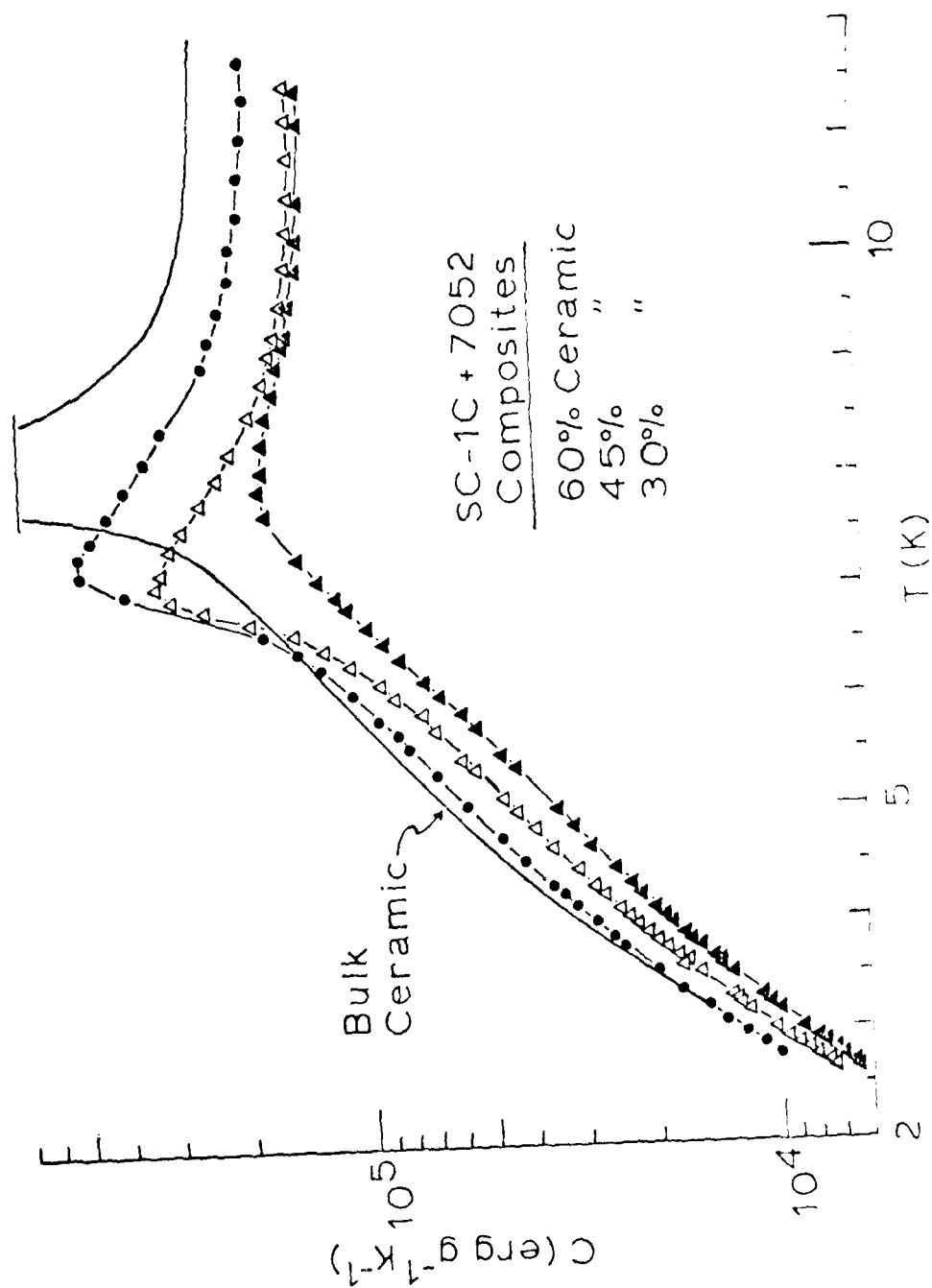


Figure 1. Specific heat  $C_p$  of SC-1C + 7052 composites at 0, 4, and 60 wt % ceramic. The curves are for composites with 0, 4, and 60 wt % ceramic. The curves are for composites with 0, 4, and 60 wt % ceramic.



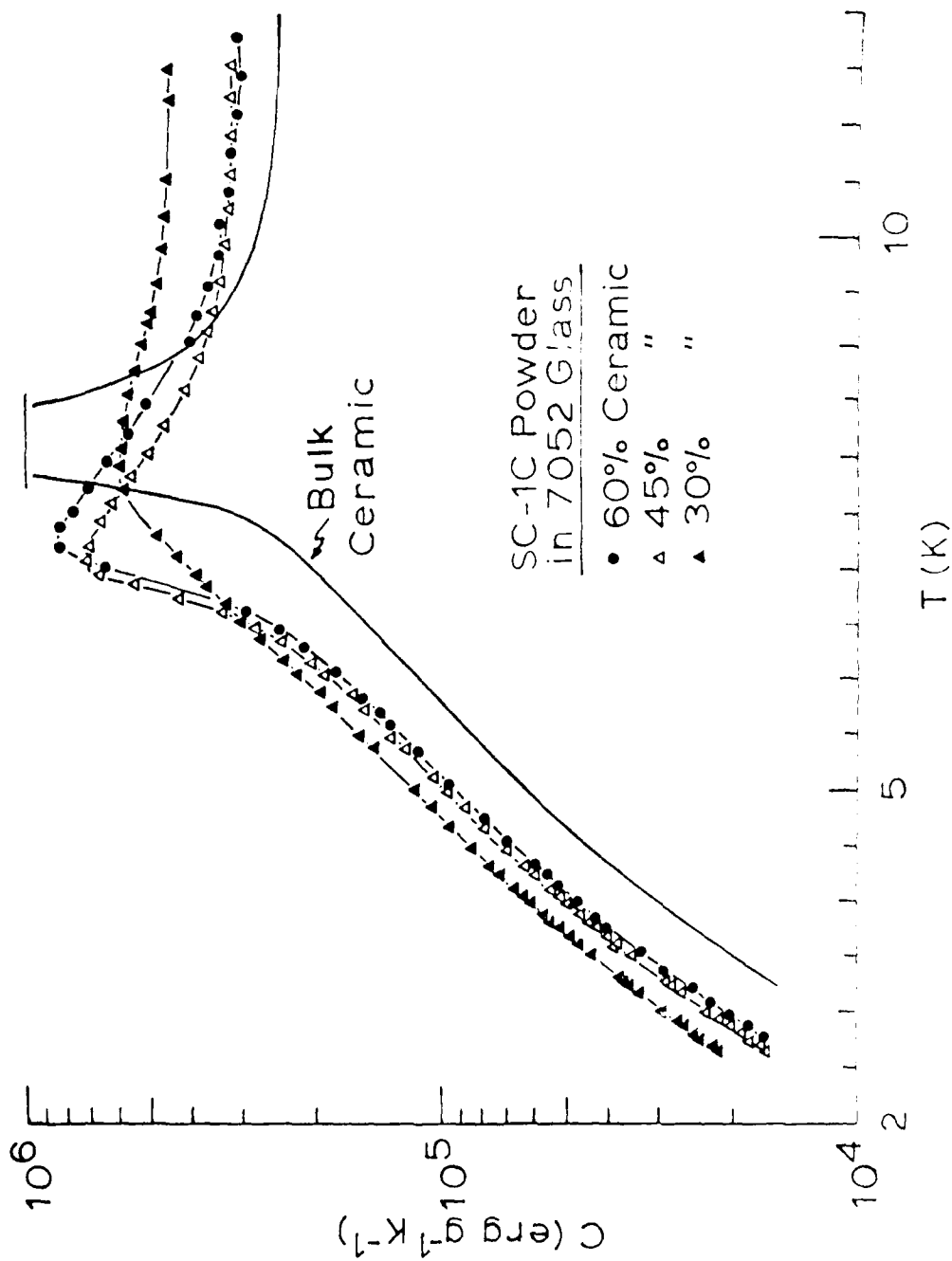
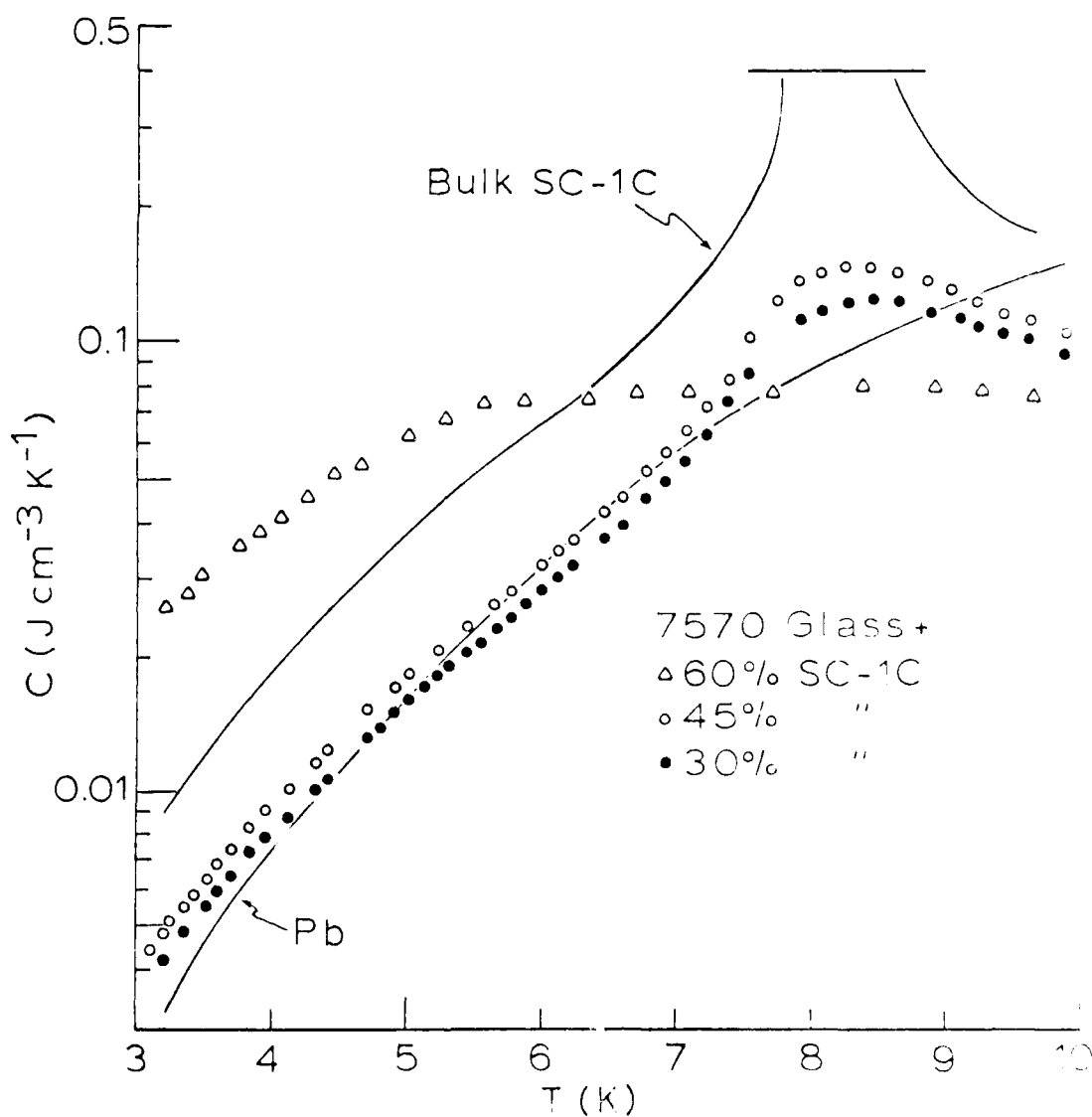


Figure 17. Specific heat for the SC-1C powder, glass, in the composition with 7052 glass, which that is low about 2 K. The peak in the 7052 glass matrix have very small contribution to the total specific heat with a small temperature.



**Figure 38.** Specific heat data for the SC-1C + 7570 composites at 30, 45, and 60 wt % of the ceramic powder. Also shown for comparison are specific heat data for the bulk SC-1C ceramic, and note that the 60% composite has a larger specific heat than the bulk ceramic below 6.5 K.

AD-A131 857

ENTHALPY - IMPROVED DIELECTRIC INSULATION FOR  
SUPERCONDUCTING WIRES(U) LAKE SHORE CRYOTRONICS INC  
WESTERVILLE OH W N LAWLESS ET AL. MAY 82

2/2

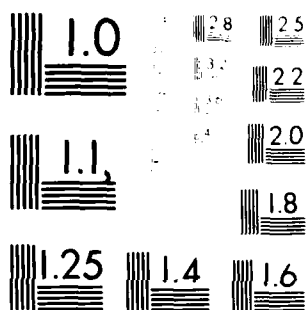
UNCLASSIFIED

AFWAL-TR-82-2056 F33615-80-C-2022

F/G 11/2

NL

END  
DATE  
FILMED  
9-83  
DTIC



MICROCOPY RESOLUTION TEST CHART  
NATIONAL BUREAU OF STANDARDS-1963-A

To appreciate the significance of the 60% composite data in Fig. 38, recall that the bulk SC-1C ceramic is quite refractory (1350°C sinter temperature) and so cannot be used directly as a wire coating but only in combination with a vehicle, such as glass. The significance here lies in that fact that, when combined with the 7570 glass vehicle, the resulting composite has a specific heat superior to that of the bulk ceramic below 6 K.

The results in Fig. 38 for the 60% composite were of such potential significance that it was decided to repeat the measurements. In any material having such a huge specific heat, thermal diffusivity within the sample can be problematic in a specific heat measurement. Consequently, great care was taken in the repeat measurements to leave no question as to thermal diffusivity: The original pellet was cut into quadrants on a diamond saw, copper foil was varnished to the cut surfaces, and the pellet was re-assembled with varnish. A duplicate pellet was similarly fixtured. The measurements made on these two pellets are shown in Fig. 39 and compared to the original-pellet data. As seen in Fig. 39, the favorable specific-heat phenomenon in the 60% SC-1C + 40% 7570 composite is reproducible.

Finally, as was done in the previous composites, the specific heats of the SC-1C powder only in the 7570 composites were determined, and these data are shown in Fig. 40. These data reveal a strong and favorable interaction between SC-1C and 7570 at all three mixing ratios, because in all cases the specific heat of the powder in the 7570 glass is larger than

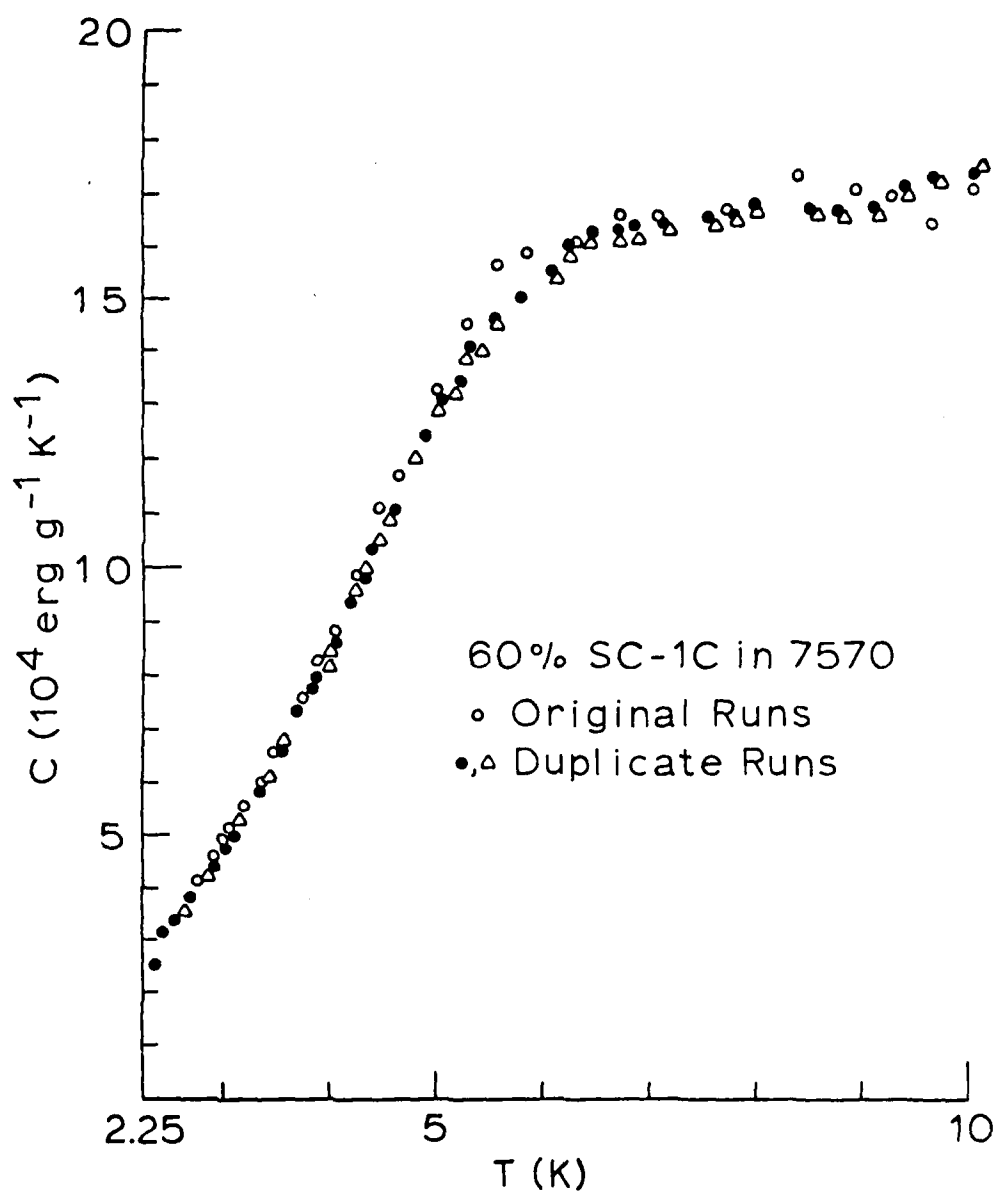


Figure 39. Repeatability of the specific heat data for the 60% SC-1C + 7570 composite.

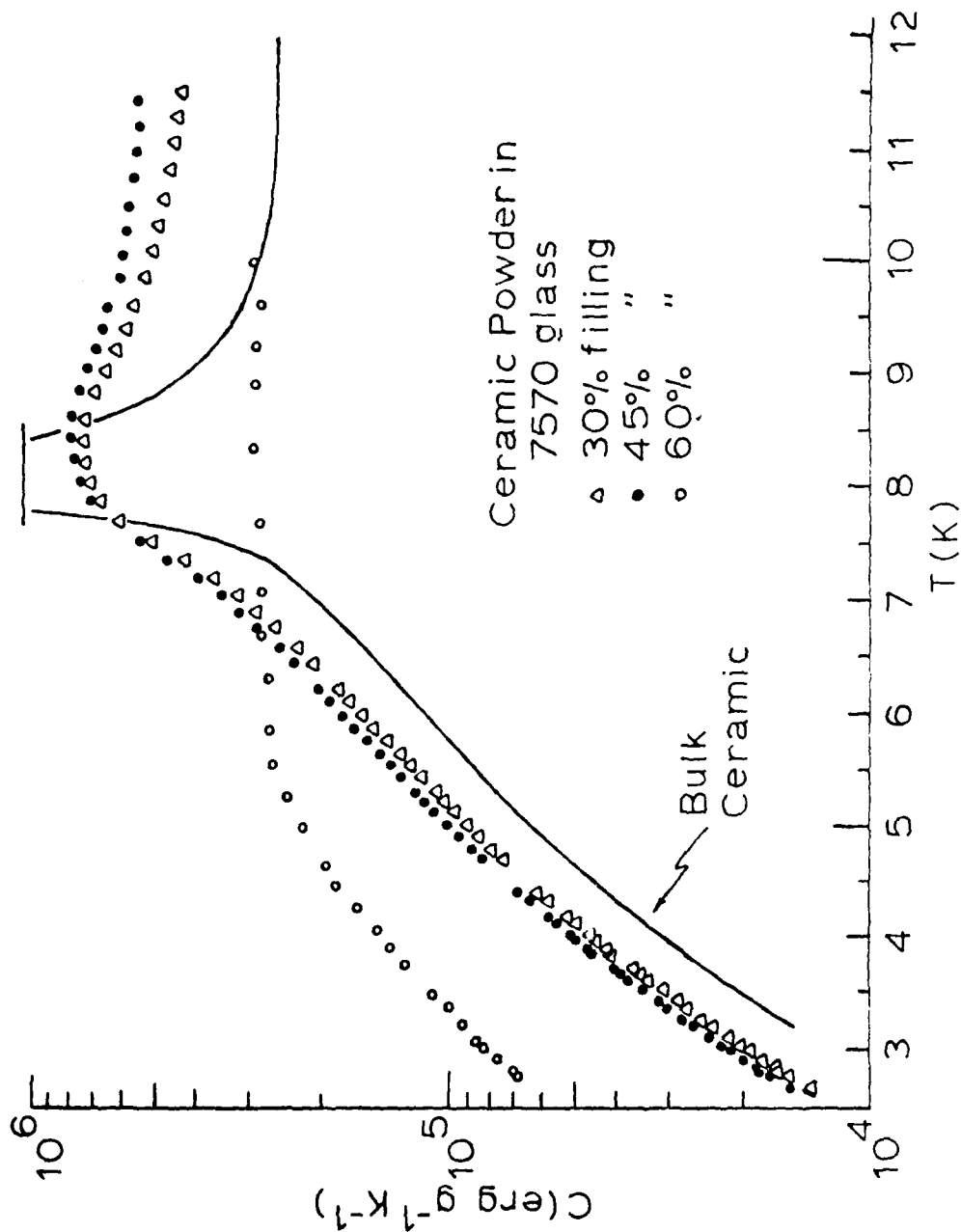


Figure 40. Specific heat data for the SC-1C powders alone in the composites with 7570 glass. Note that below about 7 K the powders in the 7570 glass matrix have larger specific heats than the bulk ceramic, indicating a solid-state reaction.

that of the bulk ceramic (except in the immediate neighborhood of the 8 K peak).

The specific heat data in Figs. 36 and 38 and the density data in Table 11 were used to calculate volumetric enthalpy data relative to 4.2 K, and these data are summarized in Table 12. As with the SC-1B composites above, only the 45 and 60% SC-1C composites were considered.

Table 12

Volumetric Enthalpies of the SC-1C + Glass Composites  
Relative to 4.2 K (in units of  $\text{mJ cm}^{-3}$ ) (a)

T (K)	7570 Glass +		7052 Glass +	
	45% Powder	60% Powder	45% Powder	60% Powder
5	11.36	43.3	7.35	8.83
6	35.98	113.8	24.20	28.34
7	81.08	190.4	67.75	76.43
8	180.7	269.2	146.4	188.6
9	324.0	349.6	200.1	265.3
10	439.4	428.9	243.1	321.3

(a) Zero Field

The large specific heat of the 60% SC-1C + 7570 composite (Fig. 38) is reflected in the enthalpy of this material in Table 12, and these are the largest volumetric enthalpy values determined in this program for a viable coating material (Note that the enthalpy values for SC-1A in Table 2 are larger than those for this composite, but, as with SC-1C, the SC-1A cannot be used as a coating directly but has to be incorporated in a vehicle.).



### Thermal Conductivity and Measurements (Zero-Field)

Thermal conductivity data measured on the SC-1C + glass composites at low temperatures are shown in Fig. 41. As was found above with the SC-1B composites (Fig. 35), the thermal conductivities of these SC-1C composites are also glasslike (i.e.,  $\lesssim 1 \text{ mW cm}^{-1} \text{ K}^{-1}$ ).

It is interesting to compare the SC-1B + 7570 and SC-1C + 7570 composites for connectivity (Recall that in all the composites with the 7570 glass, the vol. %'s of the ceramic powders are large enough to insure connectivity between the ceramic grains.). In the upper plot of Fig. 35, the thermal conductivity of the SC-1B + 7570 composites increases with increasing ceramic content; conversely, in the upper plot of Fig. 41, the thermal conductivity decreases. The explanation here is straightforward: From Fig. 5, the thermal conductivity of SC-1B is larger than that of the glass, while for SC-1C the opposite is true. Therefore, due to the connectivity between the ceramic grains, the thermal conductivities of these composites with 7570 follow the expected behavior based on the thermal conductivities of the bulk ceramics.

For both the SC-1B and SC-1C composites with 7052, the thermal conductivity decreases with increasing ceramic content (Figs. 35 and 41), but the effect is more pronounced with SC-1C.

There is some evidence for Kapitza resistance in the data for the 60% SC-1C + 7570 composite in Fig. 41. For example, at 5 K this composite has

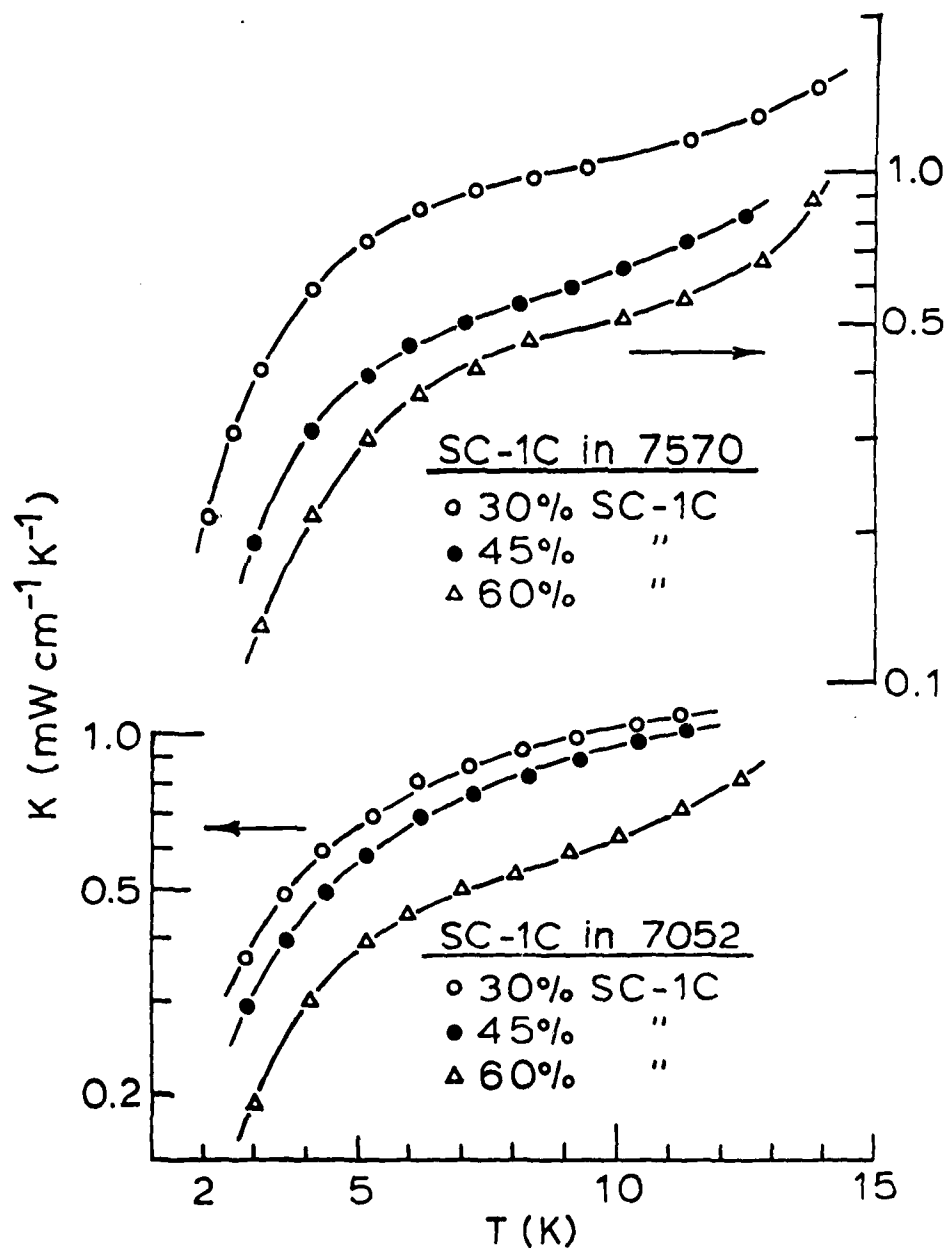


**Figure 41.** Thermal conductivities of the composites of SC-1C and 7570 glass (upper plot) and 7052 glass (lower plot).

a thermal conductivity  $\approx 0.3$ , compared to  $\approx 0.7$  for the bulk ceramic and  $\approx 1.0$  for the glass phase (in units of  $\text{mW cm}^{-1} \text{K}^{-1}$ ). This implies that there is an additional thermal resistance to the flow of heat in these composites.

Pursuing this further, thermal conductivity data on all the 7570 composites are shown in Fig. 42 at the lowest temperatures measured. There is intergranular connectivity in these composites, and all the data in Fig. 42 follow a  $T^m$  law, where  $m \approx 2$ . For two of the data sets, 30% and 60% SC-1C, several data points were measured below 4 K, and for these composites  $m = 1.67$  and  $1.88$ , respectively. It is in the temperature range below 4 K where all glasses display a  $T^2$  thermal conductivity, so one might conclude from the data in Fig. 42 that the glass phase in these composites dominates the thermal conductivity. However, were this the case, the thermal conductivity values in Fig. 42 would be up to an order of magnitude larger (see Fig. 5). On the other hand, the Kapitza resistance varies as  $T^{-n}$  with  $n \approx 2$  for dielectrics(23), and this suggests that the data in Fig. 42 are dominated by the Kapitza resistance (note that the thermal conductance is the inverse of the thermal resistance).

#### XI. WIRE COATING STUDIES (SC-2B on NbTi)

The SC-2 materials become ductile at temperatures above about  $350^\circ\text{C}$ , and it therefore seemed possible to hot-extrude these materials directly onto a wire without the use of an organic binder. The SC-2B material was

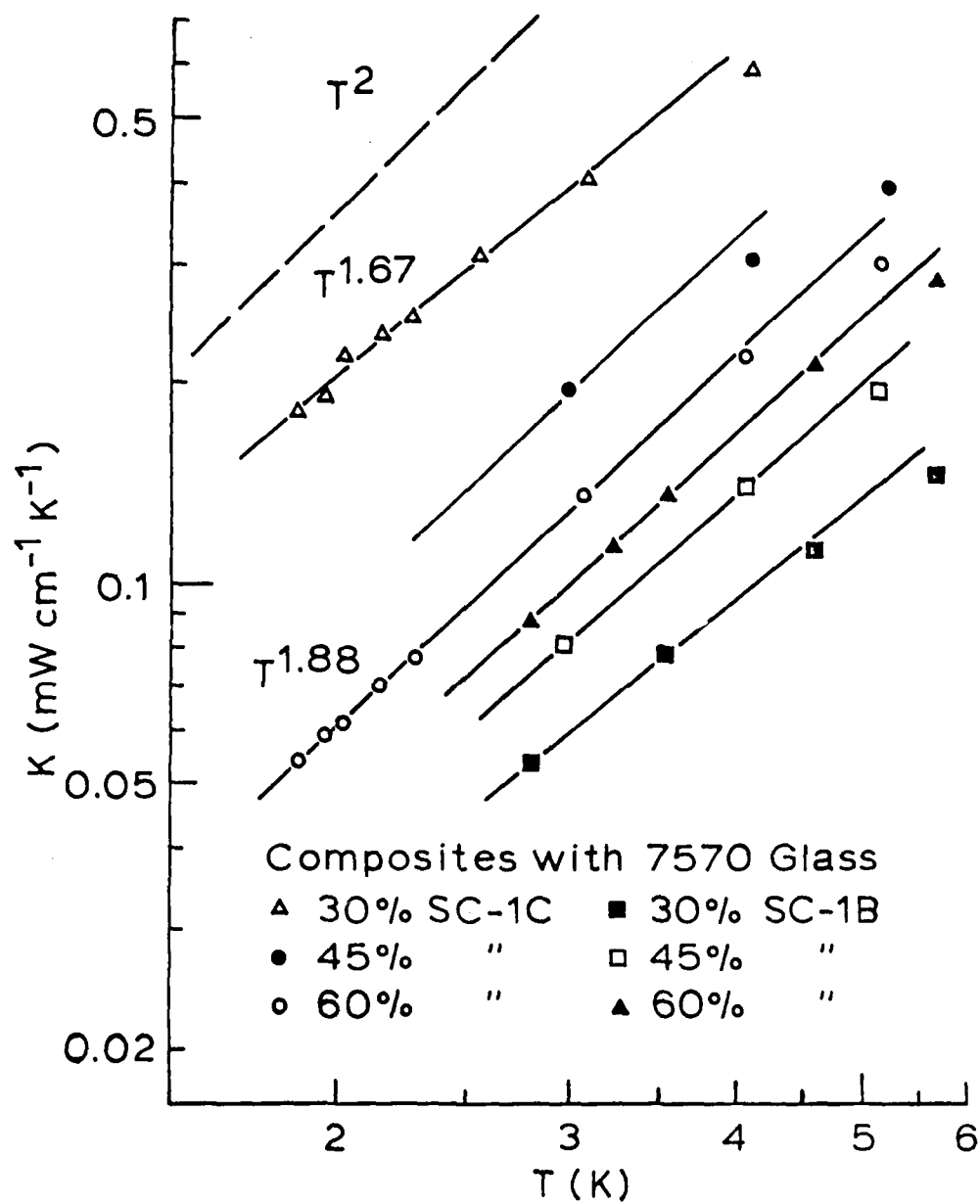


**Figure 42.** Thermal conductivities of the composites with 7570 glass at the lowest temperatures. The  $K \propto T^2$  trend in all the data suggests that Kapitza resistance may play a dominant role in the phonon transport through these composites.

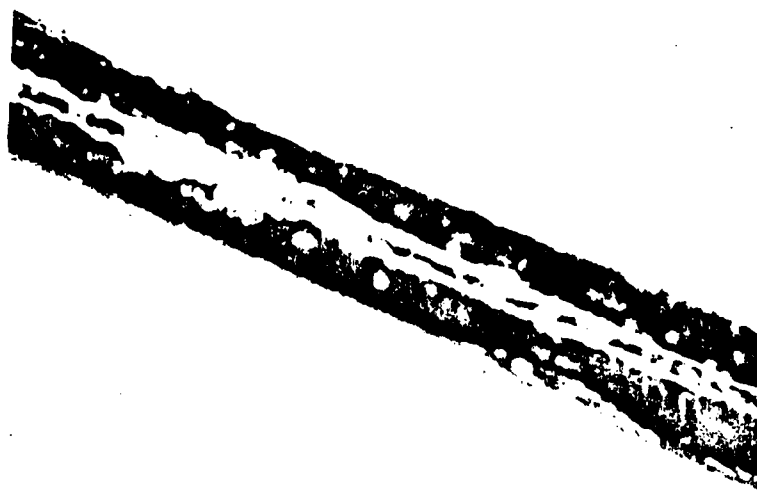
chosen for these studies because of its large specific heat (Fig. 15) and large thermal conductivity in thin sections (Fig. 18 and Table 3). These coating studies were subcontracted to Harshaw Chemical Co.

A 100-ft spool of NbTi wire was received from Intermagnetics General Corp. This was the so-called "BNL wire" and had an outside diam. 0.012". The coating on the wire was either a copper-nickel alloy or a cadmium alloy, but the coating effort did not allow a determination of this coating alloy.

In the initial coating studies, short sections of the wire were drawn through a melt of SC-2B, and the results were very favorable. In Fig. 43 are shown photographs of the coated wire (43a.) and of a 1" bend test (43b.). The SC-2B coating is about 0.0015" thick in the photographs, and there is no indication of damage to the coating in the bend test. Additional bend tests down to 1/8" showed that the coating adhered well and did not spall or flake off, although at a 1/8" bend the coating appeared to re-crystallize.

Attempts to draw longer lengths of the wire through molten SC-2B were not successful. The wire surface eventually darkened, and then the coating did not adhere. It was believed that the cadmium alloy on the wire surface was oxidizing, but performing the operation under a protective atmosphere (argon) did not alleviate the problem.

In the second coating study, the SC-1B material was hot-extruded onto



(a)



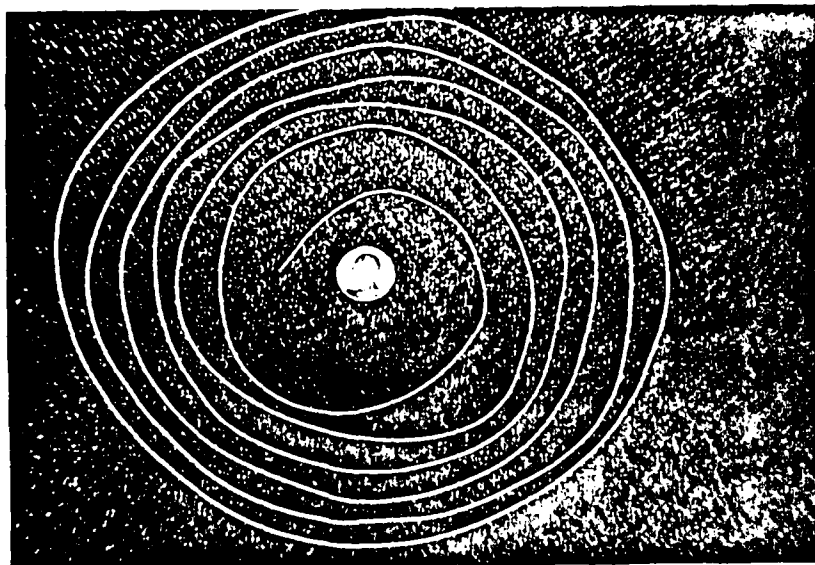
(b)

Figure 43. Photographs of short sections of NbTi wire (0.012" diam) coated with SC-2B (0.0015" thick): (a) Straight section; (b) 1" bend.

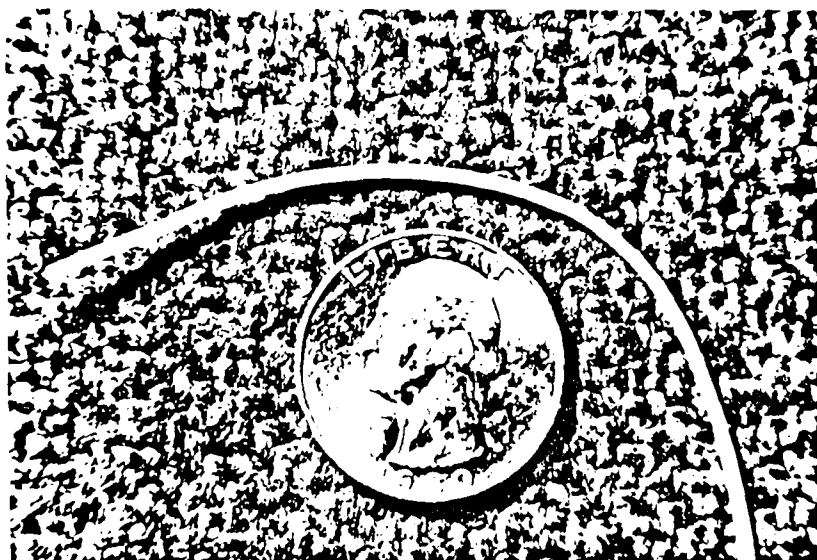
the NbTi wire. Here, a billet of SC-2B was loaded into an extrusion press, and the wire was passed through a hole in the billet along the center line. The diameter of the extrusion die was 0.050". A 16-ft section of the wire was continuously coated with this setup, and photographs of the coated wire are shown in Fig. 44. The SC-2B coating here was uniform, and there was no indication of a surface reaction on the wire.

The SC-2B coating on this 16-ft section was relatively very thin (0.019") due to the (available) die diameter, and there were indications that the coating adherence to the wire was inferior compared to the first coating attempts where the coating was much thinner (0.0015"). In particular, corona-discharge experiments at Wright-Patterson AFB revealed a gap between the wire and the thicker coating.

There are two problems involved here which these coating studies brought into focus: First, the as-received BNL wire had a metallic coating that was certainly not optimized for the SC-2B dielectric coating. And second, the compressibility of the dielectric here is much larger than that of the wire, so that in the extrusion process, which involves high pressures at the orifice of the die, the dielectric is considerably compressed. On exiting from the orifice, the dielectric relaxes, and a gap develops. This effect is magnified in thick coatings.



(a)



(b)

Figure 44. Photographs of a 16-ft section of NbTi wire (0.012" diam) coated continuously with SC-2B (0.019" thick) by a hot-extrusion process: (a) Entire 16-ft coil; (b) Approx.  $\frac{1}{2}$ " bend test.



## XII. CONCLUSIONS

In this report, a voluminous amount of new data on several, potential, dielectric-coating materials has been presented, the goal being to provide an experimental compendium of thermal properties for judging the practicality of these materials. In the course of these investigations, several new and intriguing phenomena have been uncovered, particularly in intense magnetic fields.

The experimental data measured on these materials can be encapsulated along two lines: (1) The volumetric enthalpies relative to 4.2 K; and (2) The thermal time constants relative to 5 K. The former quantity is a measure of the heat-storage capacity of a material; the latter quantity, a measure of how rapidly a material reaches steady-state following a temperature change.

The volumetric enthalpies are summarized in Table 13, where the materials are listed in order of descending enthalpy (at 5 K). Temperatures above 8 K are not considered in Table 13: The appropriate superconductors are listed in the table for easy reference, and enthalpy data for unfilled resins (Fig. 1) and for Pb are given for comparison. The data for resins were calculated from the specific heat data in Ref. 6, and the data for Pb were calculated from specific heat data for Pb measured (24) in the same calorimeter used here for the zero-field measurements.

Table 13

Volumetric Enthalpies ( $\text{mJ cm}^{-3}$ ) Relative to 4.2 K<sup>(a)</sup>

Material	Super-Conductor	5 K	6 K	7 K	8 K
Unfilled Resins	(NbTi)	3.98	13.02	28.26	49.96
Metallic Pb	(NbTi)	7.72	30.34	79.09	147.1
SC-1A(b)	-	60.94	121.1	-	-
60% SC-1C+7570	NbSn	43.3	113.8	190.4	269.2
SC-1C(b)	-	28.45	94.12	201.8	590.0
SC-1B(b)	-	19.75	49.38	84.97	127.9
60% SC-1B+7570	NbSn	19.30	64.88	96.20	121.9
SC-1C+7031	NbTi	18.80	54.58	116.9	310.9
SC-2B(c)	NbTi	15.32	50.53	104.1	178.6
60% SC-1B+7052	NbSn	13.23	44.65	63.80	78.79
45% SC-1B+7052	NbSn	12.12	39.50	57.56	72.38
45% SC-1C+7570	NbSn	11.36	35.98	81.08	180.7
SC-2C	NbTi	10.83	39.58	84.35	154.7
SC-2A	NbTi	10.65	36.47	79.86	144.6
SC-1D(b)	-	9.69	22.77	38.27	62.24
45% SC-1B+7570	NbSn	8.93	28.18	43.24	58.22
60% SC-1C+7052	NbSn	8.83	28.34	76.43	188.6
45% SC-1C+7052	NbSn	7.35	24.20	67.75	146.4
SC-3B(c)	NbSn	3.15	9.77	21.42	40.96
SC-3A	NbSn	2.10	7.20	16.37	31.80

<sup>(a)</sup> At zero magnetic field, unless noted otherwise<sup>(b)</sup> At 7.5 T<sup>(c)</sup> At 5.0 T

The ordering of the data in Table 13 according to the enthalpy at 5 K is, of course, an arbitrary selection, but in general the enthalpy data at the higher temperatures tend to scale with the 5 K enthalpy. The two exceptions are SC-1C and SC-1C + 7031 which have the largest enthalpies at 8 K (note, however, the SC-1C by itself is not a viable coating material).

The ordering of the data in Table 13 reveals some very significant experimental findings: The enthalpies of these new dielectric materials range up to an order of magnitude larger than that of the unfilled resins and up to five times larger than that of metallic Pb.

There are also some surprises in Table 13 which were unforeseen at the start of this program:

(1) On an enthalpy basis, the simple composite of SC-1C powder suspended in G.E. 7031 varnish appears to be the "best" coating for NbTi, followed closely by SC-2B (which was actually used in the NbTi-coating studies). We also note from Figs. 12 and 22 that the enthalpies of these two materials are very nearly independent of intense magnetic fields.

(2) The "best" NbSn coating is the 60% SC-1C + 7570 material which also turns out to be the best coating material in the table on an enthalpy-ordering basis.

(3) The SC-1B + glass composites in Table 13 appear very favorable for NbSn, also. However, in judging these composites, one must consider

that the enthalpy of bulk SC-1B is significantly depressed by intense magnetic fields (Fig. 9).

(4) The SC-3 materials rank last in the enthalpy table; however, these materials have thermal diffusivity advantages, which we consider next.

The enthalpy data in Table 13 tell only half the story. The thermal relaxation time measures how rapidly the coating reaches steady-state following a temperature rise in the wire. The maximum heat transfer through the coating takes place at steady-state, so the smaller the thermal relaxation time, the more rapidly will the heat generated in the wire be transmitted to the helium bath. Of course, the heat cannot be transmitted too rapidly, since otherwise deleterious film boiling will occur at the coating-helium interface. One must strive to arrange the heat transmitted through the coating such that nucleate boiling takes place at this interface, as this represents the best heat-transfer condition. This is obviously a complex problem involving the thermal properties of the coating (and the Kapitza resistances at the wire-coating and coating-helium interfaces, see below), and is beyond the scope of this study. What is clear, however, is that the thermal relaxation time ( $\tau$ ) of the coating plays a central role: If  $\tau$  is too large, nucleate-boiling is not achieved; if  $\tau$  is too small, film-boiling may occur.

The heat flow through a coating is a standard boundary-value problem in Fourier series(25), and whether one solves the cylindrical-coordinates,

Bessel function problem or approximates the coating by a slab, the transient solution always involves a characteristic time given by

$$\tau = d^2/a_j^2 k \quad (4)$$

where  $d$  is the coating thickness,  $k$  is the thermal diffusivity defined by Eq.(3), and  $a_j$  is an eigenvalue. For comparison purposes, it seems reasonable to take  $a_j = \pi$ , which corresponds to the leading term ( $j = 1$ ) in the solution of the heat flow in a slab. Note that the  $\tau$ -values given below could be used in the transient solution (cylinder or slab) which involves sums over terms containing  $\exp(-c_j t/\tau)$  terms where the  $c_j$  are just the ratios of the squares of the respective eigenvalues to  $\pi^2$ .

One must assume a reasonable coating thickness  $d$  in order to estimate  $\tau$ -values, and we will select  $d = 0.127$  mm (0.005") as a reasonable value. Note that this assumed  $d$ -value is smaller than some of the  $\lambda_b$ -values in Table 3 and 5, and this introduces a subtlety in determining the thermal conductivity,  $K$ , which enters Eq.(3). Taking SC-2A as an example,  $\lambda_b$  from Table 3 is 0.18 mm, so for a 0.127 mm thickness,  $K$  in the  $T^3$  limit will be  $0.127/0.18 = 0.71$  times the  $K$  given in Fig. 17. This follows directly from Eq.(2) for  $d < \lambda_b$ . The procedure then is to draw a line parallel to the  $T^3$  line in Fig. 17 at 71% of the measured value, and from this line the estimated  $K$ -value is found at various temperatures. This procedure applies to SC-2A (Table 3) and to the SC-3 type materials (Table 5). For these estimates we will ignore the magnetic-field dependence of the thermal

conductivity of SC-2A and -2B (Fig. 23) and of SC-3A (Fig. 28). Note that in the case of SC-3A, the dramatic maximum in the thermal conductivity at  $\sim 8$  T (Fig. 28) would tend to compensate the  $d < \lambda_D$  effect mentioned above; however, the temperature of the (isothermal) measurements in Fig. 28 is considerably higher than the  $T^3$ -regime range for this material.

For the lower thermal-conductivity materials, we will continue to assume that the thermal conductivities are magnetic-field-independent for the reasons discussed above.

For the specific-heat data entering Eq.(3), we will continue to use the magnetic-field data quoted in Table 13. Going further, we can estimate the enthalpy per unit length, given  $d = 0.127$  mm and adopting the diameter of the BNL NbTi wire, 0.305 mm (i.e., coating volume =  $7.35 \times 10^{-4}$  cm<sup>3</sup> per unit length). This estimate can be made directly from Table 13.

Finally, then, listed in Table 14 are the thermal diffusivity data from Eq.(3) at 5 K, the thermal relaxation times from Eq.(4) at 5 K (with  $a_j = \pi$ ), and the enthalpy-per-unit-length data at 6 and 8 K, for each of the materials in Table 13. The Table 14 materials are ordered on the basis of increasing thermal relaxation time. Also listed in Table 14 for convenience are the appropriate superconductors.

Table 14

Thermal Parameters for a Hypothetical Coating  
0.127 mm (0.005") thick(a)

Material	Super-Conductor	k(5K) (cm <sup>2</sup> /s)	$\tau$ (5K) ( $\mu$ s)	Enthalpy per unit length ( $\mu$ J)	
				6 K	8 K
Unfilled Resins	(NbTi)	0.123	133	9.6	36.7
Metallic Pb	(NbTi)	42	0.39	22.3	108.1
SC-3B(b)	NbSn	375	0.044	7.2	30.1
SC-3A	NbSn	348	0.047	5.3	23.4
SC-2A	NbTi	82	0.20	26.8	106.3
SC-2B(b)	NbTi	67	0.24	37.2	131.3
SC-2C	NbTi	24	0.69	29.1	113.7
SC-1D(c)	-	0.12	138	16.7	45.8
SC-1B(c)	-	0.094	173	36.3	94.0
SC-1A(c)	-	0.081	203	89.0	-
45% SC-1C+7052	NbSn	0.046	353	17.8	107.6
45% SC-1B+7052	NbSn	0.033	490	29.0	53.2
60% SC-1C+7052	NbSn	0.028	592	20.8	138.6
60% SC-1B+7052	NbSn	0.023	711	32.8	57.9
45% SC-1C+7570	NbSn	0.021	796	26.4	132.8
SC-1C(c)	-	0.014	1132	69.2	433.7
45% SC-1B+7570	NbSn	0.0136	1201	20.7	42.8
60% SC-1B+7570	NbSn	0.0080	2054	47.7	89.6
SC-1C+7031	NbTi	0.0064	2538	40.1	228.6
60% SC-1C+7570	NbSn	0.0046	3545	83.7	197.9

(a) At zero field unless noted otherwise

(b) At 5.0 T

(c) At 7.5 T

The  $\tau$ -ordering of the materials in Table 14 is qualitatively just the opposite of the enthalpy-ordering in Table 13, and the  $\tau$ -values in Table 14 span six orders of magnitude.

There appears to be a general relationship between the enthalpy and  $\tau$ -values in Table 14, and in Fig. 45 are plotted  $\tau$ -values and enthalpies-per-unit-length at 6 K for all the materials in this program. The Fig. 45 data reveal that the materials group into two categories: "Pb-like" with  $\tau < 1 \mu\text{s}$ ; and "resin-like" with  $\tau > 100 \mu\text{s}$ . For the former category, there appear to be logarithmic relationships between  $\tau$  and enthalpy, as indicated by the dashed lines in Fig. 45.

The Fig. 45 data summarize somewhat all the materials measured in this program. It is clear that all of these coating materials offer enthalpy-stabilization properties superior to resins (except for SC-3A and -3B) and, in most cases, superior to Pb, also.

Finally, we can draw the following conclusions from this study:

(1) Several potential dielectric coatings for superconducting wires, switches, etc. have been demonstrated in this program. These materials cover a broad range of thermal time constants (0.04 to 3500  $\mu\text{s}$ ) and enthalpies (equivalent to Pb ranging up to about five times larger than Pb).

(2) The most attractive coatings for NbTi appear to be SC-2B and a



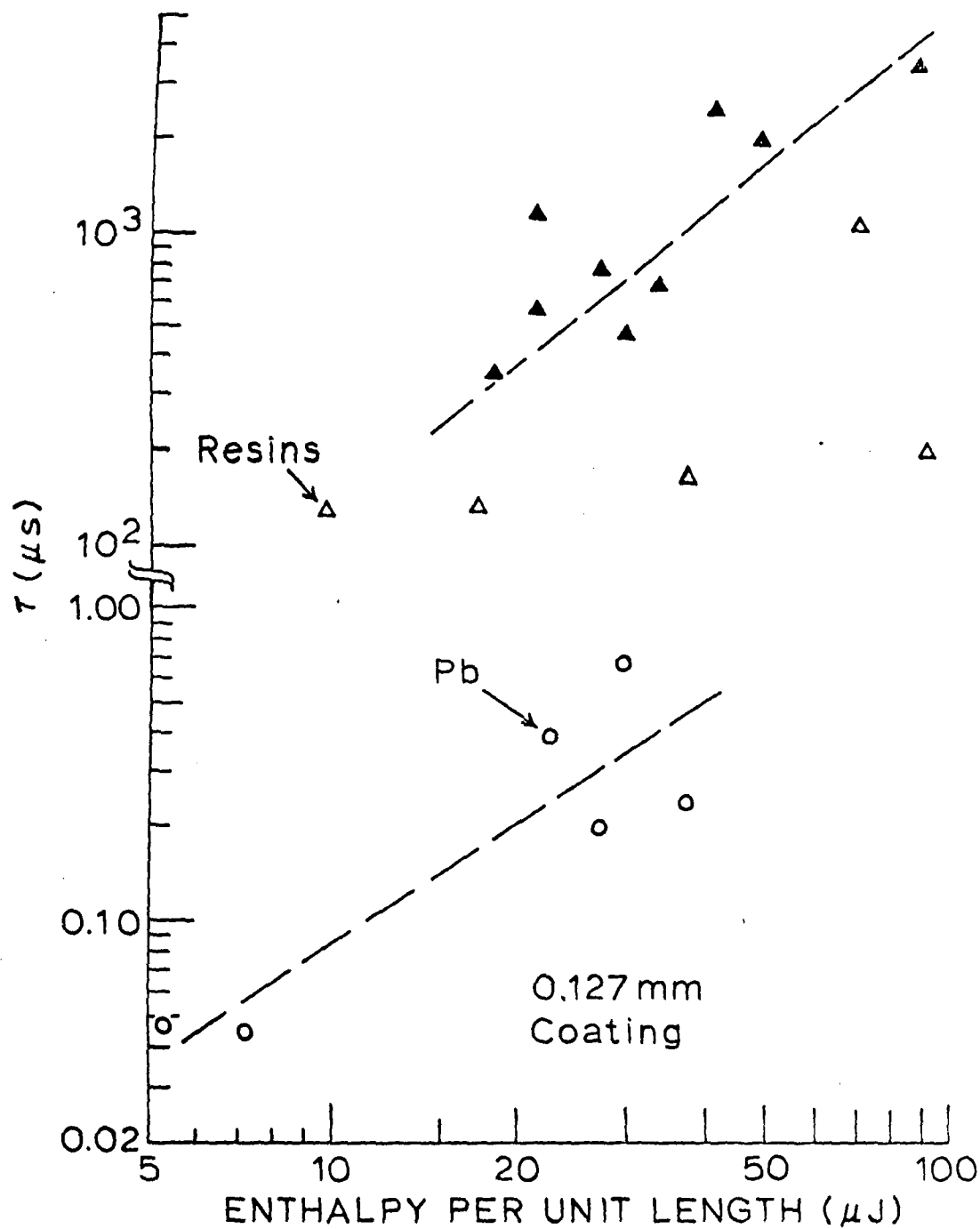


**Figure 45.** Plot of thermal relaxation time versus enthalpy per unit length for a 0.127 mm thick coating for all the materials studied (taken from Table 14). The materials fall into two categories: "Pb-like" and "resin-like."

composite of SC-1C + 7031 varnish. The former material has been coated on a NbTi wire by a hot extrusion process, and it has been demonstrated that the latter material lends itself to a dip-coating process.

(3) The most attractive coatings for NbSn appear to be the ceramic + glass composites, in particular the SC-1C + 7570 composites. The SC-1B + glass composites have attractive zero-field properties, but there is evidence (Fig. 8) that the specific heat of SC-1B is seriously depressed by an intense magnetic field.

(4) The thermal properties of the most important materials in this program are not degraded by intense magnetic fields: SC-1C (Figs. 10,12); SC-2A (Figs. 1-,23); and SC-2B (Figs. 21,23). There is also evidence that the near-metallic thermal conductivity of the latter two materials is not degraded on going to thin sections ( $\sim 0.1$ - $0.2$  mm, Table 3).

(5) There is solid-state reaction between the 7570 glass and both SC-1B (Fig. 33) and SC-1C (Fig. 40). The 7052 glass also reacts with SC-1C (Fig. 37), and in the case of SC-1C these reactions lead to enhanced specific heat properties.

(6) The ceramic + glass composites all have long thermal relaxation time constants (353 to 3545  $\mu$ s, Table 14), and there is evidence that the dominant contribution to these time constants is the Kapitza resistance within the composite.

(7) The SC-1A material has not received much attention in this study, but it has been found experimentally here that this material deserves further investigation: (a) The effect of an intense magnetic field is to increase the specific heat at 4.2 K (Fig. 6); (b) The enthalpy of this material at 6 K and 7.5 T is the largest of any material in the program (Table 13); and (c) The thermal conductivity is the largest of the SC-1 class of materials (Fig. 5).

(8) Several new and unusual effects have been discovered in intense magnetic fields: (a) The specific heat of the chromite spinel in SC-1C develops sideband structure (Fig. 11) in contrast to the chromite spinel in SC-1D (Fig. 13); and (b) The thermal conductivities of SC-2A, -2B, and SC-3A show H-field dependences (Figs. 23 and 28) despite the fact that these materials are alkali-halide-like.

(9) Several ancillary studies have been, or will be, published from this program: (a) The addendum heat capacity of the capacitance thermometer (14); (b) Thermal properties of carbon-impregnated porous glass(22); (c) Thermal conductivity and electrical resistivity of copper in intense magnetic fields(16); and (d) Method for measuring specific heats in intense magnetic fields [Appendix A1](15).

### XIII. RECOMMENDATIONS

In a study involving several new materials and several phenomena, all of which are in a pioneering vein of sorts, it is by no means straight-

forward to set priorities on subsequent studies. The specific areas for future studies can, however, be identified, and these fall into two categories: Applied Materials' Research, and Basic Materials' Research.

#### Applied Materials' Research Areas

Thermal expansion measurements and dielectric breakdown measurements (4.2 K) are needed on the most promising coating materials. For very thin coatings, however, thermal expansion mismatches may not be a problem due to the "Housekeeper's seal" effect which is well-known in glass-to-metal seals.

The solid-state reactions between SC-1C and the 7052 and 7570 glasses (Figs. 37 and 40) deserve further investigation, as one intuitively suspects that the ideal coating for NbSn will result from these systems. The nature of these reactions should be explored by making additional samples in, say, the 45 to 75% ceramic range and performing X-ray analyses, scanning-electron-microscopy, etc. Measurements of the thermal properties of such composites in intense magnetic fields are also needed to determine if these reactions are altering the magnetic-field-insensitivity of the specific heat of SC-1C (Fig. 10).

Along this line, it seems clear that the thermal conductivities of the ceramic + glass composites may be too small for several applications. One approach to improving the thermal conductivities is to add alumina powder at  $\approx 33$  vol. % to insure connectivity, and it would be worthwhile

to see if the favorable reaction between SC-1C and 7570 (Fig. 40) could be preserved in such composites. Such a three-component composite would most probably have a lowered specific heat, but this may be a small price to pay to gain the improved thermal conductivity and thereby a smaller thermal relaxation time.

Composites of SC-1A and 7052 now appear to be very promising: Presumably there would be no unfavorable reaction between the ceramic and the glass based on Fig. 34 (note that SC-1A and SC-1B are single-phase, columbite structures), and the large thermal conductivity of SC-1A (Fig. 5) may lead to large composite thermal conductivities provided the vol. % of SC-1A is large (see Table 9 and Fig. 35).

Additional experience is now needed in coating NbTi and NbSn with these materials, the eventual goal being to wrap a test coil. Several development efforts would constitute such a program, and one of the most important ingredients will be to devise appropriate intermediate coatings between the superconductor and the dielectric to achieve good adhesion.

Last, but certainly not least, is the need to develop a transient-heating model that will allow one to make judgements regarding the plethora of specific heat and thermal conductivity data reported here on these various coating materials. Such a model is being developed currently by Lt. S. Holmes at WPAFB. In this same vein, planar-geometry heat-transfer samples similar to those studied by Iwasa and Apgar(26) are

needed to perform experiments to check the model. Such samples should be coated with some of the dielectrics reported here, and in fact such samples coated with SC-2A, -2B, SC-1C + 7031, and 60% SC-1C + 7570 are in preparation for delivery to WPAFB.

#### Basic Materials' Research Areas

The role of Kapitza resistance in these dielectric coatings cannot be overemphasized, nor can the fact that it is poorly understood. Kapitza resistance occurs at the boundary between two dissimilar substances due to acoustic-phonon mismatch, and we have three interfaces to consider: between the superconductor and the coating; between the coating and liquid helium; and, in the case of composites, between the ceramic particles and the glass or varnish matrix. We have seen evidence in these studies that Kapitza resistance dominates the thermal conductivity of the composites (e.g., Fig. 42).

Very little work has been published on these three types of Kapitza resistances involving dielectric materials, and a substantial basic program could be involved here. The scope of such a program should also include measurements in intense magnetic fields.

The chromite spinels in SC-1C and -1D are new spinels which have not been investigated from a basic-physics viewpoint, to our knowledge. Because of their very large specific heats, these materials are also being studied as regenerator matrix materials for Stirling cycle cryocoolers(7), yet,

incredibly enough, their magnetic susceptibilities have not yet been measured at low temperatures. The magnetic-field-induced structure in the specific heat of SC-1C (Fig. 11) is a ripe area for further study. Moreover, there is some evidence(7) that SC-1C may be ferroelectric, and this may be the explanation for the very large specific heat of this material: There would then be three contributions to the specific heat -- the Debye background plus the "ferroelectric" mode(4) plus the magnetic contribution. Basic studies of these spinels should involve single crystals and measurements of both ferroelectric and magnetic properties, including measurements in intense magnetic and electric fields. We remark here that the presumed magneto-electric coupling in these spinels could in itself prove to be a very fruitful area of research.

The SC-2 and SC-3 materials are poorly understood, in particular as regards the "ferroelectric" modes in the SC-2 materials (Fig. 15) and the very practical thermal conductivities of the SC-2 materials (Figs. 17 and 18). One can ask what small geometric entities in the SC-2 materials are controlling the  $T^3$ -boundary scattering and how might these entities be controlled. The effects of intense magnetic fields on the thermal conductivities of SC-2A and -2B (Fig. 23) and SC-3A (Fig. 28) were completely unexpected and appear to be real effects. Based on the slight decrease in the specific heats of SC-2A and -2B with intense fields (Figs. 19 and 21), one would expect a correspondingly slight depression in the thermal conductivities based on thermodynamic considerations, such as occurs in SC-2A (Fig. 23). The thermal conductivities of SC-2B (Fig. 23) and

SC-3A (Fig. 28) are completely anomalous. In particular, the strong maximum in the thermal conductivity of SC-3A at 9T deserves further studies at other temperatures; unfortunately, the specific heat of SC-3A was not measured in intense fields in this study, and these measurements should also be pursued.



## System Safety Hazard Analysis Report

### SC-1 Class of Insulations

This class of materials are refractory oxides which are formed into solid bodies by conventional ceramic methods at temperatures near 1300°C. These ceramics in powder form are subsequently mixed into appropriate vehicles such as epoxies, varnishes, or glasses for application to superconducting wires. Consequently, the only safety hazard that is posed occurs during the 1300°C ceramic process which is conventionally carried out in a furnace with appropriate fume control. The hazard results from possible toxic gases emanating from the ceramics.

SC-1A. No hazard

SC-1B. No hazard

SC-1C. This material contains cadmium, so there is a potential hazard in firing this ceramic due to cadmium vapor if adequate fume control measures are not taken. The recommended maximum allowable (8-hr-day) concentration of cadmium vapor in air is 0.1 mg/m<sup>2</sup>. We point out, however, that cadmium loss is detrimental to the physical properties of this ceramic, so the ceramic is always sintered in a tight enclosure to eliminate cadmium loss as a practical matter.

SC-1D. No hazard

### SC-2 Class of Insulations

This class of materials are intended to be applied to superconducting wires by either a hot extrusion process or drawing through a melt. All of the SC-2 materials contain thallium, so there is the hazard of heavy-metal toxicity and these materials must be handled with care (See "Occupational Diseases - A Guide to Their Recognition" - Rev. Ed. June, 1977; USDHEW Emergency & First Aid Procedures). The threshold limit value of thallous halides is 0.1 mg/m<sup>3</sup>. Handling of thallous compounds may be a skin irritant and sensitizer, and for skin contact the affected area should be washed

thoroughly with soap and water. With any cutting or grinding operation, a local exhaust should be used to maintain exposure below the threshold value. Dust and cutting chips should be vacuumed promptly. At temperatures between about 500-600°F, these materials will volatilize thallium compounds, so any melt or extrusion operations should be done with appropriate fume control. If ventilation is inadequate, NIOSH/MESA approved respiratory protection should be used [see DHEW (NIOSH) Publication #77-159, Data Sheet #S306].

SC-3 Class of Insulations

No hazard.

#### REFERENCES

- (1) For a discussion of enthalpy stabilization in magnets, see R. Hancox, Proc. 2nd Int'l Conf. on Magnet Tech., Oxford (1967); and H.R. Hart, Jr., GE Publ. 68-1.-297 (1968).
- (2) R. Hancox, IEEE Trans. on Magnetics, vol. mag. -4, no. 3, pg. 486 (1968).
- (3) S.S. Rosenblum, H. Sheinberg, and W.A. Steyert, IEEE Trans. on Magnetics, vol. mag. -13, no. 1, pg. 834 (1977).
- (4) W.N. Lawless, Ferroelectrics 17, 341 (1977); Phys. Rev. Lett. 36, 478 (1976); Phys. Rev. B14, 134 (1976); Ferroelectrics 15, 61 (1977); Phys. Rev. B16, 433 (1977); Phys. Rev. B17, 1458 (1978); Phys. Rev. B18, 2394 (1978).
- (5) W.N. Lawless and A.C. Anderson, Phys. Rev. B23, 3886 (1981); Ferroelectrics 37, 627 (1981).
- (6) G. Hartwig, Paper U-9, 1975 Cryo Eng. Conf., Queen's Univ., Kingston, Ontario.
- (7) W.N. Lawless, Final Report, NBS Contract NB81RAC10007, "High Specific Heat Ceramics for Cryocooler Regenerator Applications," Dec. 1981.
- (8) W.N. Lawless, Cryogenics 15, 273 (1975).
- (9) W.N. Lawless, Rev. Sci. Instrum. 48, 361 (1977).
- (10) W.N. Lawless, Rev. Sci. Instrum. 42, 561 (1971).
- (11) L.G. Rubin and W.N. Lawless, Rev. Sci. Instrum. 42, 571 (1971).
- (12) W.N. Lawless, Rev. Sci. Instrum. 46, 625 (1975).
- (13) W.N. Lawless and E.A. Panchyk, Cryogenics 12, 196 (1972).
- (14) W.N. Lawless, Rev. Sci. Instrum. 51, 1567 (1980).
- (15) W.N. Lawless, C.F. Clark, and R.W. Arenz, Rev. Sci. Instrum. (in press).
- (16) R.W. Arenz, C.F. Clark, and W.N. Lawless, Phys. Rev. B (in press).
- (17) K.W. Garrett and H.M. Rosenberg, J. Phys. D: Appl. Phys. 7, 1247 (1974).

- (18) G.E. Childs, L.J. Ericks, and R.L. Powell, NBS Monograph 131, Nat'l Bureau St'ds, Boulder, Sept. 1973.
- (19) W.N. Lawless (unpublished data).
- (20) J.L. Cude and L. Finegold, Cryogenics 11, 394 (1971).
- (21) W.N. Lawless, Rev. Sci. Instrum. 43, 1743 (1972).
- (22) W.N. Lawless, Rev. Sci. Instrum. 52, 727 (1981).
- (23) N.S. Snyder, Cryogenics 10, (1970).
- (24) W.N. Lawless, J. Low Temp. Physics 41, 339 (1980).
- (25) R.V. Churchill, Fourier Series and Boundary Value Problems (McGraw-Hill, New York, 1941).
- (26) Y. Iwasa and B.A. Apgar, Cryogenics May 1978, p. 267.

APPENDIX A1

Method for Measuring Specific Heats  
in Intense Magnetic Fields at Low  
Temperatures using Capacitance Thermometry

Method for Measuring Specific Heats  
in Intense Magnetic Fields at Low  
Temperatures using Capacitance Thermometry<sup>(a)</sup>

by

W.N. Lawless, C.F. Clark, and R.W. Arenz  
CeramPhysics, Inc., Westerville, Ohio 43081

(Abstract)

A drift method is described for measuring specific heats in intense magnetic fields at low temperatures. Capacitance thermometry is used, and an automated data-collection system utilizes the imbalance of a transformer-ratio-arm bridge to process the capacitance data. The zero-field specific heat must be known, and measurement of the in situ drift in zero-field calibrates the thermal link. Additional calibration of the link is required if the link's magneto-thermal conductivity effects are significant, and a specific example of a copper-wire link is presented. The method resolves complex structure in the specific heat near a steep  $\lambda$ -type anomaly, as illustrated by measurements on a chromite spinel at 7.5 T. The uncertainty in the method is estimated to be  $\approx \pm 7\%$ .

## INTRODUCTION

Calorimetry in intense magnetic fields at low temperatures generally involves resistance thermometers.<sup>1</sup> The magnetoresistance of these thermometers is handled either by calibrating the magnetoresistive effect or by locating the thermometer out of the field region (e.g., coupling the sample and thermometer by a long Au wire). The capacitance thermometer<sup>2</sup> is unaffected by intense fields,<sup>3</sup> yet except for brief mention by Pratt *et al.*<sup>4</sup> there appears to have been no effort to use capacitance thermometry in magnetic-field calorimetry. There are probably two reasons for this: First, unencapsulated capacitor units are somewhat large ( $0.16 \times 0.16 \times 0.77 \text{ cm}^3$ , 82 mg) and so could constitute a large addendum; and second, a transient ( $\sim 30 \text{ min}$ ) drift in this thermometer at low temperatures<sup>5</sup> and poor reproducibility necessitates calibrating the unit each run.

The need to perform specific heat measurements in intense fields at low temperatures on ceramics of potential use as dielectric insulation materials for superconductors led us to develop a calorimetric method using capacitance thermometry. The purpose of this paper is to describe this method. In our case, samples could be made of any size, and these ceramics have very large specific heats at low temperatures ( $\sim 0.1 \text{ J g}^{-1} \text{ K}^{-1}$ ) so the addenda correction is very small. Pursuant to this method, the addendum heat capacity of the (unencapsulated) capacitance thermometer was recently published.<sup>6</sup> The method reported here is a version of the so-called "calibrated-wire" technique wherein the sample slowly drifts in temperature from 20 to 3 K in an intense H-field. Three samples per run could be measured in a 14 T Bitter magnet, and the data collection was automated.

## EXPERIMENTAL METHODS

The basic scheme of the method is to arrange the sample to drift slowly in temperature between about 20 and 3 K and to convert the resulting capacitance-time data to specific heat-temperature data. In this section, we will first describe the theory of the method followed by a description of the experimental techniques and the data-collection system.

### Theory of the Method

Consider a sample of total heat capacity  $\mathcal{C}$  coupled to a reservoir through a (dominant) thermal link of thermal conductance  $G$ . If at time  $t$  the sample temperature is  $T$  and the reservoir temperature is  $T_0$ , then in a time interval  $dt$  the sample temperature will change an amount  $dT$  according to

$$\mathcal{C}_H (dT/dt) = -G_H (T - T_0) \quad (1)$$

provided there is no power flow to the sample. The subscript  $H$  refers to the magnetic field intensity. Strictly speaking,  $G_H$  is a function of  $T$ ,  $T_0$ , and  $H$ , depending on the thermal link, and we shall return to this point in detail below.

For convenience, define

$$\phi_H = -(T - T_0) / (dT/dt) \quad (2)$$

so that

$$\mathcal{C}_H = \phi_H G_H. \quad (3)$$

The heat capacity has two contributions,

$$\mathcal{C}_H = m_s C_H + a(T), \quad (4)$$

where  $m_s$  and  $C_H$  are the mass and specific heat of the sample, respectively, and  $a(T)$  is the total addenda contribution. Assuming that the addenda are field-independent, Eqs.(3) and (4) yield

$$C_0 - C_H = [C_0 + a(T)/m_s] (1 - \beta_H \phi_H / \phi_0) \quad (5)$$

for the field-dependent specific heat,  $C_H$ , relative to the zero-field



specific heat,  $C_0$ . Here,  $\beta_H$  is the parameter which calibrates the H-field dependence of the thermal link,

$$\beta_H = C_H/C_0 \quad (6)$$

Consequently, if  $C_0$  and  $\beta_H$  are known, Eq.(5) relates  $C_H$  to the zero-field drift data,  $\phi_0$ , and to the drift data in an intense field,  $\phi_H$ . In our case here,  $C_0$  was measured on the same samples in a conventional calorimeter described elsewhere.<sup>7</sup>

#### Experimental Techniques

A schematic drawing of the experimental arrangement is shown in Fig. 1. The sample (1) in the form of a pellet ( $\sim 1$  cm diam) is thermally linked to a copper reservoir (6) by a spiralled copper link (5), 0.07 mm diam, oriented so the axis of the spiral is parallel to the magnetic field. This copper link is the dominant thermal link, and the very large specific heat of our ceramic samples necessitated using a copper link. This complicated the link calibration,  $\beta_H$ , as will be seen below; for samples with smaller specific heats, a more convenient manganin link would suffice.

A second, mechanical link (4), 0.13 mm diam manganin wire, was wrapped around the sample. Both links, (4) and (5), were indium-soldered to a copper post (3) mounted in the reservoir (6). The mechanical link (4) wrapped tightly on the sample was particularly necessary in the case of samples containing paramagnetic ions to provide mechanical stability when changing field strengths.

The pellet sample (1) was grooved to accept the capacitance-thermometer element (2) to provide good thermal diffusivity, and the thermometer leads were tempered to the sample. It was determined in zero-field drifts that with this arrangement there was a negligible difference ( $< 10$  mK) between the sample temperature and the thermometer temperature for drift rates as high as 10 mK/sec, even in the case of a chromite spinel with a very large

specific heat maximum at 7.99 K (see below).

Each sample was outfitted with a manganin heater (7),  $\sim 200\Omega$ , and G.E. 7031 varnish was used in the sample assembly (The sample heater was used for convenience only, see below.). All sample hook-up leads were 0.03 mm diam manganin wires. Addenda weights were determined by cumulative weighings.

The copper reservoir (6) accommodated three samples arranged vertically, and all three samples were located within the homogeneous field region of the magnet. The reservoir was attached to the flange of a single-can, immersion cryostat with a stainless-steel link chosen to provide a convenient balance between cooldown time versus helium-boiloff during temperature control of the reservoir (i.e., no helium exchange gas was used). All electrical leads were thermally anchored to the cryostat flange and to the top of the copper reservoir, and the pumping line was radiation-baffled. A micro-miniature coaxial cable was the common lead to all capacitance thermometers to minimize stray capacitance. The other individual capacitance leads were twisted, 0.08-mm diam, phosphor bronze wires which were encased in a long, stainless-steel tube (.318 cm diam) with a webbing of 7031 varnish. This small tube ran the length of the pumping line and was grounded, and the purpose of this tube was to eliminate any relative motion between the capacitance leads and ground due to mechanical vibrations (this motion causes noise in the capacitance signal).

A brass can (3.81-cm outside diam to fit the magnet bore) was bolted to the flange with an indium seal, and zeolite pellets were placed in the bottom of the can. The inside of the can was lined with aluminized mylar, and an estimate of the radiation cooling of the samples yielded  $\sim 2 \mu\text{W}$  under worst conditions (i.e., sample at 20 K, can at 1.5 K). For our samples, this translates into a contribution to the drift rate  $\leq 10 \mu\text{K/sec}$ , which is orders of magnitude smaller than drift rate due to the copper link (5). Finally, the reservoir (6) was outfitted with a heater ( $30\Omega$ ), a silicon

diode thermometer, a calibrated germanium thermometer, and a capacitance thermometer. The reservoir heater and the silicon diode were connected to a temperature controller.

The cryostat was evacuated at room temperature, pre-cooled in liquid nitrogen, and inserted into the bore of the magnet filled with liquid helium. About 4-6 hr were required to cool the samples to helium temperatures through the various thermal links under the high vacuum conditions, and this long cooldown eliminated the transient drift of the capacitance thermometers.<sup>5</sup> The reservoir post stabilized at  $\approx 3$  K when the helium bath was pumped to  $\sim 1.5$  K.

The capacitance thermometers were first calibrated against the germanium thermometer in zero field, and about seven calibration points 4-20 were taken (the capacitance thermometer is nearly linear in this range). Bringing the samples into equilibrium with the temperature-controlled reservoir was facilitated by using the sample heaters which could be individually activated.

Next, the zero-field drift,  $20 \pm 3.2$  K, was carried out to determine  $\phi_0$ , Eq.(5). With the reservoir at  $\sim 3$  K, the sample heaters were used to bring the samples to  $\sim 20$  K, and removing the heater powers initiated the T-t drift. The subsequent drifts in intense fields were carried out in the same fashion. Heating the samples to  $\sim 20$  K prior to a drift heated the reservoir to  $\sim 6$  K. When the power to the sample was removed, the reservoir temperature,  $T_0$  in Eq.(2), rapidly drifted back to  $\sim 3$  K, and this reservoir drift was measured with the capacitance thermometer mounted on the reservoir post.

#### Data Collection and Reduction

The calibrated germanium thermometer was measured by the usual four-lead potentiometric method with current reversal, and for calibration purposes the capacitance thermometers were measured with a General Radio

transformer ratio-arm bridge (Model 1615-A) driven by a Krohn-Hite Model 4022R oscillator. The resulting capacitance ( $c$ )-temperature ( $T$ ) data were fitted to the fourth-order expansion,<sup>8</sup>

$$T = \sum_{n=0}^4 a_n c^n, \quad (7)$$

which results in an uncertainty  $\leq \pm 15$  mK in determining the absolute temperature in this temperature range.

The drift data were automatically collected as follows: Before the start of a drift with the sample at  $\sim 20$  K, the capacitance bridge was approximately balanced. During the drift, the bridge imbalance was supplied to a PAR Model 129 two-phase, lock-in amplifier with the quadrature adjusted so the signal input was pure capacitive. The lock-in amplifier was externally referenced by the Krohn-Hite oscillator, and the d.c. output of the amplifier was fed to a Digital Equipment Corporation Data Collection System, Minc 11. An EC Model 5105 pulse generator connected to the Minc 11 triggered voltage readings every 15 sec (set with an HP Model 5302A Universal Counter), and these voltages were stored by the Minc System on a disc. Voltage readings were thus taken at temperature intervals  $\leq 150$  mK. From 20 to 3 K, the capacitance thermometer typically changes from 22.5 to 19.0 nF, respectively, and the gain of the amplifier was set such that  $\pm 0.5$  nF corresponded to  $\approx \pm 60\%$  scale deflection. Consequently, the bridge setting was changed in 1 nF increments (between voltage readings) during the drift. Three bridge-amplifier systems were used for the three samples, and the Minc 11 recorded the three voltage signals simultaneously.

The data-collection systems were calibrated using standard capacitors in the range 17 to 23 nF, and these calibration data were fitted to

$$c = c_n + A_1 V + A_2 V^2 \quad (8)$$

where  $c_n$  is the null capacitance and  $V$  is the amplifier voltage. The

quadratic term in Eq.(8) was always small, indicating that the amplifier was in the linear range. In some cases,  $A_1$  and  $A_2$  in Eq.(8) were found to be slightly dependent on  $c_n$ .

To summarize, the amplifier V-data at 15-sec intervals were converted to c-data using Eq.(8), then to T-data using Eq.(7). These T-t data sets were then used to generate the  $\phi_o$  and  $\phi_H$  data according to Eq.(2). The initial, rapid reservoir drift between  $\sim 6 \rightarrow 3$  K mentioned above was accurately described by a single exponential,  $T_o(t) - T_o(\infty) \propto \exp(-t/\tau)$ , and was also incorporated in Eq.(2).

#### Wire Calibration ( $\beta_H$ )

In this section, we will describe the calibration of the 0.07 mm diam copper wire used as the dominant thermal link for the high specific heat samples. It should be noted, however, that if the thermal conductance of the dominant thermal link is magnetic-field independent, then  $\beta_H = 1$  from Eq.(6). In this case, the zero-field drift calibrates the link.

In the general case, as defined by Eq.(1),

$$G_H = (A/\ell)(T-T_o)^{-1} \int_{T_o}^T K_H dT \quad (9)$$

from Eq.(1), where  $A/\ell$  is the geometric factor for the link and  $K_H$  is the thermal conductivity.

Copper has a significant magneto-thermal conductivity effect which is anisotropic, and this complicates the calibration of the copper wire. The spiralled link (5) in Fig. 1 has both transverse and longitudinal components, and introducing thermal resistivities, which are additive, in Eq.(9) yields

$$G_H = A(T-T_o)^{-1} \int_{T_o}^T (\ell_t \gamma_t + \ell_\ell \gamma_\ell)^{-1} dT \quad (10)$$

where  $\gamma_t$  and  $\gamma_l$  are the transverse and longitudinal thermal resistivities, respectively. The effective lengths of the two components,  $l_t$  and  $l_l$ , are found directly from the physical dimensions of the spiral. Finally, the calibration parameter,  $\beta_H$  of Eq.(6), is determined by the ratio of the integrals defined by Eqs.(9) and (10), and the area of the wire cancels in the ratio.

Consequently, the wire calibration here necessitated measuring the transverse and longitudinal thermal conductivities of the copper wire (RRR = 108) in intense fields at low temperatures, and these measurements are reported elsewhere<sup>9</sup> (It was found that the Wiedemann-Franz ratio was unreliable for determining  $\gamma_t$  and  $\gamma_l$  from the corresponding electrical resistivities.). In Fig. 2 are shown thermal resistivities for this copper wire at 0, 5, and 10 T (Data at 2.5 T intervals up to 15 T are available from the authors.).

The total length of the copper links were chosen for our high specific heat samples such that the drift rate did not exceed 10 mK/sec. This could be determined adequately from the time constant,  $\tau = C/\dot{Q}$ . A complicating feature arose, however, from drift rates that were too slow at the very high field levels, as may be judged from Fig. 2. It was found necessary to shorten the copper links by about one-half for fields above 7.5 T.

#### EXPERIMENTAL RESULTS

A typical T-t drift record as generated on an HP 7221B plotter is shown in Fig. 3. The sample here was the chromite spinel mentioned above. To generate  $\phi$ -T data from a T-t record according to Eq.(2), it proved necessary to smooth the data before forming the  $dT/dt$  derivatives. The most satisfactory method for data smoothing consisted of dividing the T-t record into several overlapping regions, drawing the best curve through the experimental data, and digitizing the curves on an HP 7221B plotter. A third-order spline fit<sup>10</sup> was applied to the digitized data prior to generating the derivative data. The  $\phi$ -T data generated in this fashion from the T-t data in Fig. 3

are shown in Fig. 4. A flat region in the T-t data, such as near 8 K in Fig. 3, indicates a peak in  $\phi$  according to Eq.(2) and a maximum in the specific heat according to Eq.(3).

Finally, the specific heat data at 7.5 T of the chromite spinel sample mentioned above, as determined by this method, are shown in Fig. 5. The  $\phi_0$  and  $\phi_{7.5}$  data were determined as discussed above, and the  $\beta_{7.5}$  calibration parameter was determined from the magneto-thermal conductivity data according to Eqs.(6) and (10). The independently measured  $C_0$  data on this sample are also shown in Fig. 5. The addenda term,  $a(T)$  in Eq.(5), was determined from the addenda weights using literature data for the 7031 varnish and metals. The capacitance-thermometer addendum was taken from recently published data.<sup>6</sup> For this spinel sample, the addenda correction was very small; for example, at 10 K,  $a(10) \approx 5500 \text{ erg K}^{-1}$  whereas  $\mathcal{L} \approx 4 \times 10^5 \text{ erg K}^{-1}$  from Fig. 5 (i.e., 2 g sample), so the addenda constitute about 1.4% of the total heat capacity at 10 K.

The  $C_{7.5}$  data in Fig. 5 show considerable structure in the neighborhood of the zero-field specific heat maximum at 7.99 K. These  $C_{7.5}$  data between 7-9 K are shown separately in Fig. 6, and a second peak appears at 8.32 K together with satellite peaks at 8.10 and 8.41 on the high-temperature wings of the two main peaks at 7.5 T. The first peak at 7.99 K is unaffected in height or temperature by the 7.5 T field.

## DISCUSSION

The results presented here demonstrate that this drift method employing capacitance thermometry is a very sensitive technique for measuring specific heat data in intense magnetic fields. The versatility of the method is evident in Fig. 6 where a considerable amount of structure is resolved within a relatively narrow temperature range. The method is especially well-suited for resolving such data near a maximum, as in Fig. 6, because the drift rate slows considerably and  $\Delta T$ 's  $\sim 10 \text{ mK}$  are involved. By contrast, the conventional pulse method involves  $\Delta T$ 's  $\sim 200 \text{ mK}$  at, say, 8 K, and consequently there is some rounding of the data near the maximum. The ability

to collect calorimetric data on three samples simultaneously is a distinct advantage, and the problems of calibrating the capacitance thermometers in situ and accommodating the transient drift with a long cooldown seem far less formidable than calibrating the magnetoresistance of resistance thermometers.

The major disadvantage of the method as presented here was the calibration of the copper link wire, which grew into a separate study.<sup>9</sup> However, the copper wire was dictated by the very large specific heats of the samples measured, whereas for samples with smaller specific heats a manganin link [such as (4) in Fig. 1] would suffice. Moreover, a manganin link offers a considerable calibration advantage compared to copper because the magnetoresistive effect in manganin is negligibly small.<sup>11</sup> Consequently, for manganin,  $\beta_H \approx 1$  (recall that the zero-field drift calibrates the thermal link provided there are no magneto-thermal conductivity effects).

The capacitance thermometer element may appear to represent a significant addendum for samples with small specific heats, but at 10 K this element represents only about 20% of the total addenda quoted above (5500 erg  $g^{-1} K^{-1}$ ). If one sets an upper limit of 50% on the addenda contribution to the specific heat, then the sample specific heat should be at least  $\sim 3 \times 10^3$  erg  $g^{-1} K^{-1}$  at 10 K for a 2-g sample for using this method. For comparison, the specific heat of glass is  $\sim 5 \times 10^4$  erg  $g^{-1} K^{-1}$  at 10 K.

There is a certain degree of arbitrariness in smoothing the T-t drift data as described above. As an internal check, the experimental T-t data leading to the  $C_{7.5}$  data in Fig. 6 were independently smoothed two different ways. The two sets of resulting  $C_{7.5}$  data in the range 7-9 K, measured in two independent runs, matched identically, as regards major structure, and this was a stringent test of the method due to the structure in the data (note the logarithmic scale in Fig. 6).

Finally, we consider the sources of error in the method: Referring to Eq.(5), the largest source of error most probably is due to  $C_0$ , the



zero-field specific heat which must be measured independently. In the case of our materials, the uncertainty in  $C_0$  was no larger than  $\pm 5\%$ . Depending on the thermal link, the uncertainty in  $\beta_H$  can be very small. In the extreme case of the copper link used here, the uncertainty in the thermal conductivity values used is  $\approx \pm 5\%$ .<sup>9</sup> However, since a ratio of integrals is involved in  $\beta_H$ , the uncertainty in  $\beta_H$  is smaller than the uncertainty in the thermal conductivities. The uncertainty in the addenda term,  $a(T)$ , is negligible in our case, and the uncertainty in the ratio of  $\phi$ 's in Eq.(5) is certainly below  $\pm 2\%$ , except when  $dT/dt$  is small (near a peak in  $C$ ). Since all these sources of error are independent, we estimate that the upper limit on the uncertainty of the method is  $\approx \pm 7\%$ . A major source of error is not apparent from Eq.(5); namely, at a high drift rate the sample will not be in thermal equilibrium with the thermometer. This thermal lag, however, can easily be circumvented by embedding the thermometer in the sample such that the longest thermal diffusion path is commensurate with the diffusivity of the material.

#### Acknowledgement

The authors are grateful for the hospitality of the Francis Bitter National Magnet Laboratory and to L.G. Rubin, in particular, for technical assistance in these measurements.

#### REFERENCES

(a) Work supported by the U.S. Air Force.

1. See the review of low-temperature calorimetry by R.W. Hill in Experimental cryophysics, F.E. Hoare, L.C. Jackson, and N. Kurti, Editors (Butterworths, London, 1961).
2. W.N. Lawless, Rev. Sci. Instrum. 42, 561 (1971).
3. L.G. Rubin and W.N. Lawless, Rev. Sci. Instrum. 42, 571 (1971); note that the loss tangent, the in-phase component of the capacitance signal, is related to the a.c. conductivity and therefore can be H-field dependent.
4. W.P. Pratt, S.S. Rosenblum, W.A. Steyert, and J.A. Barclay, Cryogenics, Dec. 1977, pg. 689.
5. W.N. Lawless, Rev. Sci. Instrum. 46, 625 (1975); C.A. Swenson, Rev. Sci. Instrum. 48, 489 (1977).
6. W.N. Lawless, Rev. Sci. Instrum. 51, 1567 (1980).
7. W.N. Lawless, Phys. Rev. B14, 134 (1976).
8. W.N. Lawless and E.A. Panchyk, Cryogenics 12, 196 (1972).
9. R.W. Arenz, C.F. Clark, and W.N. Lawless, Phys. Rev. B (in press).
10. C.F. Gerald, Applied numerical analysis (Addison-Wesley, London, 1978).
11. L.G. Rubin (private communication).

#### FIGURE CAPTIONS

- Figure 1. Schematic drawing of the experimental arrangement for measuring specific heat in intense magnetic fields at low temperatures. The sample (1) containing a capacitance thermometer element (2) and a heater (7) is linked to a copper reservoir (6) by a mechanical link (4) and a dominant thermal link (5).
- Figure 2. Longitudinal and transverse thermal resistivity data for the copper thermal link wire at 0, 5, and 10 T. These are representative data from Ref. 9 which are used to evaluate the integral in Eq.(10).
- Figure 3. Example of a time-temperature drift record generated by the data collection system. The sample here was the chromite spinel mentioned in the text and the field level was zero.
- Figure 4. Example of the  $\phi$ -T data generated according to Eq.(2) by the method discussed in the text. These  $\phi$  data were generated from the T-t drift data in Fig. 3.
- Figure 5. Specific heat of a chromite spinel at 7.5 T measured by the drift method described in the text. The independently measured zero-field specific heat data are shown for comparison, and the peak at 7.99 K is not affected by the field.
- Figure 6. Specific heat data at 7.5 T of the chromite spinel of Fig. 5 in the range 7-9 K. At this field level, a second peak appears at 8.32 K and satellite structures appear at 8.10 and 8.41 K.

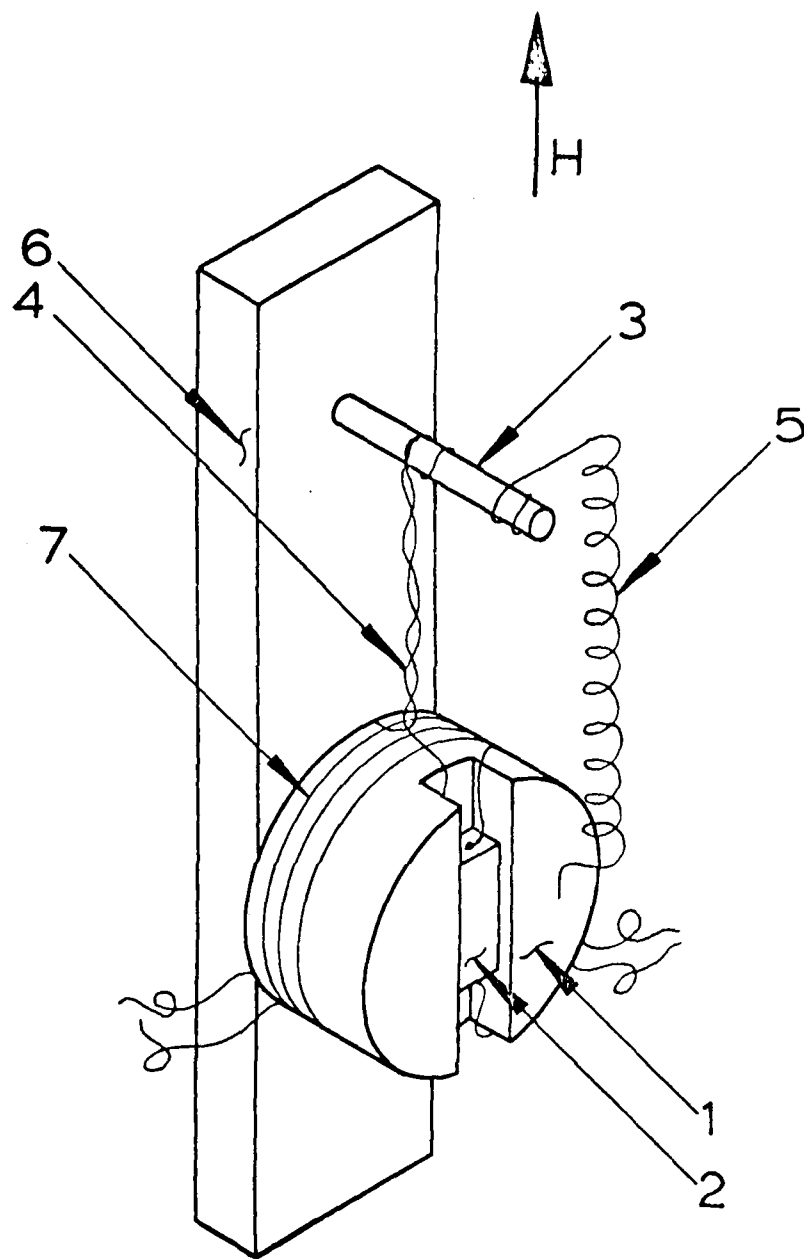


Figure 1.

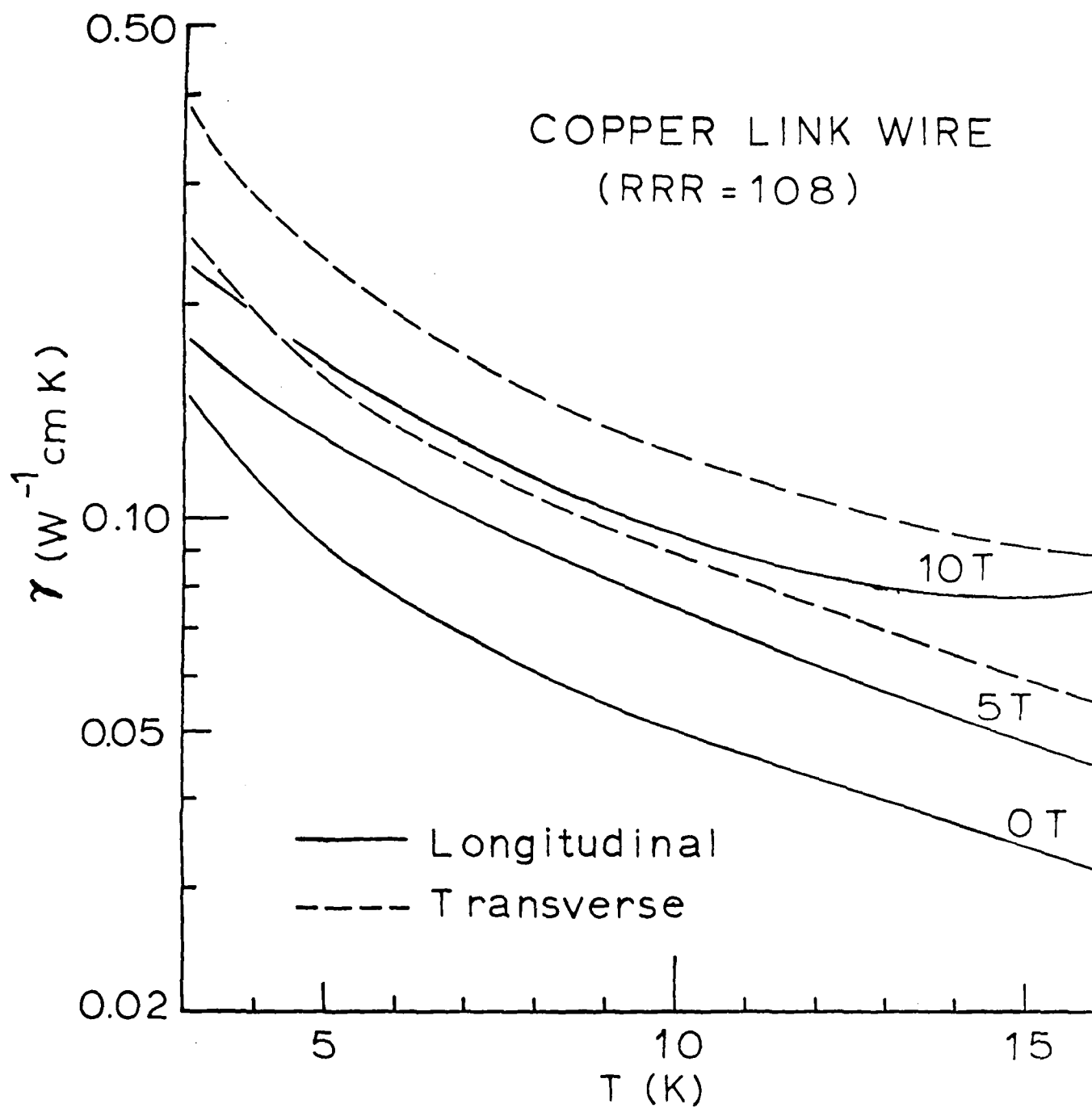


Figure 2.

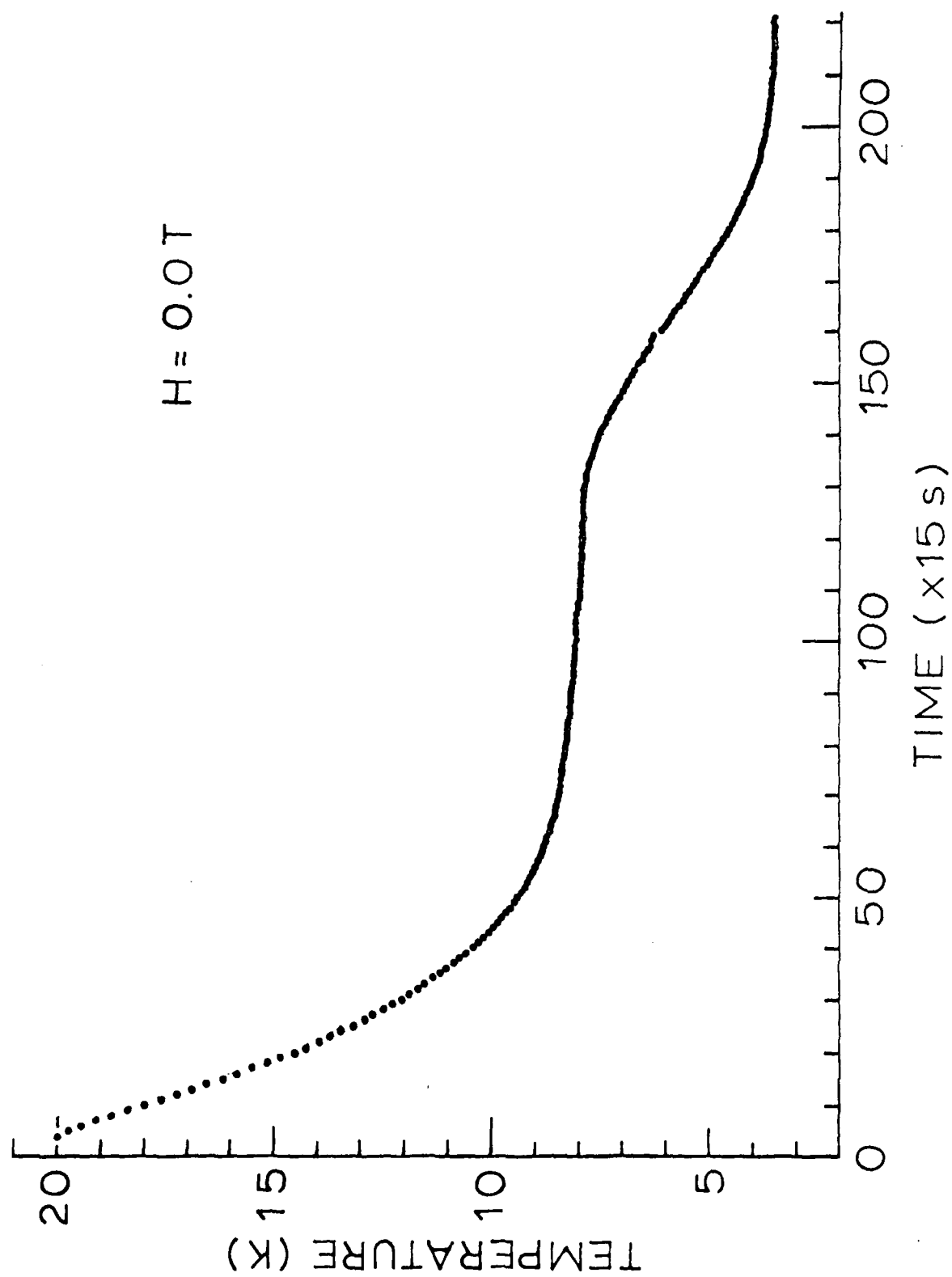


Figure 4

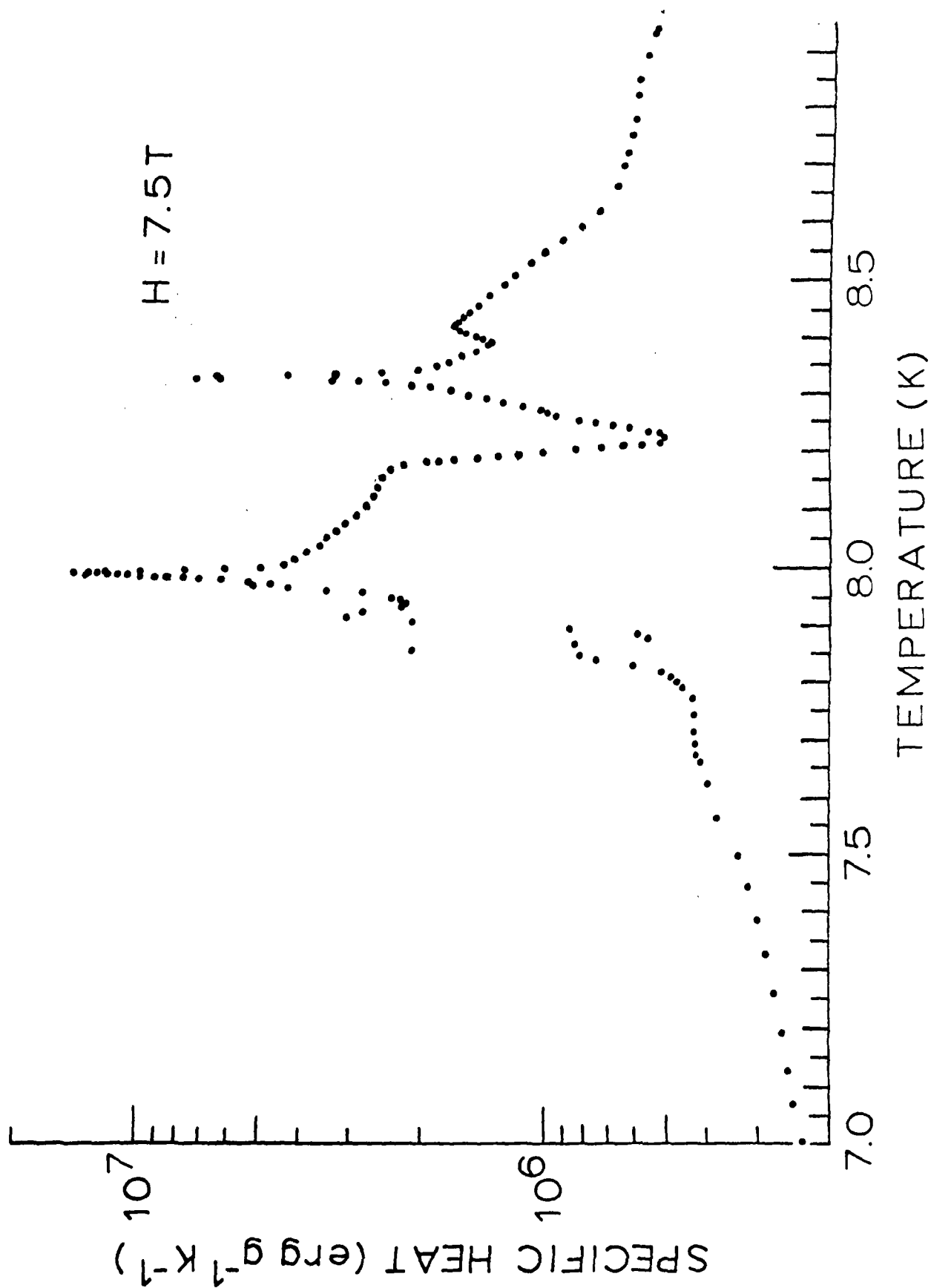


Figure 4.

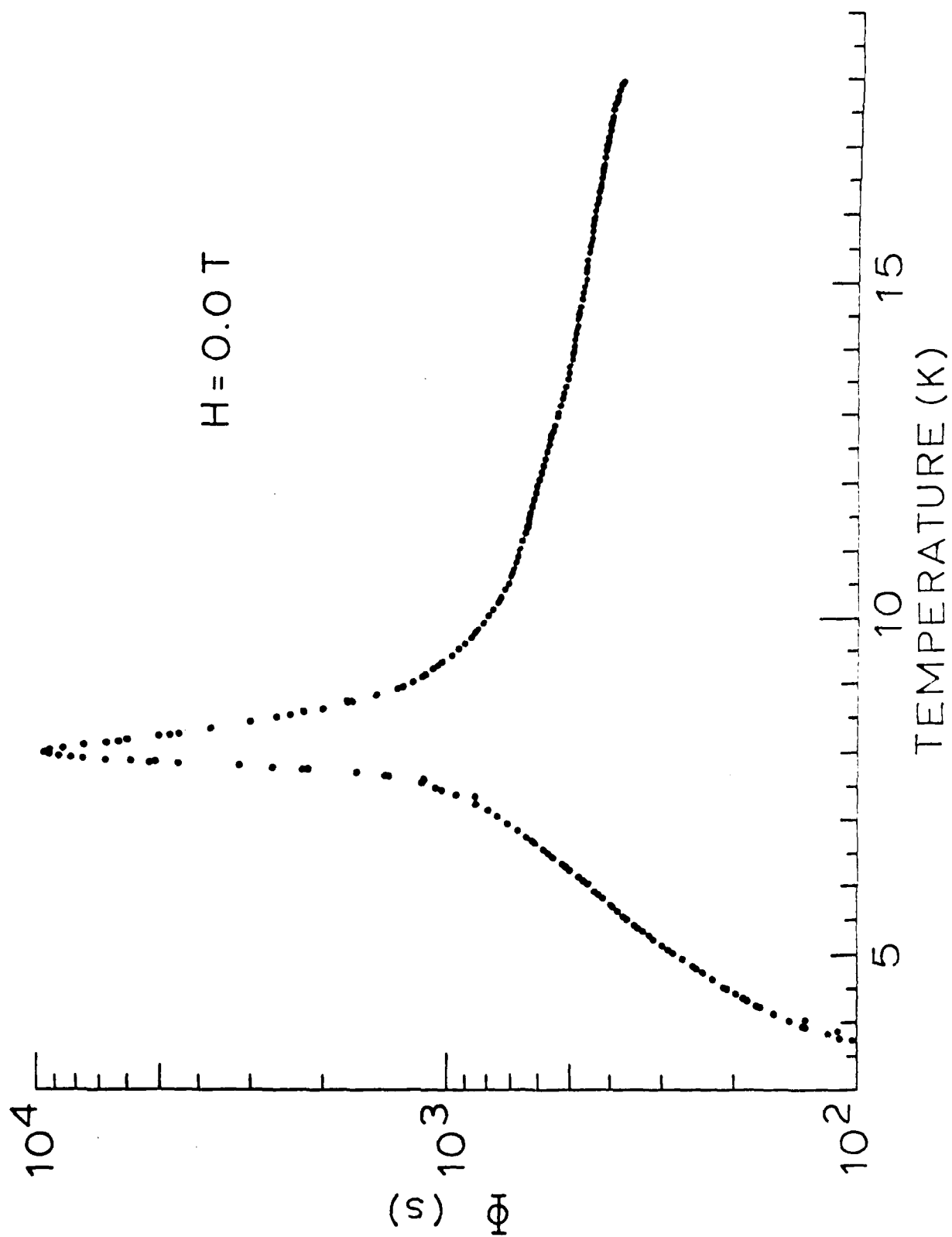


Figure 3



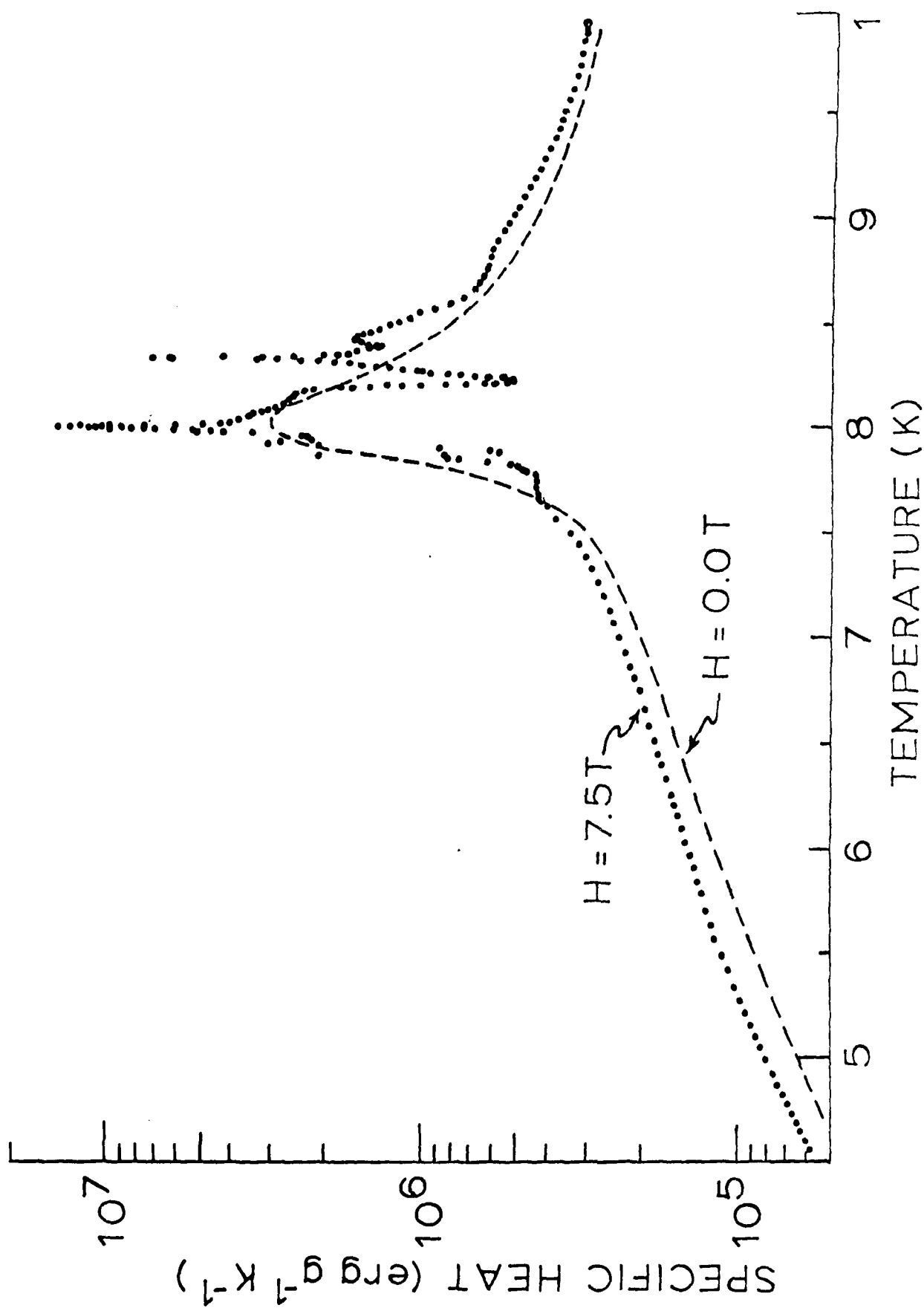


Figure 6.

DATE  
FILME